DESIGN AND DEVELOPMENTAL ASPECTS OF HIGH POWER ULTRA-WIDEBAND 3DB HYBRID COUPLER FOR ICRF HEATING IN TOKAMAK

By

Rana Pratap Yadav

ENGG06201104003

INSTITUTE FOR PLASMA RESEARCH, GANDHINAGAR

A thesis submitted to the
Board of Studies in Engineering Sciences

In partial fulfillment of the requirements

For the Degree of

DOCTOR OF PHILOSOPHY

of

HOMI BHABHA NATIONAL INSTITUTE

June, 2014

Homi Bhabha National Institute

Recommendations of the Viva Voce Board

As members of the Viva Voce Board, we recommend that the dissertation prepared by **Rana Pratap Yadav** entitled "Design and developmental Aspects of High Power Ultra-wideband 3dB Hybrid Coupler for ICRF Heating in Tokamak" may be accepted as fulfilling the dissertation requirement for the Degree of Doctor of Philosophy.

-- **Date :**
Chairman : Dr. Anurag Shyam

-- **Date :**
Convener : Dr. S.V. Kulkarni

-- **Date :**
Member : Mr. Sunil Kumar

-- **Date :**
Member : Prof. S. Mukharji

-- **Date :**
Member : Dr. S. K. Pathak

Final approval and acceptance of this dissertation is contingent upon the candidate's submission of the final copies of the dissertation to HBNI.

I hereby certify that I have read this dissertation prepared under my direction and recommend that it may be accepted as fulfilling the dissertation requirement.

-- **Date :** Oct. 9, 2014
Guide : Dr. S. V. Kulkarni

STATEMENT BY AUTHOR

This dissertation has been submitted in partial fulfillment of requirements for an advanced degree at Homi Bhabha National Institute (HBNI) and is deposited in the Library to be made available to borrowers under rules of the HBNI.

Brief quotations from this dissertation are allowable without special permission, provided that accurate acknowledgement of source is made. Requests for permission for extended quotation from or reproduction of this manuscript in whole or in part may be granted by the Competent Authority of HBNI when in his or her judgment the proposed use of the material is in the interests of scholarship. In all other instances, however, permission must be obtained from the author.

Rana Pratap Yadav

DECLARATION

I, hereby declare that the investigation presented in the thesis has been carried out by me. The work is original and the work has not been submitted earlier as a whole or in part for a degree/diploma at this or any other Institution or University.

Rana Pratap Yadav

To my Family

ACKNOWLEDGEMENTS

Foremost, I would like to express my sincere gratitude to my thesis supervisor Dr. S.V. Kulkarni for her excellent guidance, help and the time he spent throughout my period of association with his. He always encouraged me for everything. The positive attitude I learnt from him will remain with me for ever.

I am extremely grateful to Mr. Sunil Kumar for all experimental and technological discussions during my thesis period. Each time I discussed, I learnt a lot and got enriched with several novel ideas. Meeting with him was always an experience for me. I thank him for everything he did for me to make my Ph.D. a success.

I would like to thanks Prof. Anurag Shyam, Dr. Subrato Mukharji and Dr. Surya Kumar pathak for their useful suggestions.

A special thanks to Prof. P. K. Kaw and Prof. D. Bora for their continuous support and encouragement.

A special thanks to (Mr.) Srinivas, Bhavesh R. Kadia, Atul, H.M. Jadav, Kirit Parmar, Ramesh Joshi, Manoj and Gaytri of ICRH group for their support.

I would also like to convey my sincere thanks to IPR library, IPR administration and computer center staff for their kind support during my thesis period.

A Special thanks to Dr. Sanjay Mishra to provide me the help in proof reading of my publications.

A Special thanks to (Mr.) G. Vedaprakash and Pravesh Dhyani for always being supportive for me at academic and personal front. Thanks to my senior(Dr.) Sekhar, Ujjwal, Vikram Narang, Sanat Tiwari, Jugal, Prabal, Khitish, Ashwin, Deepak, Sharad, Vikrant, Rajneesh, Susil, Gurudatt Swati, Sita, Satish, Kamal Kant and Ajay for being friendly and helpful towards me on various occasion. I enjoyed the friendly hostel life at IPR. Greetings and best wishes to my dear Aditya, Somen, Sayak, Manjit, Neeraj, Vikram Dharodi, Roopendra, Vibhu, Vara Prasad, Akanksha, Vidhi, Deepa, Mangilal, Harish, Megharaj, Surbhi, Bhumika, Arghya, Debraj, Modhuchandran, Naran, Amit, Ratan, Sonu and Umesh.

A special thank to my colleagues and friends Mr. Veda Prakash, Md. Zuber, Sandeep Rimza and Dushant for their help in numerous occasions.

Special thank to my wife for encouraging and supporting me at every front and decision making. This is unconditional and selfless support of her which will encourage me to come out of all sort of odds through out my Ph.D tenure. At last my heartfelt gratitude to my parents and brothers for their goodwill and support all through my life.

List of Publications

List of publication:

- **Design and Development of the 3dB patch compensated tandem hybrid coupler**,
  Rana Pratap Yadav, Sunil Kumar and S. V. Kulkarni
  Review of Scientific Instruments 84.1 (2013): 014702-014702.

- **An analysis of junction discontinuity effects in multi-element coupled lines and its diminution at designing stage**,
  Rana Pratap Yadav, Sunil Kumar and S. V. Kulkarni
  Progress In Electromagnetics Research B, Vol. 56, 25-49, 2013.

- **Design and development of ultra-wideband 3dB hybrid coupler for ICRF heating in Tokamak**,
  Rana Pratap Yadav, Sunil Kumar and S. V. Kulkarni
  Review of Scientific Instruments 85, 044706 (2014).

- **Junction discontinuity effect in multi-element coupled lines and its ompensation**,
  Rana Pratap Yadav, Sunil Kumar and S. V. Kulkarni
  proceeding of TENSYMP-2014 in IEEE explore,
  http://dx.doi.org/10.1109/TENCONSpring.2014.6863051.

- **Design and development of ultra-wideband 3dB hybrid coupler for ICRF heating in fusion grade reactor**,
  Rana Pratap Yadav, Sunil Kumar and S. V. Kulkarni
  To be submitted

Conferences/Schools:

International Participation

- Design and development of a 3dB high power hybrid coupler for the ultra wideband frequency range. (Poster)
  Rana Pratap Yadav, Sunil Kumar and S. V. Kulkarni
  International Conference on Complex Processes in Plasmas and Non Linear Dynamical Systems(ICCPPNDS-2012), Institute for Plasma Research, Gandhinagar, India, 6-9 November, 2012.

- Design and development of a 3dB high power hybrid coupler.(Poster)
  Rana Pratap Yadav, Sunil Kumar and S. V. Kulkarni
  6th ITER International School Ahmedabad, India, 02-06 December 2012.

- Junction discontinuity effect in multi-element coupled lines and its compensation. (Talk)
  Rana Pratap Yadav, Sunil Kumar and S. V. Kulkarni
  IEEE Region 10 Symposium, Kuala lumpur, Malaysia, April 2014.

National Participation

- Design aspect of the tandem 3dB hybrid coupler using matching stub for the rf heating of plasma in tokamak.(Talk)
  Rana Pratap Yadav, Sunil Kumar and S. V. Kulkarni
  2nd ISRC, 21st October 2011, IPR Gandhinagar, India.

- Design aspect of the tandem 3dB hybrid coupler for the ultra wide band frequency range of (32-112)MHz. (Poster)
  Rana Pratap Yadav, Sunil Kumar and S. V. Kulkarni
  1st ASRC, July, 3-4, 2012 , IPR Gandhinagar, India.

- Design aspect of 91.2MHz 3dB hybrid coupler using two 8.34dB coupled lines. (Poster)
  Rana Pratap Yadav, Sunil Kumar and S. V. Kulkarni
  PSSI-2011, December 20-23, 2011 at Birla Institute of Technology, Patna, Bihar, India.

- Design and development of a multi-element 3dB high power hybrid coupler. (Talk)
  Rana Pratap Yadav, Sunil Kumar and S. V. Kulkarni
  National Symposium on High Power RF and Microwave,IPR Gandhinagar, India, Sept. 04-06, 2013.

Contents

Abstract

The ICRH system of tokamak utilizes continuous wave rf power above 100kW and upto few MW at many frequencies in the range of 20 to 120MHz. The frequency depends upon geometry of the tokamak, desired plasma parameters and toroidal magnetic field at the center of tokamak vessel. The ICRF generators are used to feed the rf power to the plasma with ICRH antennae. These should ideally be operated into matched load. The antennae load impedance not only depends on the antennae geometry but also on the boundary conditions of plasma which offer continuously variable mismatch. Due to the mismatched loading, significant amount of the rf power is reflected back and causes inconsitant performance or damage to the generator. The conventional matching systems operate on slower time scale and may fails to cope with the faster variation of plasma impedance. The 3dB hybrid coupler is used to provide the essential protection to the rf generator from the reflected power. The 3dB hybrid coupler can also be used as power combiner, divider and to protect the rf source by coupling of reflected power to the isolated port.

The 3dB hybrid coupler is a 4-port device in which input of rf power at port-1 is equally divided into the port-2 and port-3 with a phase difference of 90°, whereas port-4 is remain isolated. In case, reflected powers due to mismatched load at port-2 and port-3 that are connected to antennae are equal in magnitude and phase, the total reflected power goes to port-4. Thus, rf generator is protected from reflected power. The high power hybrid couplers that are developed and presently available for these purposes are rated for narrow frequency band and do not cover full operational frequency range of the proposed ICRH experiments. Many 3dB hybrid coupler, at various discrete frequencies are required in the ICRF

range. Therefore, hybrid coupler and the coupling mechanism needs to be altered with change of operating frequency. The development of broadband 3dB hybrid coupler in the high power rating is not yet reported. Therefore, the need is felt and the author is motivated to intensify his research interest in this domain. The work has been completed in following steps:

1. A strip line based prototype 3dB tandem hybrid coupler of rating, 91.2±15MHz and 2.5 kW has been developed to create the process for indigenous development at any frequency in the range of HF and VHF.

2. Design of broadband multi-element coupled lines for high power handling capability is successfully completed.

3. A 200kW and 38 to 116MHz, ultra-wideband novel 3dB hybrid coupler is designed, developed, fabricated and tested for the desired performance.

4. Design and fabrication drawings of the 1.5MW ultra-wideband 3dB hybrid coupler for the ICRF heating in fusion grade reactor is completed.

List of the Symbols

R, L, G, C	are series resistance, series inductance, shunt conductance and shunt capacitance per unit length of an arbitrary transmission line
ω	Angular frequency
α, β	are the attenuation phase constant
γ	propgation constant
v_p	phase velocity
λ	frequency wavelength
Z_0	characteristic impedance per unit length
ϵ_r	relative permittivity
w_e	effective width of strip line
w	width of strip line
t	thikness of strip line
b	spacing beteween ground conductor of the the strip line
α_c	attenuation constant due to the conductor
α_d	attenuation constant due to the dielectric
R_s	skin resistance of the transmission line
η_0	skin resistance of the stripline conductor
P_p	Peak power
V_{peak}	Peak voltage
ΔT	Temprature rise of inner conductor with respect to the outer conductor
$\Delta T_{perwatt}$	Temprature rise of inner conductor per watt
P_c, P_d	power dissipation due to the conductor and dielectric
P_T	Total incident power in watt
G_t	Thermal conductance
T_{amb}	ambient temprature
T_{max}	Maximum operating temprature
μ	Magnetic permeability
σ	conductance of the strip line conductor
δ	Surface rougness
C_e	even mode capacitance
C_o	odd mode capacitance
C_v	coupling cofficient
C_{11}	self capacitance of the strip 1 with respect to ground
C_{12}	capacitance between of the strip 1 and 2
Z_{ce}, Z_{co}	even and odd mode impedance of the coupled lines
$K(k)$	elliptical integral of first kind
C_{p1}, C_{p2}	face capacitance of the upper and lower side strip line conductor
C_{f1}, C_{f2}	fringing capacitance of the upper and lower side strip line conductor
Z_c, Y_c	coupled line impedance and cpacitance

Z_m, Y_m	patch impedance and cpacitance
A_c	amplitude of signal appears at isolated port-4 of uncompensated coupler
A_{wc}	amplitude of signal appears at isolated port-4 of uncompensated coupler
A_1, A_2, A_3, A_4	amplitude of signal emerging from coupled element-A from port 1,2,3 & 4
T_{0e}, T_{0o}	transmitted wave amplitude in even and odd mode
Γ_{0e}, Γ_{0o}	reflected wave amplitude in even and odd mode
Z_c, Y_c	coupled line impedance and cpacitance
Z_m, Y_m	patch impedance and cpacitance
A_c	amplitude of signal appears at isolated port-4 of uncompensated coupler
A_{wc}	amplitude of signal appears at isolated port-4 of uncompensated coupler
A_1, A_2, A_3, A_4	amplitude of signal emerging from coupled element-A from port 1,2,3 & 4
T_{0e}, T_{0o}	transmitted wave amplitude in even and odd mode
Γ_{0e}, Γ_{0o}	reflected wave amplitude in even and odd mode
Z_{0eA}, Z_{0oA}	even and odd mode impedance of element-A
Z_{0eB}, Z_{0oB}	even and odd mode impedance of element-B
C_x	coupling cofficient of an arbitrary element-x
C_A, C_B	coupling cofficient of element-A and element-B
L_{jeB}, C_{joB}	even and odd mode inductance and capacitance associated to the element-B due to the junction discontinuity effect.
L_{joA}, C_{jeA}	odd and even mode inductance and capacitance associated to the element-A due to the junction discontinuity effect
f_0	center frequency
$Z_{eB(eff)}$, $Y_{oB(eff)}$	even and odd mode effective impedance and admittance of element-B
$Y_{eA(eff)}$, $Z_{oA(eff)}$	even and odd mode effective admittance and impedance of element-A
θ	electrical length of the coupled lines at frequency f.
θ_0	electrical length of the coupled lines at frequency f_0.
$\begin{bmatrix} A_{Be'} & B_{Be'} \\ C_{Be'} & D_{Be'} \end{bmatrix}$	even mode transmission matrix parameter of element-B including junction discontinuity effect.
$\begin{bmatrix} A_{Bo'} & B_{Bo'} \\ C_{Bo'} & D_{Bo'} \end{bmatrix}$	odd mode transmission matrix parameter of element-B including junction discontinuity effect.
$\begin{bmatrix} A_{Ae'} & B_{Ae'} \\ C_{Ae'} & D_{Ae'} \end{bmatrix}$	even mode transmission matrix parameter of element-A including junction discontinuity effect.
$\begin{bmatrix} A_{Ao'} & B_{Ao'} \\ C_{Ao'} & D_{Ao'} \end{bmatrix}$	odd mode transmission matrix parameter of element-A including junction discontinuity effect.
B'_1, B'_2, B'_3, B'_4	repersent return loss, output, coupling and isolation of the coupled element-B including junction discontinuity effect.
A'_1, A'_2, A'_3, A'_4	repersent return loss, output, coupling and isolation of the coupled element-A including junction discontinuity effect.
b_3	overall coupling of 3-element coupled line section
b'_3	overall coupling of 3-element coupled line section including junction discontinuity effect

b_{3m}	overall coupling of modified 3-element coupled line section
$Z_{0ex}, Z_{0ox}, Y_{0ex}, Y_{0ox}$	even and odd impedance and admittance of the coupled element-x
ϵ_{x^+}, ϵ_{x^-}	needful increment and decrement in element-x
θ_a, θ_b	electrical length corresponding to ϵ_{x^+}, ϵ_{x^-}
X_{joex}	reactance associated to element-x due to junction discontinuity effect
C_{studs}	capacitance associated to the studs
Y_{studs}, X_{studs}	capacitive reactance associated to the supporting dielectric studs
l_{x+}, l_{x-}	length of element including required increment and decrement of ϵ_{x^+}, ϵ_{x^-} respectively

List of Figures

1

Introduction

1.1 Motivation and brief history

The energy demands in the world are dramatically increasing every year. At present more than 80% of energy need is fulfilled by the coal, oil and gas. The fossil fuels are present in limited stock. These are responsible for the huge emission of carban-dioxide and other harmful gases. Therefore, it is desirable to have an alternative energy source.

Fusion energy seems to have potential to provide sustainable solution to global energy requirements. This is the topic of active research and is supposed to be available as a future energy option by the middle of this century. This could contribute to a secured and safe energy. Fusion energy is liberated from the fusion reaction where the two light atomic nuclei of deuterium and tritium are fused together to form a heavier atom of helium. The same mechanism is considered to be responsible for the energy sources like stars and other illuminating celestial objects. In laboratory, fusion has been achieved in tokamak devices that used magnetic fields to contain and control the plasma for the production of energy. The plasma is produced with deuterium gas and tritium is added in the form of pellet in the plasma to have fusion reaction. Scientists are participating in the worldwide effort to develop magnetic fusion energy for generating electricity. International fusion experiments like JET, Tore Supra, ITER etc. aim to demonstrate the scientific and technological feasibility of fusion reactors. To achieve fusion reaction in tokamak, plasma should be heated to temperatures over 100 million degrees Celsius i.e. about 10keV. This is necessary to provide some of the heating methods to reach the temperature required for ignition. Ion Cyclotron Resonance Heating (ICRH) is a promising heating method due to its localized power deposition profile, direct ion heating at high density and established rf technology at low cost [1, 2].

Ion cyclotron heating in tokamak(ICRH)

In static magnetic field of the tokamak, charged particles (i.e. ions and electrons) of the plasma move on the spiral trajectory and rotate around magnetic field lines with frequencies that depend on: charge of particle, mass of particle and magnetic field strength. Frequency of the rotating ion is known ion cyclotron frequency (ICRF). Therefore, if an electromagnetic wave with ion cyclotron frequency is launched into the plasma, most of the ions are heated, provided that the magnetic field complements the resonant condition and also the direction of the rotation of particle is in the same direction of the direction of rotation of magnetic field so that the particle see dc electric field in their own frame of rectance. This phenomena is known as ion cyclotron resonance heating (ICRH). In tokamak, ICRF may vary from 20 to 120MHz that depends on geometry of the tokamak, desired plasma parameters and toroidal magnetic field at the center of tokamak vessel. In case of SST-1 tokamak 91.2MHz frequency is required for ICRH during 2nd harmonics heating at 3 T tokamak operation [3, 4]. ICRH system of tokamak utilizes cwrf of 100kW onwards in the frequency range of 20 to 120MHz [5]. ICRH system used in some of the well known tokamak are rated as, In ICRH system rf generator

Tokamak	**Power**	**Frequency range**
Aditya	200kW	(22-47)MHz
SST-1	1.5MW	(22-91.2)MHz
JET	36MW	(25-55)MHz
Tore Supra	12MW	(40-80)MHz
ITER plan	20MW/antenna	(40-55)MHz

feed the rf power to the plasma through one or many antennae. The antenna load impedance not only depends on the antenna geometry but also on the boundary conditions of plasma which offers continuously variable mismatched load. Due to mismatch of load impedance and generator impedance a significant amount of the rf power is reflected back to the generator. This is undesirable for the better efficiency and reliable operation of rf generator. Matching systems are used to transform the plasma impedance to that required for the optimal functioning of the ICRF generator. The conventional matching system operates on slower time scale which may fail to cope with the faster variation of plasma impedance [6–8]. The 3dB hybrid coupler may be used to protect the rf generator from reflected power.

Schematic of the the 3dB hybrid coupler is shown in Fig.1.1. It is a 4-port device in which input rf power at port-1 is equally divided into the output port-2 and coupled port-3 with a phase difference of 90°, whereas port-4 is isolated. In case, reflected power due to mismatched load at port-2 and port-3 is equal in magnitude and phase, the total reflected power goes to port-4 which is terminated with dummy the load [9–11]. Thus, the rf generator at port-1 is protected from reflected power.

In ICRH system of the Joint European Torus (JET), the 3dB hybrid coupler

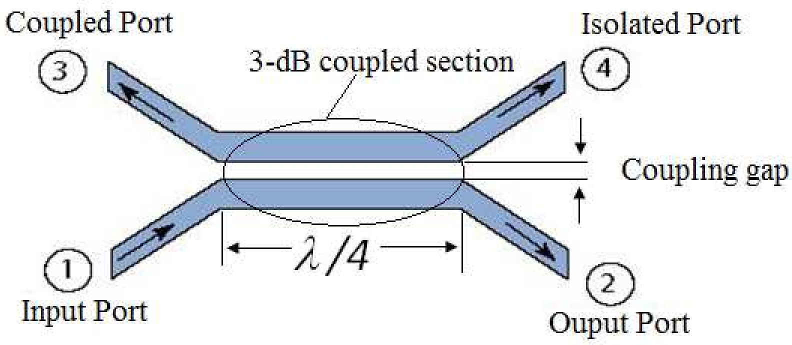

Figure 1.1: Schematic of the 3dB hybrid coupler.

is installed to feed 2MW rf power through two antennae located at different positions of the plasma. The tests showed that the reflected power during ELMs (Edge localized modes) was successfully directed to the dummy load instead of the generator and a clear improvement in coupled power is obtained [12]. This experience is utilized in ITER plan where 20MW of rf power is to be fed via four 3dB hybrid couplers with eight transmission lines to the ICRF antenna [13]. Schematic of the typical rf system used in SST-1 is shown in Fig.1.2 where rf power from the single source is divided through hybrid coupler into two identical transmission lines. Each of the transmission lines including matching networks are terminated with antennae that feed the power to the plasma in tokamak. Here hybrid coupler is used with following objectives,

1. To provide the better efficiency, reliable operation and isolation of the reflected power from the rf generator.

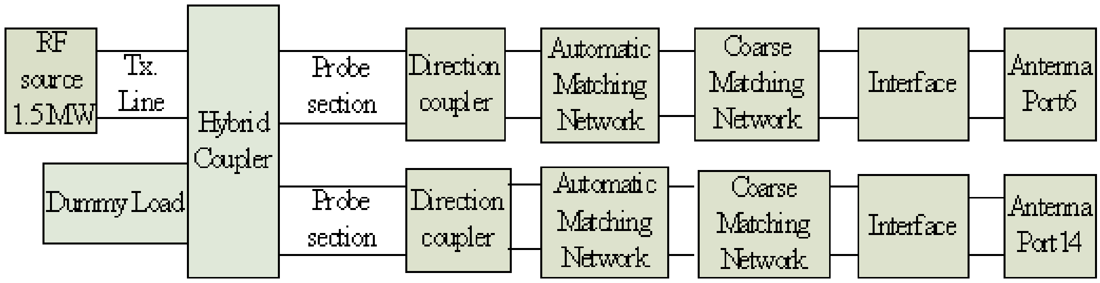

Figure 1.2: Schematic of the typical rf system used in SST-1.

2. To enhance plasma current drives by creating the phase difference of 90° between two antenna ports that are located at different positions in the tokamak.

The previously, hybrid couplers are made for narrow frequency band and are not able to cover full operational frequency range of the proposed ICRH experiments. Therefore, hybrid coupler and the coupling machnism needs to be altered with change in operating frequency. For example, in Steady State Super Conducting Tokamak-1 (SST-1), a 3dB hybrid coupler of 1.5MW power handling capability is used to feed the rf power through two antennae. This 3dB hybrid coupler is fabricated with a total of five segments that are required to be arranged in particular manner for specified operating frequencies in narrow band. Four different sets of the arrangement are procured for the specified operating frequency ranges namely 22-25MHz, 43-48MHz, 65-75MHz and 87-97MHz. The alteration in assembly of such bulky and sensitive structure consumes time, manpower and alteration in peripheral rigid coaxial transmission lines. Moreover ICRF heating experiments can not be performed outside specified narrow bands of frequencies. The development of broadband 3dB hybrid coupler for the high power rating is not yet reported. Therefore, the need is felt and the author is motivated to intensify his research interest on this topic in this domen.

High voltage breakdown due to applicable power, frequency and structure geometry, limits the power ratings of rf components [14–16]. Broadside TEM coupled stripline structures are widely used in the development of 3dB hybrid couplers due to simple design, cost effectiveness and ease of fabrication. In a particular environmental condition, peak power handling capability of any strip-line is decided by the spacing between the stripline conductors and ground plane. The maximum permissible spacing is governed by the onset of TE and TM modes. The lowest order TE modes can propagate when the width of the strip conductor and spacings are such that average circumferential distance exceeds about one wavelength [17]. Therefore in a particular frequency range, strip width and spacings of the stripline based system is restricted and hence the maximum power handling capability is limited. TEM coupled strip-lines are also well known for poor impedance matching and poor isolation due to discontinuities, fabrication tolerance constraints and theoretical approximations. These effects become prominent as the size of the system increases due to high power application. Alleviation of all the above problems from the coupled stripline and development of stripline based 3dB high power hybrid coupler is the motivation of the present research work. The work is organized as follows.

1.2 Thesis Outline

Thesis deals with the design and development of the 1.5MW ultra-wideband 3dB hybrid coupler for the HF and VHF range of frequency, the fabrication and testing of 2.5 kW narrow band and 200kW ultra-wideband novel hybrid couplers have been completed at intermediate steps.

Chapter 2 covers the fundamental of transmission lines and coupled lines theory that will be needed throughout the thesis. Transmission lines and their applicability in high power is studied in detail. Generally, rigid coaxial transmission lines are used the high power application. Though, stripline type transmission line is found appropriate due to simpler geometry i.e. more suitable for broadband coupled line design. Therefore, this chapter is more concentrated on the study, design and development procedure of the stripline type transmission lines.
Chapter 3: Here, theory of coupled lines is revisited. Design and development procedure of the stripline based 3dB tandem hybrid coupler is presented. The coupled stripline structure is designed and High Frequency Structure Simulator(HFSS) is used for accurate modelling and optimization of parameters. To achieve the wider spacing between the coupled lines two 8.34dB quarter wavelength coupled lines are used in tandem for overall 3dB coupling. To demonstrate the design process, a prototype tandem coupler rated for 2.5kW at 91.2MHz, has been design, fabricated and tasted. Frequency and power handling capability of the prototype are selected in such a way that it may be useful for various applications in plasma related experiments. To get the optimum performance a novel patch compensation technique is explored, explained, applied and incorporated in development of the 3dB tandem hybrid coupler. This newly explored patch compensation technique is found substantially effective in improving the overall performance in terms of return loss and isolation. This prototype has successfully demonstrated the process for indigenous development of 2.5kW, 3dB hybrid coupler at any required frequency from 20 to 120MHz. The concept, design and development procedure have imparted sufficient experience that will be useful while making 3dB hybrid coupler of more than 100kW power rating at the various frequencies within the

range of 20 to 120MHz.

Chapter 4 has been devoted to the comprehensive review of previous works in the area of broadband development of the coupled lines and its applicability in the development of high power 3dB hybrid coupler. Broadband bandwidth can be achieved by means of cascading several quarter-wavelength elements in a particular manner, called of multi-element coupler [18–25]. In multi-element coupled lines, junctions are usually employed to connect the two different coupled elements which give rise to the undesirable reactance called junction discontinuity effect [26–30]. These effects are found prominent in the high power coupled lines for HF and VHF applications because of its large structural dimensions. In an earlier work, a theoretical approach for designing of symmetrical TEM mode multi-element coupled lines was presented [20]. The theory leads to explicit expression for essential parameters i.e. even and odd mode impedances for the elements. The theory holds good for a perfect design and yields ideal performance. However, junction discontinuity effect is not taken into consideration in this theory.
A generalized theoretical procedure has been developed where analytical equivalence of junction discontinuity effect is derived for the known parameters and verified using HFSS simulation. For the compensation of junction discontinuity effect, a modified theory is developed and applied in the designing of 3-elements 8.34±0.2dB section. The effect of junction discontinuity is found successfully compensated for the desired performance. Here the modified theory has also been extended for the n-element coupled lines section.

In chapter 5 design and development process of a 200kW, 3dB tandem hybrid coupler for 38 to 112MHz frequency range is presented. The two 8.34dB coupled lines section are connected in tandem to get 3dB coupling. To achieve the desired frequency band of 38 to 112MHz, each of 8.34$\pm$0.1dB coupled lines sections are designed with 3-coupled elements. The physical dimensions of each of the elements are calculated and configured for the design of proposed 3dB hybrid coupler. Designed model is simulated with HFSS, where results are found significantly deviated from the theoretical prediction due to junction discontinuity effect. The modified theory for the compensation of the junction discontinuity effect is revisited and compensation is applied in designed model. The fabrication of designed model is executed where broad side coupled strip-line conductors are arranged in a particular configuration and placed in the grounded metallic enclosure. Air as dielectric is used to minimize the insertion loss. The central conductors are supported with the acrylic studs. The dielectric stud induces the capacitive discontinuity. The discontinuities effect due to the junction and supporting studs are compensated using the modified theory. The fabricated model is characterized and tested. The results obtained are found in close agreement with the calculated values that take into account the effect of the discontinuities. The experience with concept, design and development procedure have imparted sufficient knowledge that can be utilize in the development of the broadband hybrid couplers for the high power applications in HF, VHF and UHF band.

Chapter 6 presents the upgradation of previous design for 1.5MW power handling capability in range of 30 to 96MHz. The presented work has imparted the new concept and sufficient research experience for the designing of the high power multi-element coupled lines. The peak power handling capability of coupled stripline transmission line is decided by the strip-width, spacing between the stripline conductors and ground plate which has maximum permissible limit. Up to the certain limit, TE and TM modes can propagate in stripline at higher frequencies and one wants to avoid these modes because of mode conversion from TEM to TE or TM. System experiences the sudden increase of the return loss and isolation while increasing the spacing and strip-width beyond the permissible limit. To increase the maximum permissible limit for the upgradation of the previous design for the desired power handling capability, a novel concept has been developed and applied in the design of the proposed 1.5MW hybrid coupler. The structural model of the hybrid coupler is simulated with HFSS and the results are found in close agreement to the calculated values. The power handling capability of the designed model has been demonstrated by using HFSS simulation.

In chapter 7, the result of the entire thesis are summarized and future work is outlined.

2

Stripline and its applicability in high power rf systems

2.1 Introduction

This chapter deals with the transmission lines and their applicability in development of the broadband high power 3dB hybrid coupler. Main intention is to give a discussion in sufficient depth for choosing the configuration, types and parameters of the transmission line structure as per desired specification and use. Generally, circular rigid coaxial transmission line is used for high power handling applications [14, 15]. However, similar configuration of stripline is found suitable for broadband coupled line design. This chapter covers the basic theory of coupled lines and related design procedures also.

2.2 Review of transmission line theory

The rf transmission line theory assumes that the physical dimensions of a network are the fraction of a wavelength. Whereas, a transmission line is a distributed-parameter network where voltage and current vary in magnitude and phase over the length. The transmission line for TEM wave propagation always have at least two conductors. Lumped equivalent of the two wire transmission line is shown in Fig.2.1.(a) and (b), where R, L, C and G are defined as series resistance, series inductance shunt conductance and shunt capacitance per unit length respectively [31, 32]. The TEM wave has a uniquely defined voltage and current which can be obtain by the given equations.

$$\frac{dV(z)}{dz} = -(R + j\omega L)I(z) \tag{2.1a}$$
$$\frac{dI(z)}{dz} = -(G + j\omega C)V(z) \tag{2.1b}$$
$$\frac{d^2V(z)}{dz^2} - \gamma^2 V(z) = 0 \tag{2.1c}$$
$$\frac{d^2I(z)}{dz^2} - \gamma^2 I(z) = 0 \tag{2.1d}$$
$$\gamma = \alpha + j\beta = \sqrt{(R + j\omega L)(G + j\omega C)} \tag{2.1e}$$

These equations represent the travelling wave in z-direction which has solutions

$$V(z) = V^+ e^{-\gamma z} + V^- e^{\gamma z} \tag{2.2a}$$

$$I(z) = I^+ e^{-\gamma z} + I^- e^{\gamma z} \tag{2.2b}$$

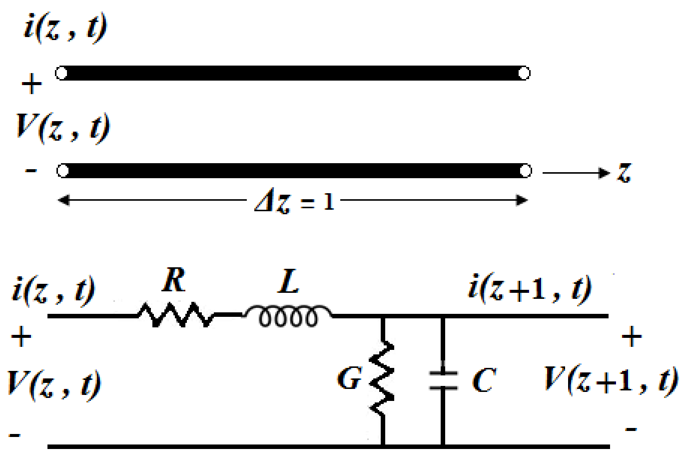

Figure 2.1: Transmission line lumped equivalent circuit.

Where the $e^{-\gamma z}$ and $e^{\gamma z}$ represent wave propagation in $+z$ and $-z$ directions respectively. In time domen this can be written as,

$$V(z,t) = V^{+}e^{-\alpha z}\cos(\omega t - \beta z) + V^{-}e^{\alpha z}\cos(\omega t + \beta z) \tag{2.3a}$$

$$I(z,t) = I^{+}e^{-\alpha z}\cos(\omega t - \beta z) + I^{-}e^{\alpha z}\cos(\omega t + \beta z) \tag{2.3b}$$

where α and β are the attenuation and propagation constant respectively. Applying equation (2.1a) to the voltage of (2.1b) gives the online current

$$I(z) = \frac{\gamma}{R + j\omega L}[V^{+}e^{-\gamma z} + V^{-}e^{\gamma z}]$$

compairing with (2.2b) shows that characteristic impedance, Z_0 can be defined as

$$Z_0 = \frac{R + j\omega L}{\gamma} = \sqrt{\frac{R + j\omega L}{G + j\omega C}} \tag{2.4}$$

We find that wavelength λ and phase velocity v_p can be given as

$$\lambda = \frac{2\pi}{\beta} \tag{2.5a}$$

$$v_p = \frac{\omega}{\beta} \tag{2.5b}$$

This is seen that the propagation constant and characteristic impedance are complex for a general transmission line including loss effects. In many practical cases loss of the line can be neglected, resulting in simplification. Substituting $R = G = 0$ gives,

$$\begin{aligned} \gamma &= \omega\sqrt{LC} \\ \text{or} \quad \beta &= \omega\sqrt{LC} && (2.6a) \\ \alpha &= 0 && (2.6b) \\ Z_0 &= \sqrt{\frac{L}{C}} && (2.6c) \\ \lambda &= \frac{2\pi}{\omega\sqrt{LC}} && (2.6d) \\ v_p &= \sqrt{\frac{1}{LC}} && (2.6e) \end{aligned}$$

2.2.1 Choice of Transmission lines

In coaxial transmission line electromagnetic field is confined to the region between the inner and outer conductors. For high power rf, air-spaced lines are used to minimize the losses but dielectric spacers are needed to support the inner conductor. Coaxial transmission line supports TEM mode which has no cut-off frequency. Thus, it may be used from very low to VHF frequency. Here, it is possible to define a voltage and a current uniquely for any given cross-section. The transmission line

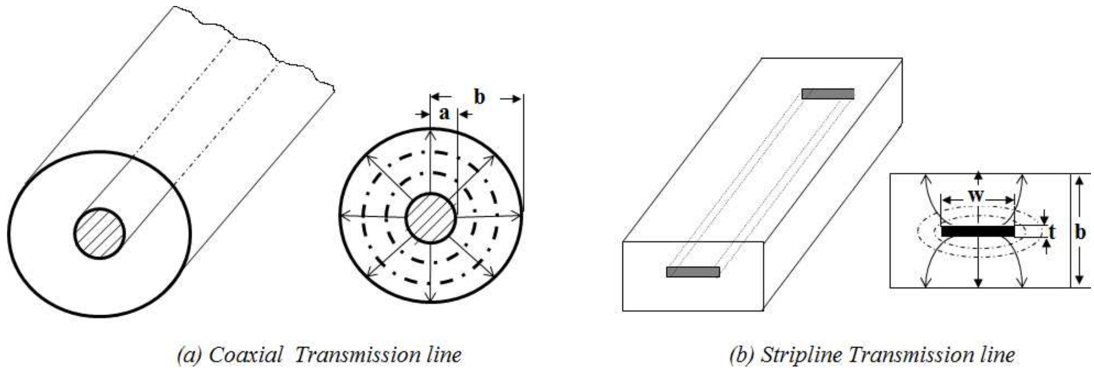

Figure 2.2: Schematic of the transmission line.

is characterized by the capacitance and inductance distributed along the length. Although, coaxial transmission line it has very good power handling capability and is not useful in the development of the complex design that is required in broadband device because of it's non-planar structural configuration. Therefore, it is necessary to look for transmission line compatible for making the complex structural of broadband hybrid coupler. The answer was realized in the form of planar stripline type transmission lines. The first planar transmission line called the strip transmission line was proposed by Barrett and Barnes [33] as early as 1951. The structure consists of a thin strip conductor surrounded by the rectangular outer conductor. Although it is similar to the coaxial transmission line; found compact in size, simpler geometry, easily fabricable and suitable for the development of the broadband device. Schematic of the coaxial and stripline is shown in Fig.2.2.(a) and (b) However, many other more reliable configurations of the planar transmission line had been proposed from the year of 1952 to 1970 like microstrip line, slotline, suspended stripline, suspended microstrip, inverted microstrip, coplanar wave guide and co-planar strips [34, 35]. Unlike the stripline these transmission lines require the a dielectric substrate of very high permittivity to confine the electro-magnetic field near the strip conductor. These transmission lines are limited to the low power applications. Therefore, stripline based 3dB hybrid coupler concept is selected for simple design, cost effectiveness and ease of fabrication.

2.2.2 Stripline

The dominant mode of propagation in stripline is the transverse electromagnetic (TEM) mode, in which the electric field is radial and the magnetic field azimuthal. The phase velocity v_p, propagation constant β and Z_0 characteristic impedance of the TEM wave are given by

$$v_p = \frac{c}{\sqrt{\epsilon_r}} \tag{2.7a}$$

$$\beta = \frac{\omega}{v_p} = \omega\sqrt{\mu\epsilon} \tag{2.7b}$$

$$Z_0 = \sqrt{\frac{L}{C}} = \frac{\sqrt{LC}}{C} = \frac{v_p}{C} \tag{2.7c}$$

where c and ϵ_r are velocity of light in free space and relative permittivity of the dielectric between the conductors. L and C are the capacitance and inductance per unit length of the line. Some of the ways to evaluate C.

1. Conformal mapping techniques,

2. Mode matching techniques,

3. Finite difference and finite element solutions.

The resulting solutions involve complicated functions; hence for practical computations simple formule are used. The two well known approximations are given as,

- *Hawe's Approximation Formula [36]:*

$$Z0 = \frac{30\pi}{\epsilon_r}\left(\frac{b}{w_e + 0.441b}\right) \tag{2.8}$$

where w_e is the effective width of the center conductor

$$\frac{w_e}{b} = \frac{w}{b} - \begin{bmatrix} 0 & \text{for } \frac{w}{b} \geq 0.35 \\ \left(0.35 - \frac{w}{b}\right)^2 & \text{for} \frac{w}{b} \leq 0.35 \end{bmatrix} \tag{2.9}$$

These formulae assume thickness $t = 0$. Their accuracy is 1% of the exact results. We see that as w increases, Z_0 decreases. While designing stripline circuits, we usually need w, whereas Z_0, b and ϵ_r are given. We can use the formulae below for this purpose,

$$\frac{w}{b} = \begin{bmatrix} x & \text{for } Z_0\sqrt{\epsilon_r} \leq 120 \\ \left(0.85 - \sqrt{0.6 - x}\right) & \text{for} Z_0\sqrt{\epsilon_r} \geq 120 \end{bmatrix} \tag{2.10}$$

where $$x = \tfrac{30\pi}{Z_0\sqrt{\epsilon_r}} - 0.441$$

Attenuation in transmission line is mainly caused due to dielectric and conductor i.e. termed as α_d and α_c respectively. Thus the total attenuation constant $\alpha = \alpha_c + \alpha_d$. As α_d is of the same form to that for the other TEM lines and is given by

$$\alpha_d = \frac{\beta \tan\delta}{2} \quad \text{Np/m(TEM waves)}, \tag{2.11}$$

Where $\tan\delta$ is known as dielectric loss tangent [32].

The attenuation due to conductor losses, α_c can be calculated by proper perturbation technique. An appropriate result for the α_c is,

$$\alpha_c = \begin{bmatrix} \dfrac{2.7\times 10^{-3} R_s \epsilon_r Z_0}{30\pi(b-t)} A & \text{for } Z_0\sqrt{\epsilon_r} \leq 120 \\ \dfrac{0.16 R_s}{Z_0 b} B & \text{for} Z_0\sqrt{\epsilon_r} \geq 120 \end{bmatrix} \tag{2.12}$$

with

$$\begin{aligned} A &= 1 + \frac{2w}{b-t} + \frac{1}{\pi}\frac{b+t}{b-t} ln\left(\frac{2b-t}{t}\right), \\ B &= 1 + \frac{b}{(0.5w+0.7t)}\left(0.5 + \frac{0.414t}{w} + \frac{1}{2\pi} ln\frac{4\pi w}{t}\right) \end{aligned}$$

where t is thickness of the strip

- *Collin's Approximate Formula [37]:*

$$Z_0 = \begin{bmatrix} \dfrac{\pi\eta_0}{8\sqrt{\epsilon_r}\left(ln2 + \pi\frac{2}{2b}\right)} & \text{for } w \geq 0.2b \\ \dfrac{\eta_0}{2\pi\sqrt{\epsilon_r}} \ln\left(\dfrac{8b}{\pi w}\right) & \text{for} w \leq 0.2b \end{bmatrix} \tag{2.13}$$

If we denote the attenuation constant due to the center conductor as α_{c1} and the attenuation constant due to the ground planes as α_{c2}, then we have the following approximate formulas:

$$\begin{aligned} \alpha_{c1} &= \frac{R_s\sqrt{\epsilon_r}}{b\eta_0} \frac{\ln\left(\frac{4b}{\pi T_e}\right)\frac{\pi w}{2b}}{ln2 + \frac{\pi w}{2b}} && \text{for } w \geq 0.2b \\ \alpha_{c2} &= \frac{\pi R_s\sqrt{\epsilon_r} w}{4\eta_0 b^2\left(\ln 2 + \frac{\pi w}{2b}\right)} && \text{for } w \geq 0.2b \\ \alpha_{c1} &= \frac{2R_s\sqrt{\epsilon_r}\ln\left(\frac{4\pi}{T_e}\right)}{\pi\eta_0 w \ln\frac{8b}{\pi w}} && \text{for } w \leq 0.2b \\ \alpha_{c2} &= \frac{R_s\sqrt{\epsilon_r}}{\eta_0\left(\frac{8\pi}{w}\right)} && \text{for } w \leq 0.2b \end{aligned}$$

Where $T_e = e^{\pi/2}\sqrt{\frac{4wt}{\pi}}$ and $R_s = \sqrt{\frac{\omega\mu}{2\sigma}}$

Both of the formulae gives the approximately equal results. By using these formule one can calculate dimensions of the stripline for the given impedance.

2.2.3 Power handling capability of stripline

The peak power handling capability of the stripline like any other transmission line is limited by dielectric breakdown whereas an increase in the temperature due to conductor and dielectric losses limit the average power rating.

Peak power handling capability

The calculation of the peak power handling capability of the stripline depends on the maximum voltage that can be applied without causing dielectric breakdown. If Z_0 is the characteristic impedance of the stripline and V_0 is the maximum voltage that line can withstand, the maximum peak power P_p is given by

$$P_p = \frac{V_0^2}{2Z_0}. \tag{2.14}$$

The separation between the inner to ground conductor can support higher voltage. At the atmospheric temperature and pressure the breakdown strength of dry air is approximately 30.0kV/cm [16]. Thus the maximum electric field on the surface of the strip conductors should be lesser than this value. This has no margin of safety and therefore allowances must be made for changes with altitude, humidity and presence of dust particles in the air.

Average Power Handling Capability

Average power handling capability of stripline is determined by the temperature rise in the strip conductor and homogeneous dielectric losses. The parameters that play important role in calculation of average power handling capability are given by [38, 39],

1. Transmission line losses
2. The thermal conductivity of the dielectric medium.
3. Surface area of the dielectric strip conductor
4. Maximum allowable temperature of the stripline structure.
5. Ambient temperature.

A loss of electromagnetic power in the stripline conductor and dielectric medium generates heat in the stripline. Due to the good conductivity of the strip metal, heat generation is uniformely distributed along the width of the conductor. Because the ground plane of the stripline configuration is held at ambient temperature, heat flows from the strip conductor to the ground plane. The heat flow can be calculated by considering the analogous electric field distribution [40].
The temperature rise ΔT of inner conductor with respect to the outer conductor can be determined by the following relation.

$$\Delta T = \frac{P_c + P_d}{G_t} \tag{2.15}$$

Where, P_c and P_d represent the dissipation per unit length of the line due to the losses in inner conductor and dielectric respectively, and G_t represent the thermal conductance of the strip conductor. The P_c, P_d and G_t can be expressed as,

$$P_c = 2\alpha_c P_T \tag{2.16a}$$

$$P_d = 2\alpha_d P_T \tag{2.16b}$$

$$G_t = \frac{120\pi g}{Z_0\sqrt{\epsilon_r}} \tag{2.16c}$$

Where, P_T incident power in watts, α_c and α_d are loss coefficients of the conductor and dielectric(neper/perunit-length), g is thermal conductivity of dielectric medium and Z is characteristic impedance of the stripline. Substituting these in (2.15),

$$\Delta T = \frac{(\alpha_c + \alpha_d)Z_0\sqrt{\epsilon_r}P_T}{60\pi g} {}^\circ C \tag{2.17}$$

That means, the per one watt of incident power temperature rise $\Delta T_{perwatt}$ is,

$$\Delta T_{perwatt} = \frac{(\alpha_c + \alpha_d)Z_0\sqrt{\epsilon_r}}{60\pi g} {}^\circ C/W \tag{2.18}$$

- **Maximum average power handling capability:** A stripline can handle the maximum average power, P_{av} that a stripline can handle with rise of temperature from T_{amb} to T_{max} is given by [40]

$$P_{av} = \frac{T_{max} - T_{amb}}{\Delta T_{perwatt}} \tag{2.19}$$

where ΔT denotes rise in temperature per watt, T_{amb} is temperature of the outer conductor and T_{max} is the maximum operating temperature. The maximum operating allowable temperature of the stripline circuits is limited due to change of substrate properties with temperature and change of physical dimensions with temperature. The maximum operating temperature of a stripline circuit to be the one at which its electrical and physical characteristics within the acceptance limits. For Example, the maximum temperature for polystyrene is known to be $100°C$. So T_{max} is limited for $100°C$ in this case. Hence maximum allowable temperature can be safely taken as $100°C$ for average power handling calculation.

Example A cross sectional view of the copper material and air spaced, 50Ω stripline is shown in Fig.2.2. Structural parameters are given as, strip width $w = 44mm$, strip thickness $t = 3.0mm$, spacing of the ground plane $b = 50mm$. Estimate the average and maximum power handling capability of the stripline at 100MHz, where maximum allowable operating temperature is $100°C$ i.e. 65°C above from ambient *Solution*

For copper, $\sigma = 5.813 \times 10^7$ s/m, magnetic permeability of air $\mu = 4\pi \times 10^{-7}$

$$
\begin{aligned}
R_s &= \sqrt{\frac{\mu\omega}{2\sigma}} = 0.0.00261 \\
A &= 1 + \frac{2w}{b-t} + \frac{1}{\pi}\frac{b+t}{b-t} ln\left(\frac{2b-t}{t}\right) = 4.12 \\
\alpha_c &= \frac{2.7 \times 10^{-3} R_s \epsilon_r Z_0}{30\pi(b-t)} A = 0.000327 \text{ Nepers/meter} \\
\alpha_d &= 0 \text{ for air dielectric} \\
\Delta T &= \frac{(\alpha_c + \alpha_d) Z\sqrt{\epsilon_r}}{60\pi g} = 0.00542498°C/W \\
P_{av} &= \frac{(T_{max} - T_{amb})}{\Delta T} = \frac{50-35}{0.00131672} = 11981.6 \approx 12.0kW
\end{aligned}
$$

It means that on rise of 65° temperature stripline can withstand the 12kW rf average power.

It must be remembered that this figure provides no margin of safety and that allowances must be made for changes with altitude, strip surface roughness, impurity of copper material and condition of of medium (this can be defined terms of moisture content, dust particle etc) [41, 42]. The α_c in term of surface roughness is given as,

$$\alpha_c' = \alpha_c[1 + (2/\pi)\tan^{-1} 1.4(\delta_r/\delta)^2] \tag{2.20}$$

Where α_c' is new value of attenuation coefficient after considering the surface roughness δ_r.

2.3 Review of the theory of the coupled lines

In 1954, Oliver [9] and Firestone [43] showed that the natural electric and magnetic coupling between pair of TEM transmission line produces directional coupling. Specifically, a wave propagating along one line induces a wave on the other line that propagates in the opposite direction. The TEM mode quarter-wave coupled transmission lines coupler is shown schematically in Fig.2.3. The coupler has the following properties, when a rf source is connected to Port 1:

1. There is transfer of power from Port 1 to Port 2.
2. There is transfer of power from Port 1 to Port 3.
3. There is no transfer of power from Port 1 to Port 4.
4. There is no reflected wave out of Port 1.
5. The two outputs at Ports 2 and 3 differ in phase by 90 degrees.

Cross sectional view of the various coupled-pair are shown in Fig.2.4. Structural configuration of the coupled lines can be selected on the basis of the coupling

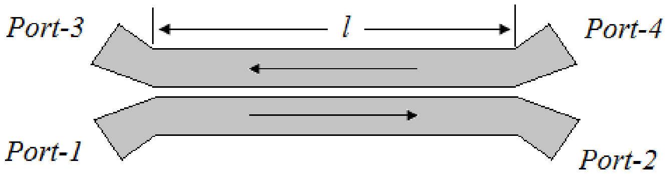

Figure 2.3: Schematic of the coupled stripline pair

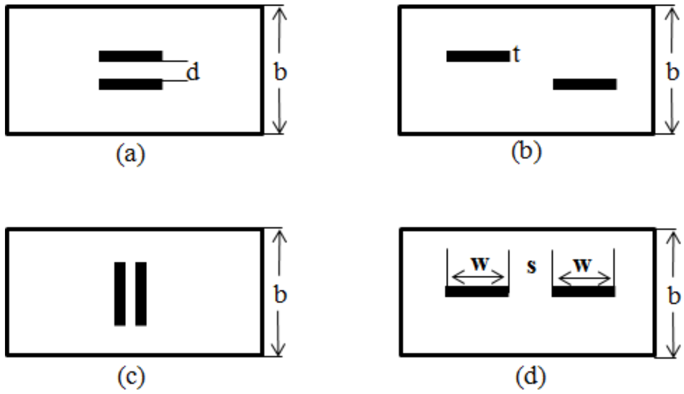

Figure 2.4: Cross-sectional views of four widely used TEM coupled line pair.

values. The configuration shown in part (a) and (c) is used if tight coupling (6dB or grater) is required where part (a) is often used in the design of 3dB couplers. For the loose coupling, coplanar stripline arrangement shown in part (b) and (d) are most common. The coupled lines shown in Fig.2.4, consist of three conductor and represent the two transmission lines with common ground. An arbitrary excitation of the coupled lines can be treated as a superposition of appropriate amplitude of even and odd mode [32]. In even mode, currents in strip conductor are equal in amplitude and same in direction, and in odd mode, where currents in strip conductor are equal in amplitude but opposite in direction. The electric and magnetic field for these two cases are sketched in Fig.2.5. For the even mode, the electric field has even symmetry about the center line and no current flows between the two strip conductors. This leads the equivalent circuit shown in Fig.2.5(b), where C_{12} is effectively open-circuited. The effective capacitance of either line to ground for the even mode is

$$C_e = C_{11} = C_{22} \tag{2.21}$$

assuming that the two strip conductor are identical in size and location.

$$Z_{0e} = \sqrt{\frac{L}{C_e}} = \frac{1}{v_p C_e} \tag{2.22}$$

For the odd mode, the electric field lines have an symmetry about the center line and a voltage null exists between two strip conductors. We can imagine this as a ground plane through the middle of C_{12}, which leads the equivalent circuit as shown in Fig.2.5(b). In case effective capacitance between either strip conductor and ground is

$$C_o = C_{11} + 2C_{12} = C_{22} + 2C_{12}, \tag{2.23}$$

and characteristic impedance for the odd mode is

$$Z_{0o} = \frac{1}{v_p C_o}. \tag{2.24}$$

In words, Z_{0e} or Z_{0o} is the characteristic impedance of one strip conductors relative to ground when the coupled lines operate in even or odd mode respectively. The overall characteristic impedance of the coupled lines is given by

$$Z_0 = \sqrt{Z_{0e} Z_{0o}} \tag{2.25}$$

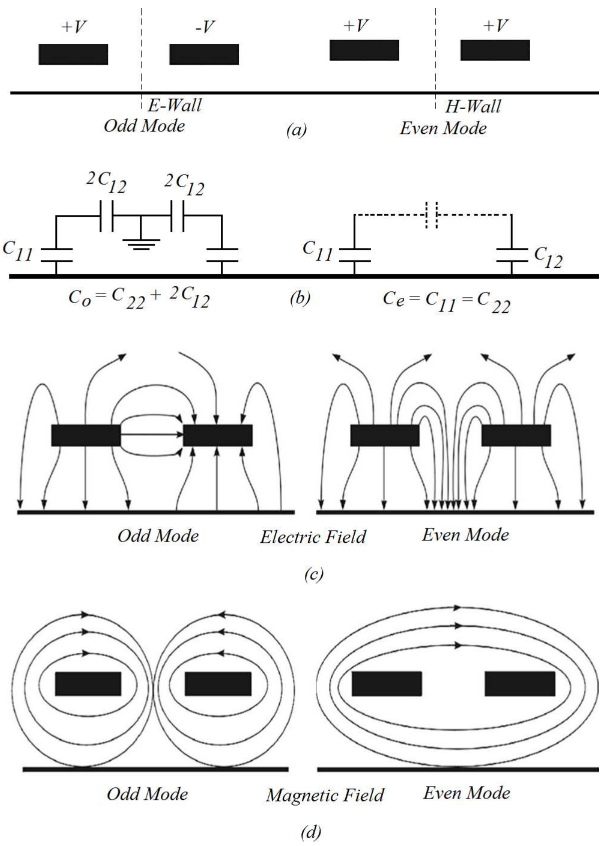

Figure 2.5: Definition of the even-odd mode theory of coupled stripline (a)Even and odd mode excitations (b)Lumped equivalent circuit for the even and odd mode (c)Electric field lines for even and odd mode (d)Magnetic field lines for even and odd mode.

Coupling coefficient i.e. C of the coupled lines depends on the even and odd mode impedance values that is given by

$$C = \frac{Z_{0e} - Z_{0o}}{Z_{0e} + Z_{0o}} \tag{2.26}$$

From (2.25) and (2.26), Z_{0e} and Z_{0o} also can be expressed as

$$Z_{0e} = Z_0\sqrt{\frac{1+C_v}{1-C_v}}, \quad Z_{0o} = Z_0\sqrt{\frac{1-C_v}{1+C_v}} \tag{2.28}$$

2.3.1 Multi-element coupled lines coupler

Single quarter wavelength coupled line based hybrid coupler works in narrow frequency band and has limited use. The broadband bandwidth can be achieved by means of cascading several quarter-wavelength coupled elements in a certain configuration called multi-element coupler.

The total voltage at coupled port of the cascaded coupler in Fig.2.6 can be expressed as,

$$V_3 = 2jV_1 \sin\theta e^{-jN\theta}\left[C_1\cos(N-1)\theta + C_2\cos(N-3)\theta + ...\frac{1}{2}C_M\right], \tag{2.29}$$

where $M = (N+1)/2$. In earlier studies, there are many theoretical procedures are presented for calculation of coupling coefficient [18,20–22]. Using these theories one can calculate the appropriate values of the coupling coefficient $(C_1, C_2, C_3.......C_N)$ for the desired coupling response of broadband coupler. In multi-element coupler multi-octave bandwidth can be achieved but coupling level must be low. Because of the larger electrical length it is more critical to have equal even and odd mode phase velocities than in single-section coupler. This usually means that stripline

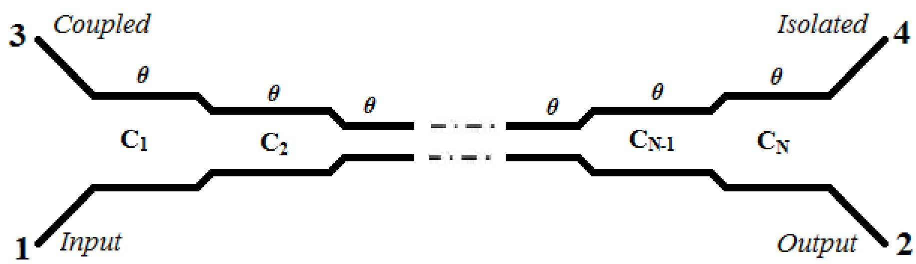

Figure 2.6: N-element coupled lines coupler.

is preferred medium for such coupler. Mismatched phase velocities, junction discontinuities, load mismatches and fabrication tolerance degrade the coupling performance of the coupler. These effects become prominent as the size of the system increases due to high power application. Alleviation of all the above problems from the coupled stripline and development stripline based 3dB high power hybrid coupler is the motivation of the present research work.

3

Design and development of 3dB patch compensated tandem hybrid coupler

3.1 Introduction

In a typical ICRH system, few milliwatts of cwrf with desired modulation and pulsing is multistage amplified to high power rf, which is coupled into the tokamak with the help of two or more transmission lines. Output from the intermediate 2kW rated pre pre-driver stage of the multistage amplifier may be divided to drive two amplifier chains of high power output of 100kW onwards each. These outputs can drive two antennae in the known phase or can be combined to drive one antenna whereas rf power output from one amplifier chain is not sufficient. Sometimes, the rf power output of few MW is divided to drive two antennae that are arranged in a certain configuration.

A 3dB hybrid coupler can be used as power combiner, power divider or to protect the rf source by coupling of reflected power to the isolated port. This is an integral part of the rf systems like satellite communication, cellular, broadcast, defense, aerospace etc. It has several useful applications in the rf and plasma related experiments also. The rf and plasma related small experiments are carried out at various frequencies from 20 to 120MHz and up to 2.5kW. The 3dB hybrid coupler is required in some of the experiments to provide the rf power from one source to two electrodes in desired phase. Thus, it has become imperative to understand, design, optimize and indigenously develop the hybrid couplers for various plasma experiments in the frequency range of 20 to 120MHz.

Therefore, in the first step, the development of prototype 2.5kW 3dB hybrid coupler at 91.2±15MHz is proposed. This prototype is aimed mainly to create a process of indigenous fabrication of 2.5kW, 3dB hybrid coupler at any required frequency from 20 to 120MHz for plasma experiments etc. The concept, design and development procedure should also be applicable while making hybrid coupler of more than 100kW power rating at the various frequencies within the range of 20 to 120MHz.

In this chapter, design and development procedure of the stripline based 2.5kW, 91.2MHz 3dB tandem hybrid coupler is presented. The coupled stripline structure is designed and electromagnetic analysis software is used for accurate modelling and optimization of parameters. To achieve the wider spacing between the coupled lines, two 8.34dB quarter wavelength coupled lines are used in tandem for 3dB overall coupling. Frequency and power handling capability of the prototype are selected in such a way that it may be useful for the several applications in plasma related experiments.

Broadside TEM coupled strip-line structures are widely used in the designing of 3dB couplers due to simple design, cost effectiveness and ease of fabrication. Air dielectric is used to minimize the insertion and other losses. It renders the upgradation from prototype to high power application easier. TEM coupled strip-lines are well known for poor impedance matching and poor isolation due to discontinuities, fabrication tolerance constraints and theoretical approximations in strip-lines. To get the desired results these problems are to be compesated. In the broadside coupled strip-line couplers, capacitors are connected to the ground in shunt capacitive compensation technique [27–29]. Recently, Slawomir, *et al.* [30] have presented the technique to compensate parasitic reactance of the coupled lines by connecting the shunt capacitances to both coupled and signal lines.

The conventional methods for the compensation use lumped capacitors or shunt open stubs that have limitations with high power application. Commercially available high power lumped rf capacitors are large in size and lossy above 20MHz frequency. Connecting shunt capacitor in coupled line affects the coupling and therefore compensation will be needed in the coupling gap also. If open stubs are used, high electric field exists on edges that may result in arcing.

A novel patch compensation technique is explored, explained, applied and incorporated in development of a 3dB tandem hybrid coupler to get the optimum performance . This newly explored patch compensation technique is found substantially effective in improving the overall performance in terms of return loss and isolation. In this chapter, section-4.2 describes the concept, design and optimization of the hybrid coupler, section-4.3 explains the theory of patch compensation and section-4.4 illustrates the power handling capability of the hybrid coupler. The fabrication process is described in section-4.5 while test results are presented and discussed in section-4.7. Finally, conclusion on the hybrid coupler including novel patch compensation technique is drawn in section-4.8.

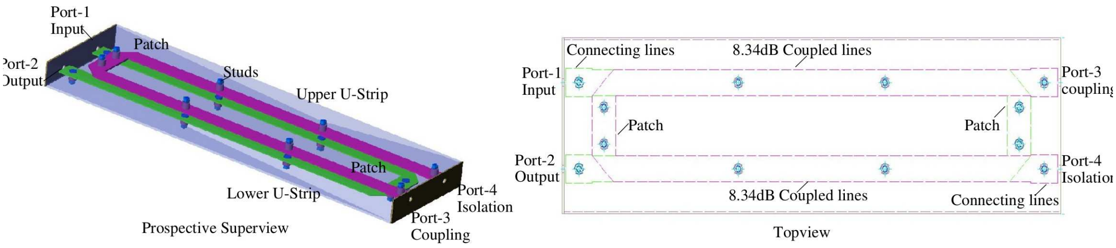

Figure 3.1: Proposed tandem 3dB hybrid coupler.

3.2 Concept, Design and Optimization

The tandem 3dB hybrid coupler is designed by connecting two 8.34dB coupled lines in tandem. It consists of two rectangular strip-line central conductors that are arranged one above the other and placed in the grounded metallic enclosure as shown in Fig. 3.1. The design can be divided into coupled and non-coupled sections. The electrical length of the coupled line is taken as quarter wavelength at desired frequency with Z_{ce} and Z_{co} as the characteristic impedances for even and odd modes respectively. Thus, the design and fabrication procedure may be generalized to implement at other frequencies also.

The width of coupled lines and the gap between them decides the degree of coupling. The non-coupled sections are constituted with connecting signal lines and the patch of Z_0 characteristic impedance. The patch is a small segment i.e. ($\leq \lambda/15$) of strip-line which is used to connect two 8.34dB coupled strip lines in tandem. Air within the grounded metallic enclosure is used as dielectric and the strip-line conductors are supported by teflon studs.

3.2.1 Coupled Strip-line Design

The schematic of 8.34dB broad sided coupled strip-lines of the tandem hybrid coupler is illustrated in Fig. 3.2. Here t, w, d and b represent the thickness,

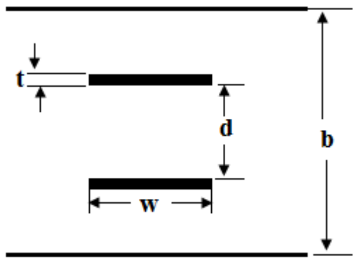

Figure 3.2: Schematic diagram Single 8.34dB Coupled strip-line.

width, spacing between coupled lines and the height of grounded box, respectively. An arbitrary excitation of coupled lines characteristic impedance Z_0 is treated as superposition of amplitudes of even and odd modes given by,

$$Z_{ce} = Z_0\sqrt{\frac{1+C_v}{1-C_v}}, \quad Z_{co} = Z_0\sqrt{\frac{1-C_v}{1+C_v}}, \text{ which gives } Z_0 = \sqrt{Z_{ce}Z_{co}}. \tag{3.1}$$

Here Z_{ce} and Z_{co} are the coupled lines characteristic impedances of coupled lines for even and odd modes, respectively. For 8.34dB coupled lines, the value of coupling coefficient C_v corresponds to 0.3828. For $Z_0 = 50\Omega$ impedance Z_{ce} is 78.84Ω and Z_{co} is 22.23Ω. In order to calculate Z_{ce} and Z_{co} we have used following equations which are given by Cohn [35]

$$
\begin{aligned}
Z_{ce} &= \frac{59.952\pi}{\sqrt{\epsilon_r}} \frac{K(k')}{K(k)}, \\
Z_{co} &= \frac{94.172\pi(d/b)}{\sqrt{\epsilon_r \tanh^{-1}(k)}}, \\
\text{where } k &= \left[1 - \left(\frac{0.5 \exp^{\pi\frac{K(k)}{K(k')}} - 1}{0.5 \exp^{\pi\frac{K(k)}{K(k')}} + 1}\right)^4\right]^{1/2} \quad \textit{and}
\end{aligned}
$$

$$
\frac{w}{b} = \frac{2}{\pi}\left[\tanh^{-1}\sqrt{\frac{\left(k-\frac{d}{b}\right)}{\left(1-k\frac{d}{b}\right)}} - (d/b)\tanh^{-1}\sqrt{\frac{\left(k-\frac{d}{b}\right)}{k\left(1-k\frac{d}{b}\right)}}\right], \tag{3.2}
$$

where $k' = \sqrt{1-k^2}$, $K(k')$ and $K(k)$ are the complete elliptic integrals of first kind. The value of $K(k')/K(k)$ can be found in Ref. [44] and references therein that gives Z_{ce} and Z_{co} for the specified value of d/b and w/b. Using $b = 5$cm in above equations, we get strip-width $w = 4.125$cm and $d = 2.475$cm. In Eqn.3.1, it can be seen that all design parameters are calculated in terms of ratio d/b and w/b. That means, w and d are dependent upon b that is calculated for the required power rating. The value of b as explained in section-IV is 5.0cm for the 2.5kW rated prototype. Therefore, the device can be upgraded in terms of power by increasing b, w and d as shown by Eqn.3.1.

3.2.2 Non Coupled Strip-line Design

With certain approximations, one can provide [44] the relationship of characteristic impedance with the shunt capacitances of homogeneous strip-line placed at arbitrary distance from the ground plane as shown in Fig. 3.3. The characteristic

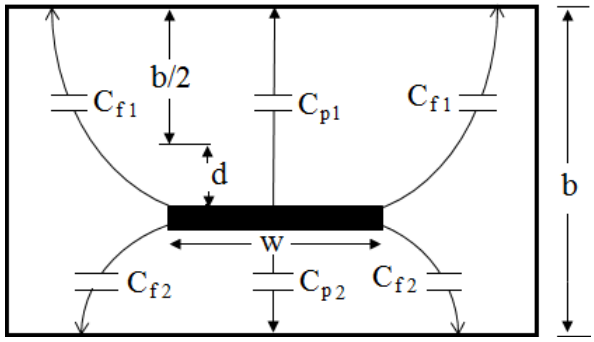

Figure 3.3: Strip-line with off-set rectangular strip.

impedance Z_0 is given as,

$$Z_0 = \frac{376.7\sqrt{\epsilon_r}}{C_t} \tag{3.3}$$

where ϵ_r is dielectric constant of the medium and C_t is total capacitance given by

$$C_t = C_{p1} + C_{p2} + 2C_{f1} + 2C_{f2}.$$

Note that C_{p1} is face capacitance on upper side, C_{p2} is face capacitance on lower side, C_{f1} is fringing capacitance on upper side and C_{f2} is fringing capacitance on lower side. These are expressed as.

$$C_{p1} = \epsilon_r \left(\frac{2\frac{w}{b-2d}}{1 - \frac{t}{b-2d}} \right), \tag{3.4}$$

$$C_{p2} = \epsilon_r \left(\frac{2\frac{w}{b+2d}}{1 - \frac{t}{b+2d}} \right), \tag{3.5}$$

$$C_{f1} = \frac{\epsilon_r}{\pi} \left[\frac{1}{1 - \frac{t}{b-2d}} \ln \left(\frac{1}{1 - \frac{t}{b-2d}} + 1 \right) - \left(\frac{1}{1 - \frac{t}{b-2d}} - 1 \right) \ln \left(\frac{1}{\left(1 - \frac{t}{b-2d}\right)^2} - 1 \right) \right], \tag{3.6}$$

$$C_{f2} = \frac{\epsilon_r}{\pi}\left[\frac{2}{1-\frac{t}{b+2d}}\ln\left(\frac{1}{1-\frac{t}{b+2d}}+1\right)-\left(\frac{1}{1-\frac{t}{b+2d}}-1\right)\ln\left(\frac{1}{(1-\frac{t}{b+2d})^2}-1\right)\right]. \tag{3.7}$$

Here, connecting lines are 0.8cm away from the center therefore $2d = 1.6$cm, $b = 50$cm, $Z_0 = 50\Omega$, $t = 0.3$cm and $\epsilon_r = 1$ give $w = 5.75$cm. These dimensions and the effect due to teflon studs are optimized by using HFSS software and performance has been calculated in term of S-parameters. The optimized design dimensions are shown in Fig.3.4. Using these dimensions, a tandem 3dB hybrid coupler has been

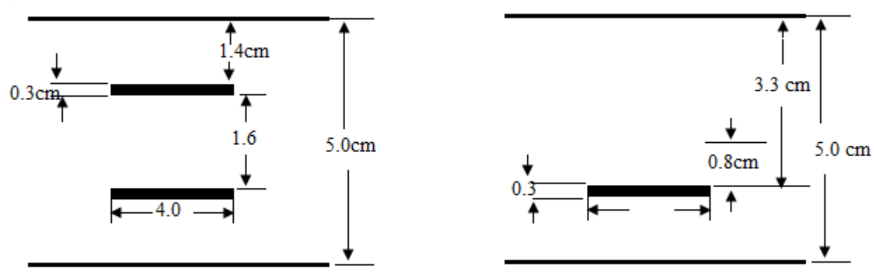

Figure 3.4: Final dimension of the coupled and non-coupled line sections.

fabricated and tasted with VNA. HFSS optimized design results and the measured S-parameters without compensation are shown in Fig.3.5, where stripline patch of length λ/m is used to connect the two 8.34dB coupled section. It can be seen that the measured values of return loss and isolation are inferior due to the fabrication tolerance constraints and theoretical approximations. Therefore, compensation is required for overall better performance. A novel idea of patch compensation technique has been explored as illustrated in the next section.

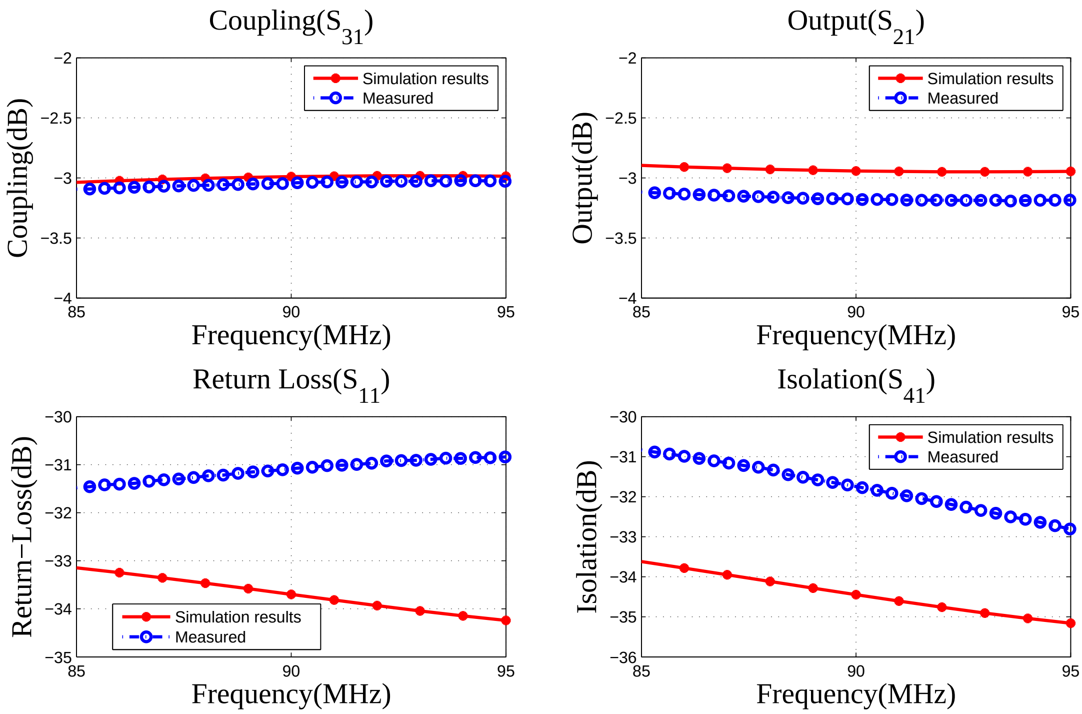

Figure 3.5: HFSS optimized design results and the measured S-parameters without compensation.

3.3 Patch Compensation Theory

In tandem 3dB hybrid coupler, patch is small segment of the stripline used to connect the two 8.34dB coupled lines. The terminology used with a U-shaped coupled strip-line and its equivalent circuit is shown in Fig.3.6. Here, Z_c and Y_c

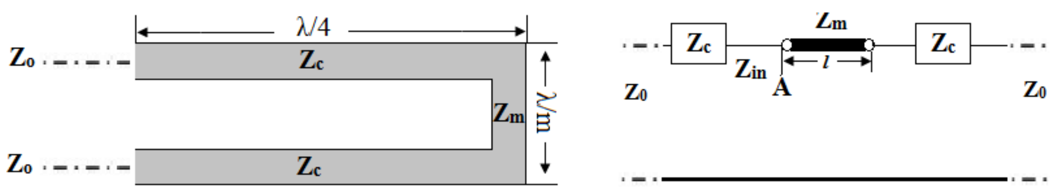

Figure 3.6: U-shaped coupled strip-line and equivalent circuit diagram.

are coupled lines impedance and admittance, Z_m and Y_m are patch impedance and admittance, Z_0 and Y_0 are the characteristic impedance and admittance of the system, Z_{in} and Y_{in} are transform impedance and admittance at point A, β is propagation constant and $l = \lambda/m$ is patch length. Admittance transformation equation is given as,

$$Y_{in} = Y_m \frac{Y_c + jY_m\beta l}{Y_m + jY_c\beta l}. \tag{3.8}$$

For the small section of high impedance i.e. $Y_c \leq 1$ and $\beta l << 1$, it implies $Y_c\beta l <<< 1$. This gives

$$Y_{in} = Y_c + jY_m\beta l. \tag{3.9}$$

From the above equation it can be seen that a small line section behaves like shunt capacitance of $Y_m\beta l/\omega$ Farad. Now, the resulting equivalent circuit of the single strip-line of the tandem coupler is as shown in Fig.3.7. The corresponding

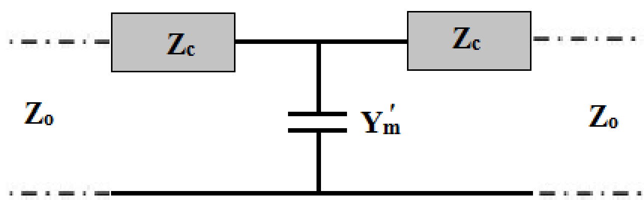

Figure 3.7: Equivalent circuit diagram of strip-line of tandem coupler.

transmission matrix is,

$$\begin{bmatrix} A & B \\ C & D \end{bmatrix} = \begin{bmatrix} 0 & jZ_c \\ \frac{j}{Z_c} & 0 \end{bmatrix} \begin{bmatrix} 1 & 0 \\ Y'_m & 1 \end{bmatrix} \begin{bmatrix} 0 & jZ_c \\ \frac{j}{Z_c} & 0 \end{bmatrix} = \begin{bmatrix} -1 & -{Z_c}^2 Y'_m \\ 0 & -1 \end{bmatrix}, \tag{3.10}$$

where patch is replaced with lumped admittance of $Y'_m = Y_m\beta l = Y_m\beta\lambda/m$.

The transmission matrix for matched U-shaped strip-line of length $(\lambda/2 + \lambda/m)$

can be written as

$$\begin{bmatrix} \cos(\pi+\beta\lambda/m) & jZ_0\sin(\pi+\beta\lambda/m) \\ j\sin(\pi+\beta\lambda/m)/Z_0 & \cos(\pi+\beta\lambda/m) \end{bmatrix} = \begin{bmatrix} -1 & jZ_0\beta\lambda/m \\ j\beta\lambda/mZ_0 & -1 \end{bmatrix}. \quad (3.11)$$

Comparing Eqn.(3.10) and (3.11) for $m \geq 15$ and by considering, $j\beta\lambda/mZ_0 << 1 \cong 0$, we get

$$Y_m = \frac{-JZ_0}{{Z_c}^2}. \quad (3.12)$$

This shows that Y_m is capacitive for $m > 15$. HFSS software is used to optimize hybrid coupler dimensions for port impedance of $Z_0 = 50\Omega$. On this basis, it is fabricated, tested with VNA and found that the port impedance is $Z_c = 56\Omega$. This deviation is found due to the discontinuities, fabrication tolerance constraints and theoretical approximations in strip-lines etc. From Eqn.(3.12), we get

$$|Y_m| = \frac{Z_0}{{Z_C}^2} = \frac{50}{56^2} = 0.0159 \;\; i.e. \;\; Z_m = 62.72\Omega. \quad (3.13)$$

Therefore, the patch impedance should be 62.72Ω for matching the coupled strip-lines to the port impedance. The proposed compensation technique improves the performance without affecting the coupling characteristic. The width of patches is calculated to be altered from 4.4cm to 3.6cm i.e. 50Ω to 62.72Ω impedance. As all ports are quarter wavelength away from patches, therefore $Z_m = 62.72\Omega$ of the patch is expected to match the coupled strip-line $Z_c = 56\Omega$ to the port impedance $Z_0 = 50\Omega$ by quarter wavelength transformer action.

Patch compensation also improves the isolation characteristic as presented here analytically. Using the Eqn.(3.13), we get

$$\begin{bmatrix} \bar{A} & \bar{B} \\ \bar{C} & \bar{D} \end{bmatrix} = \begin{bmatrix} -1 & -\bar{Z_c}^2\bar{Y}'_m \\ 0 & -1 \end{bmatrix}, \tag{3.14}$$

where $\bar{A}$, $\bar{B}$, $\bar{C}$ and $\bar{D}$ represent the normalized transmission matrices parameters. For the coupled lines impedance $\bar{Z_c} = \sqrt{\bar{Z}_{ce}\bar{Z}_{co}}$, where $\bar{Z}_{ce}$ and $\bar{Z}_{co}$ are the normalized even and odd mode impedances of the coupled section. In order to calculate transmission matrix parameters of the coupled lines for the even and odd mode which are given as.

$$\bar{Z}_{ce} = q\bar{Z}_c \text{ and } \bar{Z}_{co} = \frac{\bar{Z}_c}{q}, \text{ where } q = \sqrt{\frac{\bar{Z}_{ce}}{\bar{Z}_{co}}}. \tag{3.15}$$

By the application of Eqns.(3.14) and (3.15) even and odd mode transmission matrices for U shaped patched compensated strip-line are given as,

$$\begin{bmatrix} \bar{A}_e & \bar{B}_e \\ \bar{C}_e & \bar{D}_e \end{bmatrix} = \begin{bmatrix} -1 & -q^2\bar{Z_c}^2\bar{Y}'_m \\ 0 & -1 \end{bmatrix} \text{ and } \begin{bmatrix} \bar{A}_o & \bar{B}_o \\ \bar{C}_o & \bar{D}_o \end{bmatrix} = \begin{bmatrix} -1 & -\frac{\bar{Z_c}^2}{q^2}\bar{Y}'_m \\ 0 & -1 \end{bmatrix}. \tag{3.16}$$

The amplitude of the emerging power A_4 from the isolated port-4, is given as,

$$A_4 = \frac{1}{2}\left[T_{0e} - T_{0o}\right], \tag{3.17}$$

where T_{0e} and T_{0o} are the amplitudes of transmitted waves for the even and odd modes for two-port networks respectively. These are given as

$$T_{0e} = \frac{2}{\bar{A}_e + \bar{B}_e + \bar{C}_e + \bar{D}_e} \text{ and } T_{0o} = \frac{2}{\bar{A}_0 + \bar{B}_0 + \bar{C}_0 + \bar{D}_0}. \tag{3.18}$$

By using the Eqns.(3.16), (3.17) and (3.18) power coming at isolated port-4 of 3dB patch compensated tandem coupler is obtained as

$$A_{4c} = \frac{x(q^4-1)}{(2q^2+x)(q^2+2x)} \text{ where } x = \bar{Z}_c^2\bar{Y}_m\beta l. \tag{3.19}$$

Where A_{4c} is the amplitude of power that appears at isolated port-4. For the small patches $0 \leq \bar{Z}_c^2\bar{Y}_m\beta l \leq 1$, this means $0 \leq x \leq 1$, for all $\bar{Z}_c$ and $\bar{Y}_m$.
Before patch compensation, impedance of patches is taken as characteristic impedance ($\bar{Z}_0 = 1$). For the analysis of power emerging at isolated port-4 of uncompensated tandem coupler transmission matrix for the U-shaped strip-line can be written as,

$$\begin{bmatrix} \bar{A} & \bar{B} \\ \bar{C} & \bar{D} \end{bmatrix} = \begin{bmatrix} 0 & j\bar{Z}_c \\ j/\bar{Z}_c & 0 \end{bmatrix} \begin{bmatrix} \cos\beta l & j\sin\beta l \\ j/\sin\beta l & \cos\beta l \end{bmatrix} \begin{bmatrix} 0 & j\bar{Z}_c \\ j/\bar{Z}_c & 0 \end{bmatrix} = \begin{bmatrix} 0 & -jZ_c{}^2\sin\beta l \\ -j/(Z_c{}^2\sin\beta l) & 0 \end{bmatrix}. \tag{3.20}$$

For short length patches $\beta l \ll 1$ and therefore $\sin\beta l = \beta l$. By using Eqns.(3.17), (3.18) and (3.20) power emerging at port-4 of uncompensated coupler is derived as,

$$A_{4wc} = \frac{r^2(q^8-1)}{(q^4+r^2)(1+q^4r^2)} \text{ where } r = \bar{Z}_c{}^2\beta l, \tag{3.21}$$

Here, A_{4wc} is amplitude of power that appears at isolated port-4 of uncompensated coupler. For the small patches $0 \leq \bar{Z}_c{}^2\beta l \leq 1$; that means $0 \leq q \leq 1$, for all $\bar{Z}_c$.
From Eqn.(3.15), for 8.34dB coupled lines of the tandem coupler, q = 1.51. Using Eqns.(3.19) and (3.21), A_{4wc} and A_{4c} are plotted for $0 \leq q \leq 1$ and $0 \leq x \leq 1$ in Fig.3.8. From Fig.3.8, it is found that A_{4c} is less than A_{4wc} for the interval. It means that the isolation characteristic should also be effectively improved after compensation. It is well known that optimization of the lumped or distributed capacitors at the edges or in the center of the coupled region of the strip-line

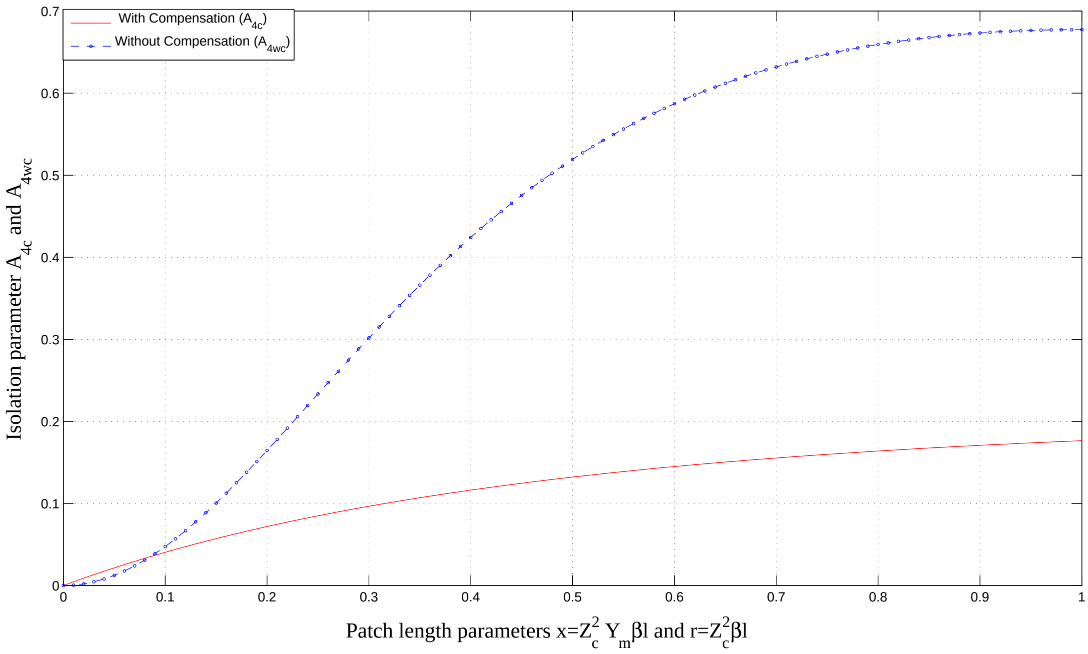

Figure 3.8: Analytic comparison of isolation of compensated and uncompensated hybrid coupler.

couplers improves the isolation characteristic. Patches behave as lumped capacitors and they are directly connected to the coupled lines of the tandem coupler. Therefore, isolation performance of the hybrid coupler is improved.

3.4 Estimation of Power Handling Capability

Power handling capability P_p of the designed 3dB Hybrid Coupler is limited by various losses and the peak voltage at strip conductor. Hybrid coupler uses air as dielectric with breakdown voltage rating of $3 \times 10^4 V_{dc}/cm$ or $1.47 \times 10^4 V_{rf(peak)}/cm$ [31]. In the presence of standing waves, this becomes $(1.47/2) \times 10^4 V_{rf(peak)}/cm$ i.e. equivalence ratio of 4.1 with respect to dc breakdown voltage. In this design, the hybrid coupler strip conductor clearance is $1.4cm$ from the ground. Therefore,

$$P_p = \frac{{V_{peak}}^2}{2Z_0} = 1.0588 \times 10^6 watt.$$

The teflon studs that hold strip conductor are tested for peak surface breakdown strength of 2kV_{dc} which is equivalent to 0.49k$V_{rf(peak)}$. This limits the hybrid coupler to the rating of 2.5kW because,

$$P_p = \frac{(4.9 \times 10^3)^2}{2 \times 50} = 2.5 \times 10^3 watt.$$

Average power handling capability (P_{av}) of the strip-line i.e. optimization of the dielectric loss and ohmic losses with the dissipation capability can be written as,

$$P_{av} = \frac{60\pi g\,(T_{max} - T_s)}{\Delta T\,(\alpha_{ic} - \alpha_{id})\, Z_0\sqrt{\epsilon_r}},$$

where T_s(strip-line temperature) = ambient 35°C,
T_{max}(maximum allowable operating temperature) = 45 °C,
g(thermal conductivity for air) = $0.0278 w/m.k$, $\quad \epsilon_r = 1$,

$$\alpha_{ic}(\text{conductor loss coefficient}) = \frac{2.7 \times 10^{-3} R_s \epsilon_r Z_0}{30\pi\,(b-t)}\left[1 + \frac{2w}{b-t} + \frac{(b+t)\,Z\sqrt{\epsilon_r}}{\pi\,(b-t)}\ln\left(\frac{2b-t}{t}\right)\right].$$

For R_s (skin resistance) = $2.4925 \times 10^3 \Omega/m$, w (strip width) = $0.044m$, b (ground conductor box height) = $0.05m$ and t (strip thickness) = $0.003m$, we get, ΔT=2.988×10^{-3}, $°C/w$, $\alpha_{ic} = 3.13 \times 10^{-4} Np/m$, and therefore, $P_{av} = 3.3kW$. The design of fabricated hybrid coupler was aimed at 2.5kW rating and the teflon studs comply with the same. Power handling capability of fabricated hybrid coupler may be extended up to 3.3kW by replacing studs of same rating.

3.5 Fabrication Process

Designed hybrid coupler is fabricated with two U-shaped 3mm thick copper strip-line conductors that are overlapping in opposite directions. The strip-widths of the coupled and non coupled sections are 4.0cm and 4.4cm respectively. Outer conductor rectangular box of dimensions $99.2 \times 26.4 \times 5.0$cm is fabricated with the aluminum sheet of thickness 0.3cm. A photograph of the fabricated hybrid coupler assembly is shown in Fig.3.9. Patch compensation is applied after testing the hybrid coupler with VNA.

Figure 3.9: Photograph of the fabricated hybrid coupler.

3.6 Results and Disscussion

In the present work, a hybrid coupler is designed and optimized with HFSS for coupling of -3 ± 0.2dB, output of -3 ± 0.2dB, return loss of less than 32dB and isolation of better than -32dB in the frequency range of 91.2 ± 15MHz. The same is for return loss of 34dB and isolation of -34dB at the center frequency 91.2MHz. Hybrid coupler is fabricated and tested with VNA. This is found providing coupling of -3 ± 0.2dB, output of -3 ± 0.2dB, return loss of less than 30.5dB and isolation of better than -30dB in the given frequency range. The same is found providing the return loss of 31dB and isolation of -32dB at the center frequency 91.2MHz. Comparison of measured values with the calculated parameters is shown in Fig.3.5. This implies that improvement is needed.

The proposed compensation technique is implemented in the designed and fabricated hybrid coupler. The modified i.e. patch compensated hybrid coupler is tested and found providing coupling of -3 ± 0.2dB, output of -3 ± 0.2dB, return loss of less than 32dB and isolation of better than -31dB in the given frequency range. The same is found providing the return loss of 40dB and isolation of -33dB at the center frequency 91.2MHz. Thus, the performance is observed greatly improved after compensation as shown in Fig.3.10.

In case of return loss, great improvement is observed at the center frequency as this compensation technique is frequency sensitive and uses the concept of quarter wavelength transformer matching whereas the isolation is improved uniformly within the given frequency range due to lumped capacitive behavior of the patches. The resulting coupling, output, return loss and isolation in the given frequency range implies 2.120W of heat dissipated for input power of 2.5kW i.e. $0.067°C/minute$ increase of the strip-line temperature at $35°C$ ambience. Estimated thermal equilibrium is found established at about $38°C$.

The cwrf high power test is conducted with the available 1kW rated source for eight hours without interruption. Schematic diagram of cwrf high power test setup and the resulting waveforms at the coupled and output port are shown in Fig.3.11 and Fig.3.12 respectively. Power meters connected with port 1, 2 and 3 give the actual power measurement. Directional coupler and the oscilloscope are connected to obtain sample of forward going power at the coupled and output ports. The performance confirms to VNA testing. Voltage withstanding level at each of the

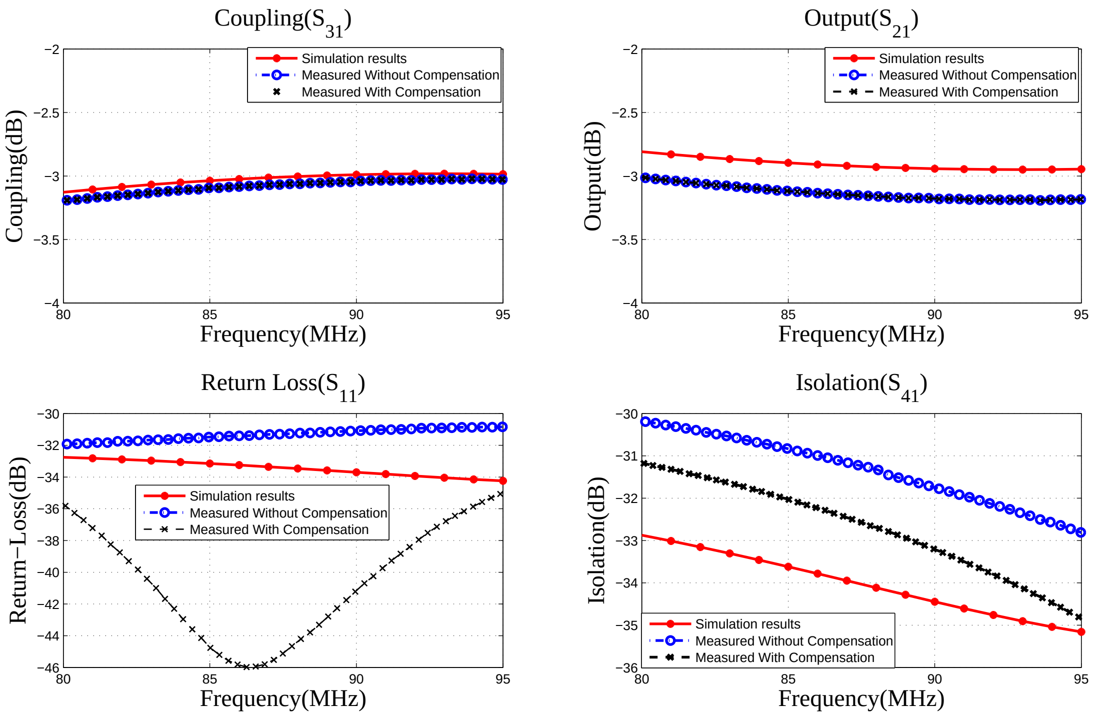

Figure 3.10: Comparison of HFSS optimized design results, the measured S-parameters without compensation and with compensation.

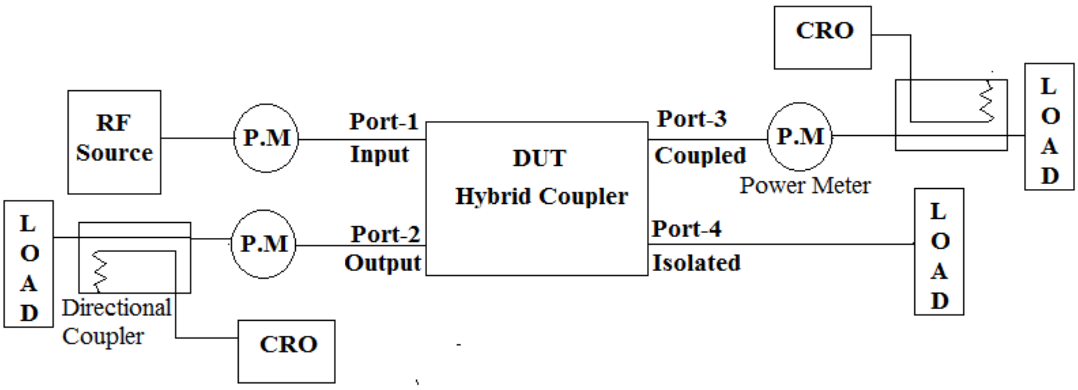

Figure 3.11: Schematic diagram of high power test setup.

ports and between the coupled lines is found 2kVdc as measured with a breakdown tester. This confirms the operational capability at 2.5kW of the patch compensated

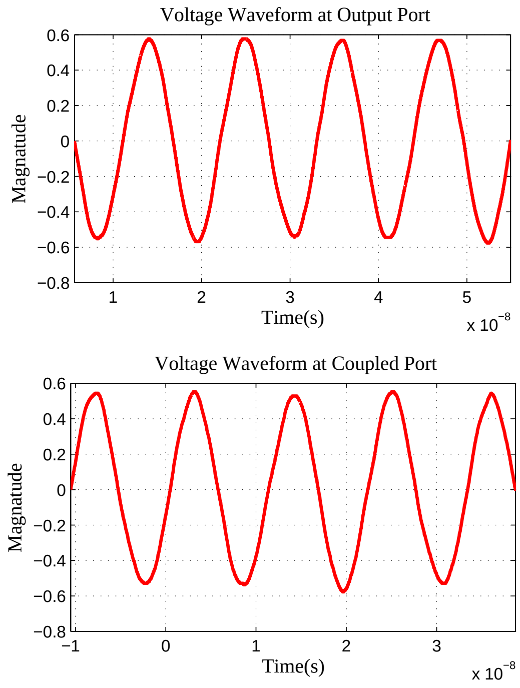

Figure 3.12: Measured voltage waveforms at coupled and output port at 1.0kW input.

3dB hybrid coupler.

3.7 Conclusion

Following are the main conclusions of the presented work,

- A novel patch compensation technique is developed to enhance the performance of tandem hybrid coupler without using lumped capacitors and open stubs. A procedure has been established for the calculation of patch impedance required for matching.
- Performance of the designed, fabricated, tested and patch compensated tan-

dem coupler is found improved and the optimum performance is obtained without affecting the coupling. The final testing shows coupling of -3 ± 0.2dB, output of -3 ± 0.2dB, return loss of less than 32dB and isolation of better than 31dB in the given frequency range of 91.2 ± 15MHz. The same is found providing the return loss of -40dB and isolation of -33dB at the center frequency 91.2MHz.

- Patch compensated prototype 3 ± 0.2dB hybrid coupler is indigenously developed and tested at 91.2 ± 15MHz for 2.5kW power handling capability.

- This prototype has successfully been created the process for indigenous development of 2.5kW, 3dB hybrid coupler at any required frequency from 10 to 100MHz.

- The concept, design and development procedure have imparted sufficient experience that will be useful while making 3dB hybrid coupler of more than 100kW power rating at the various frequencies within the range of 10 to 100MHz, mainly for the ion cyclotron resonant heating systems of plasma in the tokamaks.

4

An analysis of junction discontinuity effect in multi-element coupled lines and its diminution at the designing stage

4.1 Introduction

Our objective is to develop a broadband high power hybrid coupler for the ICRF heating system application. This chapter is devoted for the comprehensive review of previous works in the area of broadband development of the coupled lines and its applicability in the development of high power 3dB hybrid coupler. Single quarter wavelength coupled line based hybrid coupler provides the narrow frequency bandwidth. The multi-octave bandwidth can be achieved by means of cascading several quarter-wavelength elements called multi-element coupled lines. The theoretical modeling of symmetrical multi-element coupler is presented in the earlier works [10, 20, 22] where coupled elements are proposed to be cascaded in a certain configuration to achieve the desired coupling and frequency bandwidth. These theories hold good and yields ideal performance for multi-element coupled lines design.

In a practical model, junctions are employed for the joining of two different coupled elements which produce the undesirable reactive effect, abbreviated as junction discontinuity effect. This depends on junction length in addition to even and odd mode impedances. Junction discontinuity effect deteriorates the performances of the multi-element coupled lines from the theoratical prediction [45–48]. However, the existing theory does not take into consideration to the unavoidable junction discontinuity effect. This becomes more prominent in the high power coupled lines for HF and VHF applications because of larger structural dimensions. Therefore, analysis and compensation of junction discontinuity effect in a multi-element coupled line is inevitable. This chapter presents, a generalize theoretical procedure for the analysis of the junction discontinuity effect and its compensation at the designing stage.

Section-4.2 describes the analysis of the coupled lines using Cristal parameters. Concept, design and simulation of designed 3-element, 8.34dB coupled line section is explained in Section-4.3. Theory of junction discontinuity effect on multi-element coupled line performance is given in section-4.4. The modified theory for the multi-element coupled lines is illustrated in section-4.5. Application of modified theory in design of 3-element, 8.34±0.2dB coupled section is shown in section-4.7. Results and discussion of the modified theory for design and development of multi-element coupled line are discussed in section-4.8 and conclusions are given in section-4.9.

4.2 Analysis of Coupled Lines

4.2.1 Single Element Coupled Line

The coupled lines, as shown in Fig.4.1 consists of two identical lines 1-2 and 3-4 with uniform electrical spacing over electrical length θ.

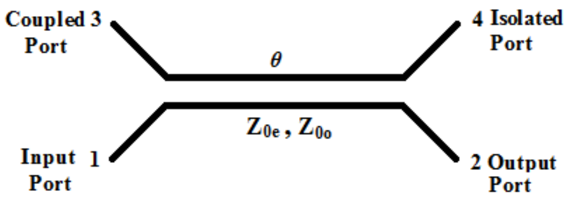

Figure 4.1: Schematic of quarter wave coupled section.

Here,

$$Z_{0e} Z_{0o} = Z_0. \tag{4.1}$$

Where Z_{0e} and Z_{0o} represent the even and odd mode impedance of coupled lines. Signals emerging from the four ports can be given as [49–51].

$$\begin{aligned} A_1 &= \frac{1}{2}\left[\Gamma_{0e} + \Gamma_{0o}\right], \\ A_2 &= \frac{1}{2}\left[\Gamma_{0e} - \Gamma_{0o}\right], \\ A_3 &= \frac{1}{2}\left[T_{0e} + T_{0o}\right], \\ \text{and } A_4 &= \frac{1}{2}\left[T_{0e} - T_{0o}\right]. \end{aligned} \tag{4.2}$$

A_1, A_2, A_3 and A_4 that represent return loss, output, coupling and isolation of coupled lines which is terminated with matched impedance. For the given two-

port network, Γ_{0e} and Γ_{0o} are the reflected wave amplitudes, whereas T_{0e} and T_{0o} are transmitted wave amplitudes for the even and odd modes respectively.
The transmission coefficient T and reflection coefficient Γ are given by the following Eqations.

$$\begin{aligned}\Gamma &= \frac{A_t + B_t - C_t - D_t}{A_t + B_t + C_t + D_t},\\ T &= \frac{2}{A_t + B_t + C_t + D_t}\end{aligned} \tag{4.3}$$

Where, A_t, B_t, C_t and D_t are transmission matrix parameter of the coupled elements. Γ and T represent transmission and reflection coefficients. Using Eqn.4.2 and Eqn.4.3, A_1, A_2, A_3 and A_4 for the matched coupled lines can be calculated as

$$\begin{aligned} A_1 &= 0,\\ A_2 &= \frac{2}{2\cos\theta + j(Z_{0e} + 1/Z_{0e})\sin\theta},\\ A_3 &= \frac{j(Z_{0e} - 1/Z_{0e})\sin\theta}{2\cos\theta + j(Z_{0e} + 1/Z_{0e})\sin\theta},\\ \text{and } A_4 &= 0. \end{aligned} \tag{4.4}$$

4.2.2 Coupled Line Section with Three Elements

Schematic diagram of the symmetrical 3-element coupled lines section is shown in Fig.4.2 where elements B, A, B are cascaded in symmetrical mannar. The A_1, A_2, A_3, A_4 and B_1, B_2, B_3, B_4 are taken as return loss, output, coupling and isolation of coupled element-A and element-B respectively. To retain the perfect voltage standing wave ratio(VSWR), each element has the same effective characteristic impedance.

$$\sqrt{Z_{0eA}Z_{0oA}} = \sqrt{Z_{0eB}Z_{0oB}} = 1. \tag{4.5}$$

Where Z_{0eA}, Z_{0eB} and Z_{0oA}, Z_{0oB} are normalized even and odd mode impedances of the element-A and element-B respectively. Initially, amplitude of emerging signal

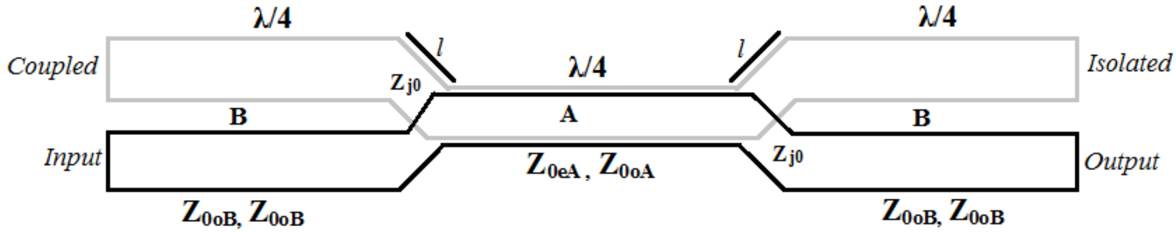

Figure 4.2: Schematic of 3-elements, 8.34dB coupled line section.

from each of the elements are computed and its combination for the multi-element coupled lines section is solved using graph network theory. The signal flow graph of the cascaded three coupled elements are shown in Fig.4.3.(a) and (b)

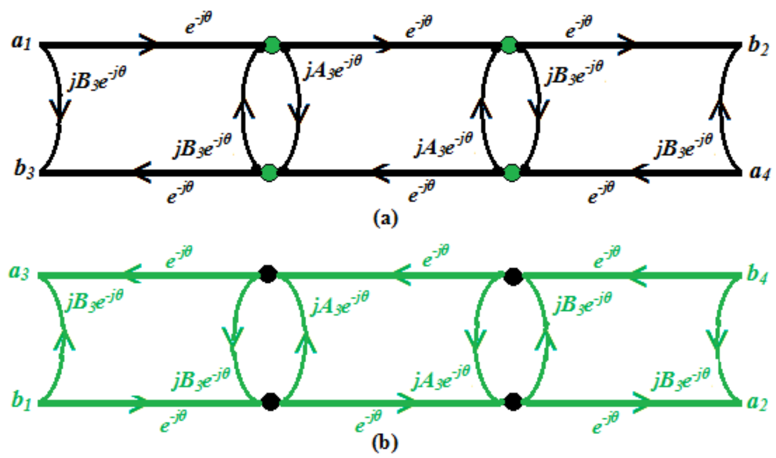

Figure 4.3: Signal flow graph of the 3-elements, 8.34dB coupled line section (a) Forward-wave (b) Backward-wave.

These two graphs are identical and represent the forward and backward-wave propagation. In perfectly matched condition, port-4 is isolated and ($a_4 = 0$). The resulting signal flow graph is shown in Fig.4.4.

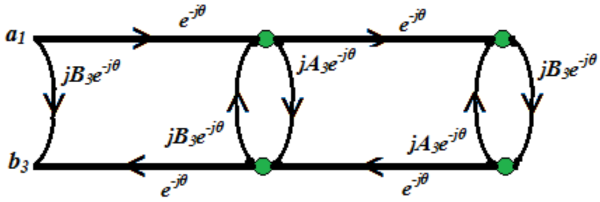

Figure 4.4: Reduced signal flow graph.

For the incident wave $a_1 = 1$, coupled output b_3 can be derived as,

$$\begin{aligned} b_3 &= jB_3.e^{-j\theta} + e^{-j\theta}.jA_3.e^{-j\theta}.e^{-j\theta} \\ &\quad + e^{-j\theta}.e^{-j\theta}.jB_3.e^{-j\theta}.e^{-j\theta}.e^{-j\theta} \\ &= jB_3.e^{-j\theta} + jA_3.e^{-j3\theta} + jB_3.e^{-j5\theta}. \end{aligned} \tag{4.6}$$

For the known coupling of element-A and element-B, coupling of the three cascaded elements b_3 can be analyzed by making use of Eqn.4.6.

The Cristal [20] table for 8.34±0.2dB, 3-element coupled lines section provides the normalized even mode impedance for element-A as $Z_{0eA} = 1.7848$ and for element-B as $Z_{0eB} = 1.07434$. Using these values in Eqn.4.4, A_3 and B_3 are calculated. Now, the overall coupling b_3 for 8.34±0.2dB, 3-element coupled lines section using Cristal tabulated parameter is analyzed and plotted using MATLAB software and shown in Fig.4.5. The result shown in Fig.4.5 represents the Cristal theoretical coupling for the 8.34±0.2dB, 3-element coupled lines section where both of the extremes are equal and shows ideal performance which one would like to achieve in their design.

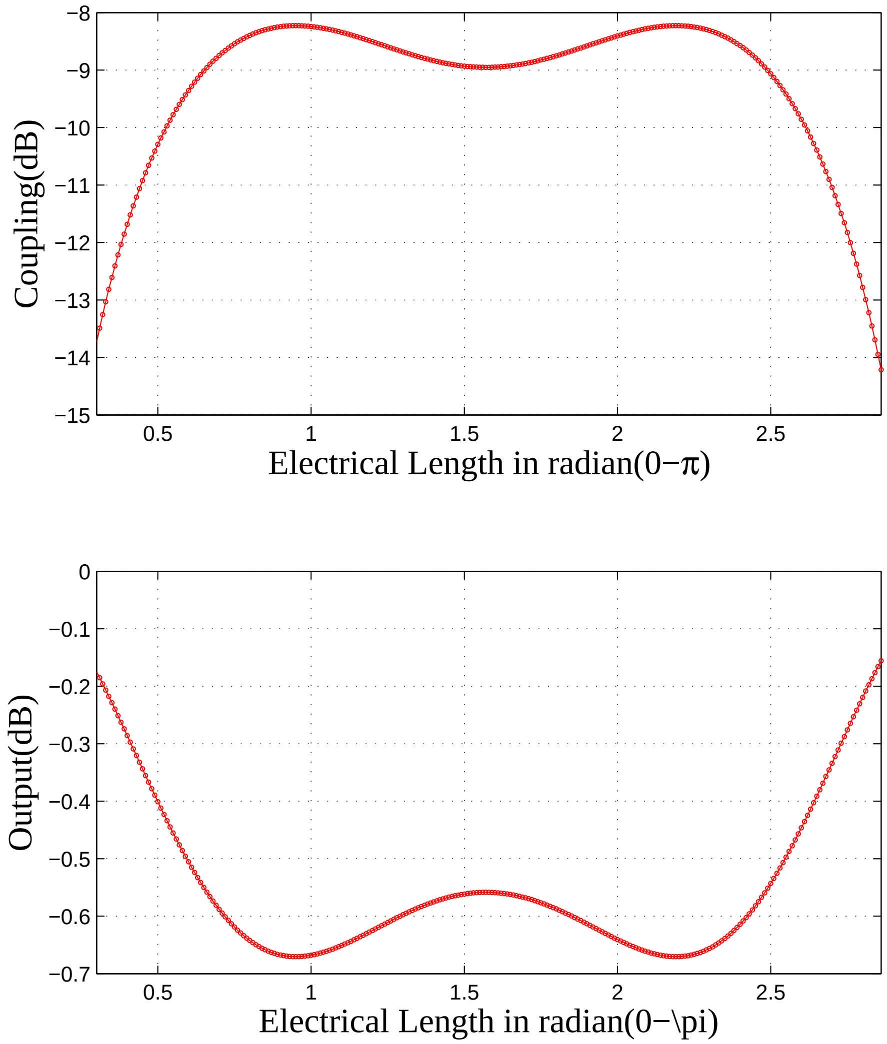

Figure 4.5: Characteristic of 3-elements, 8.34dB coupled line section using Cristal theory.

4.3 Concept, Design and Simulation

In this section design and simulation of 8.34±0.2 dB coupled section rated for 38 to 112MHz and 200kW is presented. Multi-octave bandwidth can be achieved by means of cascading several quarter-wavelength elements called of multi-element coupler. Coupling of middle element is kept higher in proportion to the number of elements used. As the number of cascaded elements is increased, coupling gap of the middle element becomes narrow that reduces the power handling capability. Therefore, only three elements namely B, A and B as shown in Fig.4.2 are designed to provide sufficient coupling gap which is essential for desired power rating.

The Cristal table [20] for 8.34 ± 0.1dB, 3-element coupled section provides the even mode impedance for element-A i.e. $Z_{0eA} = 1.7848$ and element-B i.e. $Z_{0eB} = 1.07434$.

Coupling coefficient of an element-x is given by

$$C_x = \left(\frac{Z_{0ex}^2 - 1}{Z_{0ex}^2 - 1}\right) = \left(\frac{1 - Z_{0ox}^2}{1 - Z_{0ox}^2}\right) \tag{4.7}$$

Where Z_{0ex} and Z_{0ox} are even and odd impedance of the concerned element-x. For element-A and element-B, calculated values of coupling coefficient $C_A = 0.5222{=}{-6.123}$dB and $C_B = 0.07074{=}{-22.896}$dB respectively. Dimensions of element-A and element-B are calculated for the C_A and C_B by using known equations [11, 35, 44]. The junction of length l is physically employed to join the 3-elements and simulation has been performed using HFSS.

4.3.1 Simulation of the designed Model using HFSS

The model used for the simulation of the 8.34 ± 0.2dB coupled section consisting of 3-cascaded elements is shown in Fig.4.6.

The rectangular strip-line central conductors are arranged in particular configuration and placed in the grounded metallic enclosure of dimension $310cm \times 60cm$

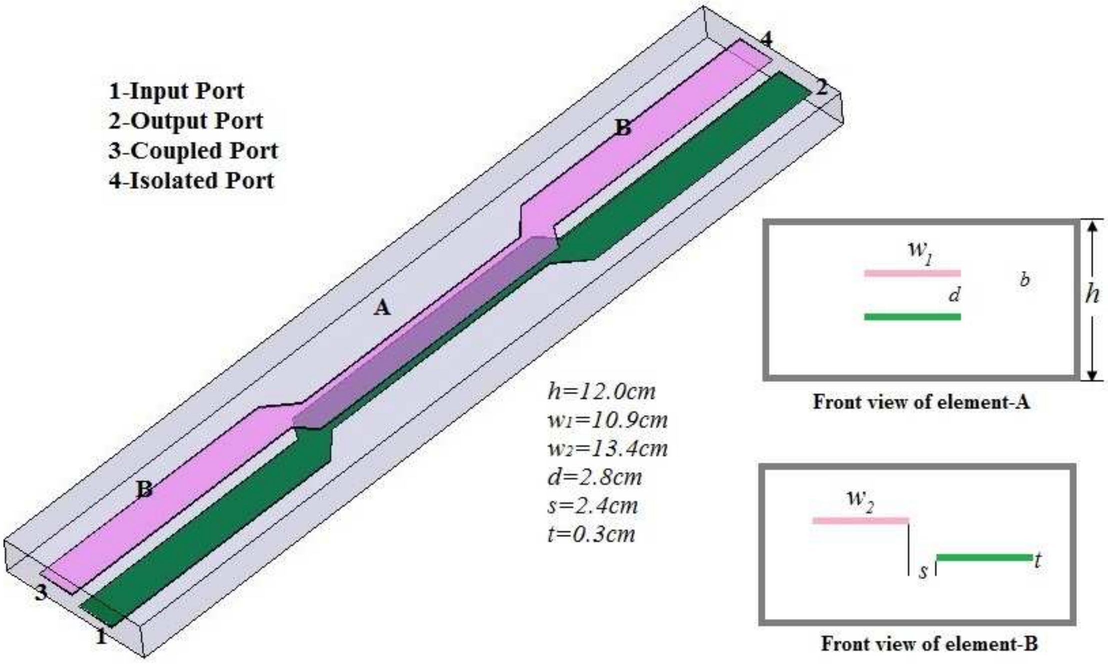

Figure 4.6: HFSS simulated model of 3-elements, 8.34dB coupled line section.

$\times 12cm$. Air within the grounded metallic enclosure is used as dielectric. The holding studs for the inner strip conductor and other transition i.e. required for practical aspect, are avoided so that junction discontinuity effect could be analyzed independently. The length of each element is taken to be 100cm i.e. quarter wavelength at center frequency 75MHz. For the given configuration junction length of 5cm is provided in each element. In first step, designed elements A and B are simulated independently and coupling performances of both are shown in Figs.4.7 and 4.8. The Illustrated performances are verified for calculated values of 6.123dB and 22.896dB at the center frequency.

In the next step, coupled strip-line junction is employed to connect these three elements namely B, A and B to achieve 8.34±0.2dB coupling and the simulation

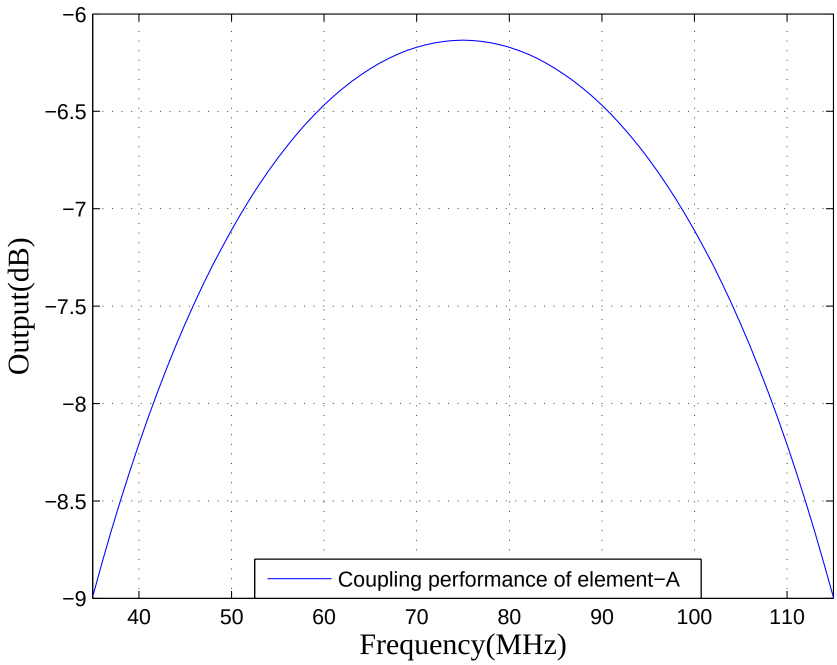

Figure 4.7: Using HFSS simulated coupling of element-A.

is performed again. The coupling and output simulation results are illustrated in Fig.4.9.

As explained in previous section, both the maxima of the coupling or output parameters should be equal in the prescribed bandwidth. In HFSS simulation results, both the maxima at upper and lower end of the frequency band are found unequal and performances are significantly deteriorated from the theoretical prediction. This anomaly does not exist in case of element-A and element-B since the coupling through simulation results are in close agreement to calculated values. This anomaly attributes to the reactive effect of junction discontinuity.

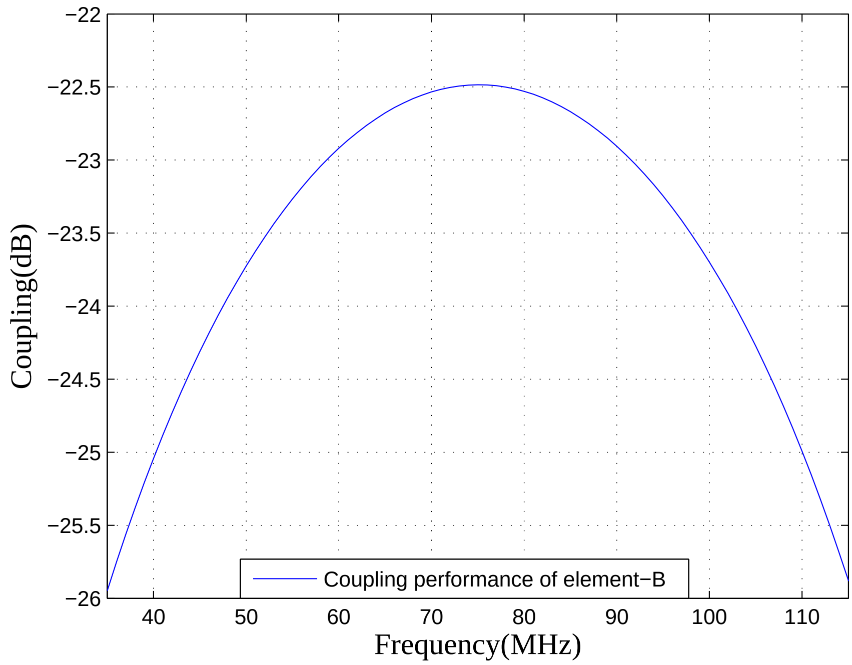

Figure 4.8: Using HFSS simulated coupling of element-B.

4.4 Theory of junction discontinuity

The coupled lines have always characterized by its even and odd modes behavior. The even and odd mode analysis of element-A and element-B including the junction discontinuity effect have been performed. Junction represents the coupled transition between element-A and element-B. The even and odd mode impedances of the junction and elements can be taken as,

$$Z_{0eA} > Z_{j0e} > Z_{0eB}, \quad Z_{0oA} < Z_{j0o} < Z_{0oB}.$$

Here, Z_{j0e} and Z_{j0o} represent the even and odd mode impedances of junction.

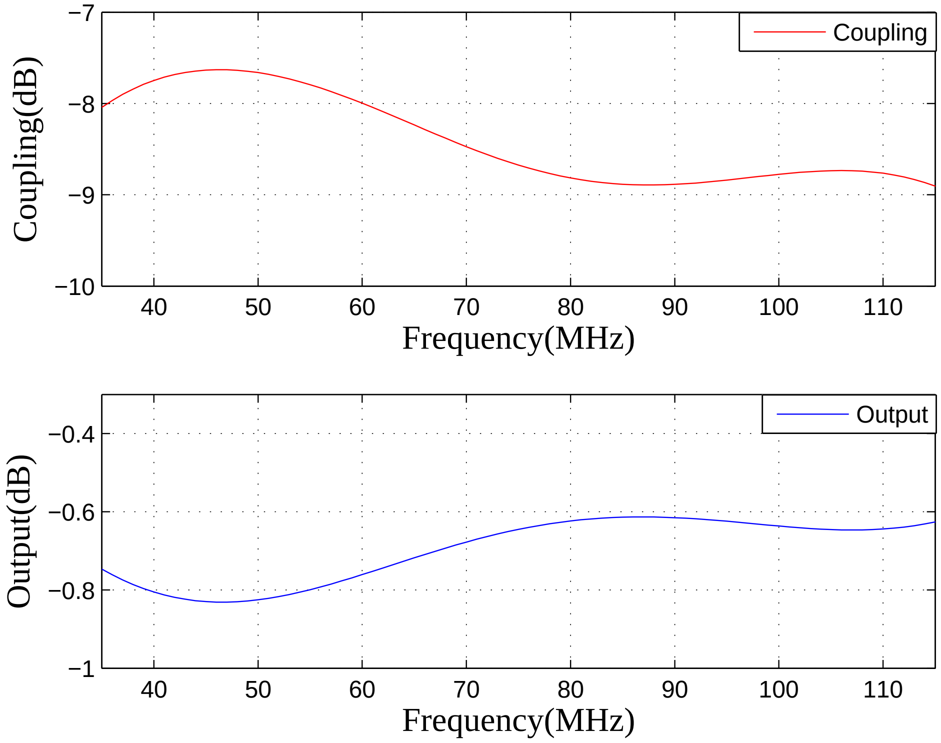

Figure 4.9: Using HFSS simulated performance of 3-elements, 8.34dB coupled line section.

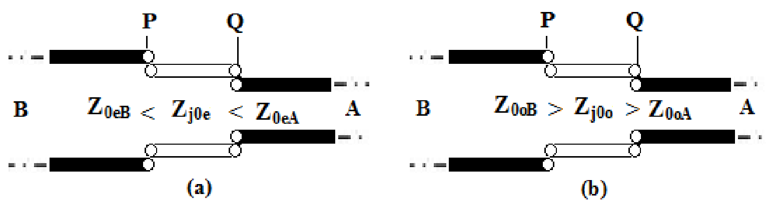

Figure 4.10: Schematic of junction between two coupled lines (a) Even mode (b) Odd mode.

Schematic of junction with coupled element A and B is shown in Fig.4.10

4.4.1 Even mode analysis of junction with the element-B

In Fig4.10.(a) input impedance at point-Q i.e. $Z_{in(eAQ)}$ is given as

$$\begin{aligned} Z_{in(eAQ)} &= Z_{j0e}\frac{Z_{0eB} + jZ_{j0e}\tan\beta l}{Z_{j0e} + jZ_{0eB}\tan\beta l} \\ &\approx Z_{j0e}\frac{Z_{0eB} + jZ_{j0e}\beta l}{Z_{j0e} + jZ_{0eB}\beta l} \text{ for } \beta l \leq \pi/6 \, . \end{aligned} \tag{4.8}$$

Where, $Z_{j0e} > Z_{0eB}$, $l \leq \lambda/25$ and $\beta l < 1$, that implies $Z_{0eB}\beta l << 1$. Therefore, $Z_{in(oAQ)}$ is approximated as,

$$Z_{in(eAQ)} \approx Z_{0eB} + jZ_{j0e}\beta l = Z_{Be_{(eff)}}, \tag{4.9}$$

where $Z_{Be_{(eff)}}$ repersents the effective impedance of element-B including junction discontinuity. The analysis shows that the junction discontinuity behaves as series inductance of $Z_{joe}\beta l/v$ with element-B in even mode.

Junction length l in terms of wavelength λ at center frequency f_0 and arbitrary frequency f can be written as.

$$l = \frac{\lambda_0}{m_0} = \frac{\lambda}{m} \Rightarrow m = m_0\left(\frac{f_0}{f}\right). \tag{4.10}$$

Where m_0 and m represent the wavelength to junction length ratio at f_0 and f respectively. Now, from the Eqns.(4.9) and (4.10), inductive reactance jX_{jeB} due to junction with element-B can be written as

$$jX_{jeB} = \frac{j2\pi Z_{j0e}}{m_0}\left(\frac{f}{f_0}\right) = \frac{j2\pi Z_{j0e}}{m_0}\left(\frac{\theta}{\theta_0}\right) = \frac{4jZ_{j0e}\theta}{m_0}. \tag{4.11}$$

Where θ and $\theta_0 = \pi/2$ are the electrical lengths of the coupled element at variable frequency f and at center frequency f_0 respectively.

4.4.2 Odd mode analysis of junction with the element-B

From Fig.4.10.(b) odd mode admittance at point-Q i.e. $Y_{in(oAQ)}$ is given by,

$$Y_{in(oAQ)} = Y_{j0o}\frac{Y_{0oB} + jY_{j0o}\tan\beta l}{Y_{j0o} + jY_{0oB}\tan\beta l}$$
$$\approx Y_{0oB} + jY_{j0o}\beta l = Y_{Bo_{(eff)}}. \tag{4.12}$$

Where $Y_{Bo_{(eff)}}$ effective admittance of the element-B including junction discontinuity effect in odd mode

Form Eqn.4.12, it can be noticed that the junction discontinuity behaves as shunt capacitance of $Z_{j0e}l/v$ with element-B in odd mode. The odd mode admittance Y_{joB} at frequency f is derived as.

$$jY_{joB} = \frac{j2\pi Y_{j0o}}{m_0}\left(\frac{f}{f_0}\right) \tag{4.13}$$

Where $Y_{j0o} = Z_{j0e}$ substituting in Eqn.4.13

$$jY_{joB} = \frac{j2\pi Z_{j0e}}{m_0}\left(\frac{\theta}{\theta_0}\right) = \frac{4jZ_{j0e}\theta}{m_0} \tag{4.14}$$

From Eqn.4.11 and Eqn.4.14, junction equivalent series inductance and shunt capacitance L_{jeB} and C_{joB} for the even and odd mode for the junction discontinuity are derived as.

$$L_{jeB} = C_{joB} = \frac{Z_{j0e}}{m_0 f_0} \tag{4.15}$$

Considering the junction discontinuity effect, the even and odd mode equivalence of element-B is shown in Fig.4.11.

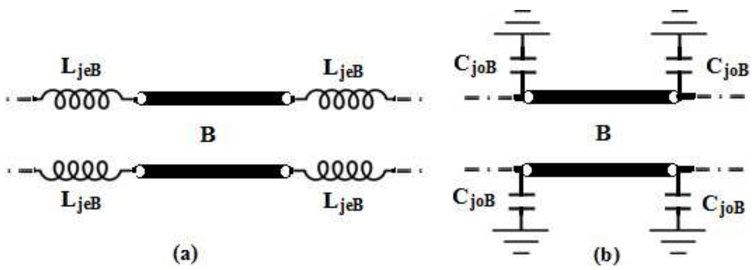

Figure 4.11: Equivalent circuit of the coupled element-B (a) Even mode (b) Odd mode.

Using equivqlent circuit of element-B, even and odd mode transmission matrix for the element-B is written as,

$$\begin{bmatrix} A_{Be'} & B_{Be'} \\ C_{Be'} & D_{Be'} \end{bmatrix} = \begin{bmatrix} 1 & jX_{jeB} \\ 0 & 1 \end{bmatrix} \begin{bmatrix} \cos\theta & jZ_{0eB}\sin\theta \\ \frac{j\sin\theta}{Z_{0eB}} & \cos\theta \end{bmatrix} \begin{bmatrix} 1 & jX_{jeB} \\ 0 & 1 \end{bmatrix}. \tag{4.16}$$

Considering $Z_{0oB} = 1/Z_{0eB}$, transmission matrix for odd mode is written as,

$$\begin{bmatrix} A_{Bo'} & B_{Bo'} \\ C_{Bo'} & D_{Bo'} \end{bmatrix} = \begin{bmatrix} 1 & 0 \\ jX_{joB} & 1 \end{bmatrix} \begin{bmatrix} \cos\theta & \frac{j\sin\theta}{Z_{0eB}} \\ jZ_{0eB}\sin\theta & \cos\theta \end{bmatrix} \begin{bmatrix} 1 & 0 \\ jX_{joB} & 1 \end{bmatrix}. \tag{4.17}$$

Where $A_{Be'}$, $B_{Be'}$, $C_{Be'}$, $D_{Be'}$ and $A_{Bo'}$, $B_{Bo'}$, $C_{Bo'}$, $D_{Bo'}$ are the even and odd mode transmission matrix parameter of element-B including discontinuity effect. Using the Eqn.4.16, Eqn.4.17 and Eqn.4.2, the emerging signals from the ports of element-B including junction is derived as.

$$
\begin{aligned}
B_1\prime &= 0,\\
B_2\prime &= \frac{j\sin\theta\left(Z_{0eB}-\frac{1}{Z_{0eB}}\right)+jX_{jeB}\left(2\cos\theta-\frac{jX_{jeB}\sin\theta}{Z_{0eB}}\right)}{2\left(1-jX_{jeB}\right)\cos\theta-j\left(Z_{0eB}-\frac{1}{Z_{0eB}}\left(1+jX_{jeB}\right)^2\right)},\\
B_3\prime &= \frac{2}{2\left(1-jX_{jeB}\right)\cos\theta-j\left(Z_{0eB}+\frac{1}{Z_{0eB}}\left(1+jX_{jeB}\right)^2\right)}\\
\text{and } B_4\prime &= 0.
\end{aligned}
\tag{4.18}
$$

Where, B_1', B_2', B_3' and B_4' are return loss, output, coupling and isolation of element-B including the effect of junction discontinuity.

4.4.3 Even mode analysis of junction with the element-A

The junction discontinuity effect with element-A is also analyzed using the same procedure as used for element-B. In Fig.4.10.(a), input admittance at point-P i.e. $Y_{in(eBP)}$ is given as

$$
\begin{aligned}
Y_{in(eBP)} &= Y_{j0e}\frac{Y_{0eA}+jY_{j0e}\tan\beta l}{Y_{j0e}+jY_{0eA}\tan\beta l}\\
&\approx Y_{j0e}\frac{Y_{0eA}+jY_{j0e}\beta l}{Y_{j0e}+jY_{0eA}\beta l} \text{ for } \beta l \leq \pi/6\ .
\end{aligned}
\tag{4.19}
$$

Where, $Y_{j0e} > Y_{0eA}$, $l \leq \lambda/25$ and $\beta l < 1$, that implies $Y_{0eA}\beta l << 1$. Therefore, $Y_{in(eBP)}$ is approximated as,

$$
Y_{in(eBP)} \approx Y_{0eA} + jY_{j0e}\beta l = Y_{Ae_{(eff)}}. \tag{4.20}
$$

Where $Y_{Ae_{(eff)}}$ is the effective admittance of the element-A including junction discontinuity effect in even mode. It can be seen that the junction discontinuity in even mode behaves as shunt capacitance with element-A. The shunt admittance Y_{jeA} can be written as

$$jY_{jeA} = \frac{4j\theta}{m_0 Z_{j0e}}. \tag{4.21}$$

4.4.4 Odd mode analysis of junction with the element-A

In Fig4.10.(b), input impedance at point-P i.e. $Z_{in(eBP)}$ is given as.

$$\begin{aligned} Z_{in(eBP)} &= Z_{j0o}\frac{Z_{0oA} + jZ_{j0o}\tan\beta l}{Z_{j0o} + jZ_{0oA}\tan\beta l} \\ \approx Z_{j0o}\frac{Z_{0oA} + jZ_{j0o}\beta l}{Z_{j0o} + jZ_{0oA}\beta l} & Z_{0oA} + jZ_{j0o}\tan\beta l. \end{aligned} \tag{4.22}$$

Where, $Z_{j0o} > Z_{0oA}$, $l \leq \lambda/25$ and $\beta l < 1$, that implies $jZ_{0oA}\beta l << 1$. Therefore, $Z_{in(eBP)}$ is approximated as,

$$Z_{in(eBP)} \approx Z_{0oA} + jZ_{j0o}\beta l = Z_{Ao_{(eff)}} \tag{4.23}$$

where $Z_{Ao_{(eff)}}$ is effective impedance of the element-A including junction discontinuity effect in odd mode. Using equivqlent circuit of element-A, junction discontinuity in odd mode behaves as series inductance with element-A. The series reactance X_{joA} is derived as

$$jX_{joA} = \frac{4j\theta}{m_0 Z_{j0e}}. \tag{4.24}$$

Using Eqn.4.21 and Eqn.4.24, the series inductance and shunt capacitance due to junction discontinuity are derived as

$$L_{joA} = C_{jeA} = \frac{1}{m_0 Z_{j0e} f_0}. \tag{4.25}$$

Where, L_{joA} and C_{jeA} are inductance and capacitance in odd and even mode with element-A due to junction discontinuity. The equivalent circuit of element-A with junction discontinuity effect is given in Fig.4.12.

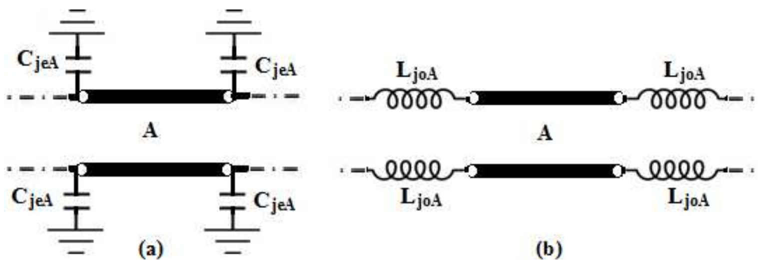

Figure 4.12: Equivalent circuit of element-A (a) Even mode (b) Odd mode.

Therefore, even and odd mode transmission matrix for the element-A can be written as

$$\begin{bmatrix} A_{Ae\prime} & B_{Ae\prime} \\ C_{Ae\prime} & D_{Ae\prime} \end{bmatrix} = \begin{bmatrix} 1 & jY_{jeA} \\ 0 & 1 \end{bmatrix} \begin{bmatrix} \cos\theta & jZ_{0eA}\sin\theta \\ \frac{j\sin\theta}{Z_{0eA}} & \cos\theta \end{bmatrix} \begin{bmatrix} 1 & jY_{jeA} \\ 0 & 1 \end{bmatrix}. \tag{4.26}$$

Considering $Z_{0oA} = 1/Z_{0eA}$ transmission matrix for odd mode is written as

$$\begin{bmatrix} A_{Ao\prime} & B_{Ao\prime} \\ C_{Ao\prime} & D_{Ao\prime} \end{bmatrix} = \begin{bmatrix} 1 & 0 \\ jX_{jeA} & 1 \end{bmatrix} \begin{bmatrix} \cos\theta & \frac{j\sin\theta}{Z_{0eA}} \\ jZ_{0eA}\sin\theta & \cos\theta \end{bmatrix} \begin{bmatrix} 1 & 0 \\ jX_{jeA} & 1 \end{bmatrix}. \tag{4.27}$$

Where $A_{Ae\prime}$, $B_{Ae\prime}$, $C_{Ae\prime}$, $D_{Ae\prime}$ and $A_{Ao\prime}$, $B_{Ao\prime}$, $C_{Ao\prime}$, $D_{Ao\prime}$ are the even and odd mode transmission matrix parameters of element-A including the effect of junction discontinuity.

The amplitude and phase of emerging signals from the ports of element-A by using Eqn.4.26, Eqn.4.27 and Eqn.4.3 is derived as

$$\begin{aligned}
A_1\prime &= 0, \\
A_2\prime &= \frac{j\sin\theta\left(Z_{0eA}-\frac{1}{Z_{0eA}}\right)+jY_{jeA}\left(2\cos\theta-\frac{jY_{jeA}\sin\theta}{Z_{0eA}}\right)}{2\left(1-jY_{jeA}\right)\cos\theta-j\left(Z_{0eA}-\frac{1}{Z_{0eA}}\left(1+jY_{jeA}\right)^2\right)}, \\
A_3\prime &= \frac{2}{2\left(1-jY_{jeA}\right)\cos\theta-j\left(Z_{0eA}+\frac{1}{Z_{0eA}}\left(1+jY_{jeA}\right)^2\right)} \\
\text{and } A_4\prime &= 0.
\end{aligned} \tag{4.28}$$

Where, A_1', A_2', A_3' and A_4' are return loss, output, coupling and isolation of element-A including the effect of junction discontinuity.

By using Eqn.4.6, amplitude of coupling for 3-element, 8.34dB coupled line section including junction discontinuity effect is written as

$$b_3' = jB_3\prime.e^{-j\theta} + jA_3\prime.e^{-j3\theta} + jB_3\prime.e^{-j5\theta}. \tag{4.29}$$

Coupling for the element-A, element-B and 3-element coupled line section by using Eqn.4.18, Eqn.4.28 and Eqn.4.29 are plotted using MATLAB and are shown in Fig.4.13, Fig.4.14 and Fig.4.15.

From Fig.4.13, Fig.4.14 and Fig.4.15, one can conclude the following facts.

1. With the aid of Fig.4.13 it can be analysed that including the junction discontinuity effect in element-A, coupling increases to left and decreases to right of prescribed frequency band, where center frequency is shifted towards left with reduced frequency band.

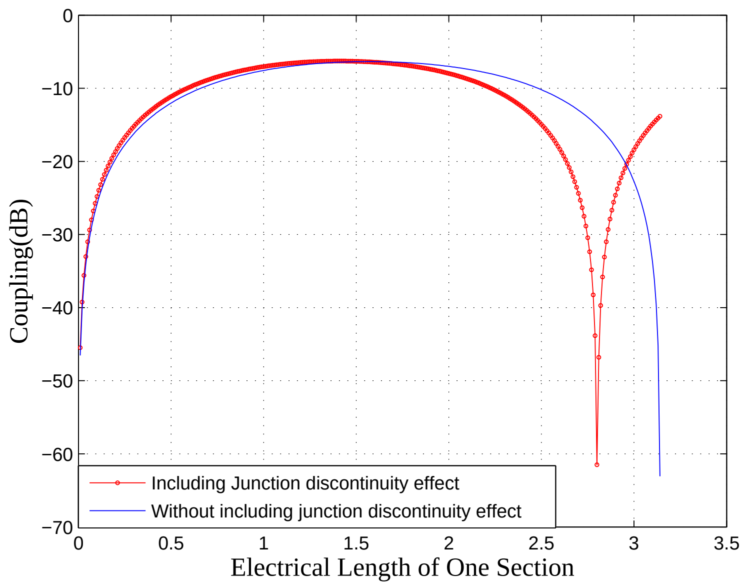

Figure 4.13: Calculated coupling of element-A.

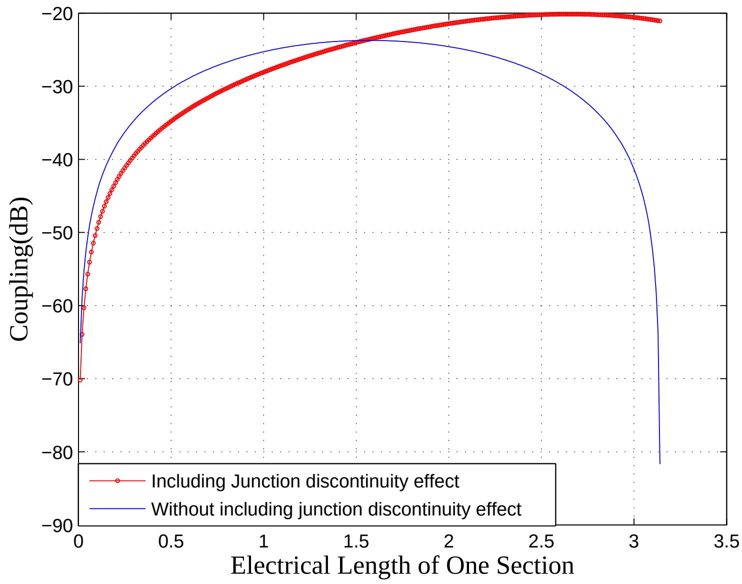

Figure 4.14: Calculated coupling of element-B.

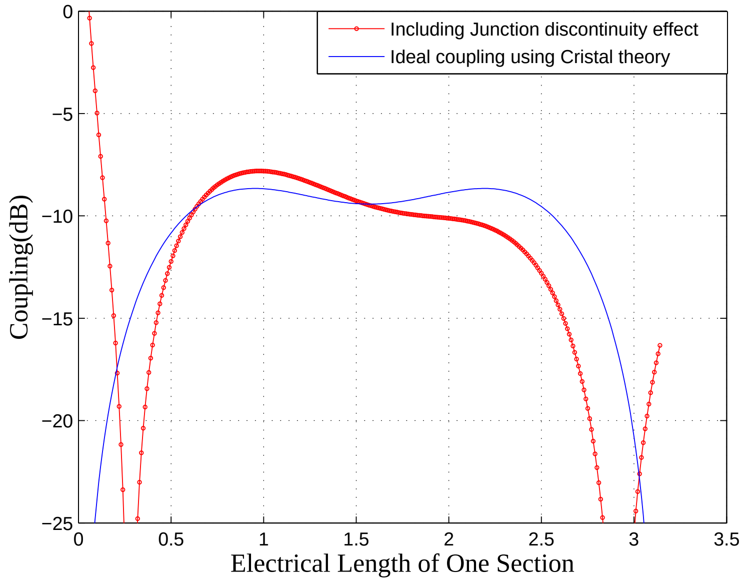

Figure 4.15: Calculated coupling of the 3-element, 8.34±0.3dB coupled line section.

2. From Fig.4.14 it can be analysed that after including the junction discontinuity effect in element-B, coupling of decreases to left and increases to right of prescribed frequency band, where center frequency is shifted towards right with extended frequency band.

3. The resultant effects of element-A and element-B is observed in coupling performance of 3-element, 8.34±0.3dB coupled section.

4. Coupling performance of 8.34±0.3dB section including the junction discontinuity effect is deviated from the Cristal theoretical results. The deviation is found in same manner as simulated result shown in Fig.4.9.

The effect due to variation of junction length λ/m_0 is shown in Fig.4.16.

In this case, coupling of the designed 3-element, 8.34±0.3dB coupled line section is found increasing in left half and decreasing in right half from the calculated

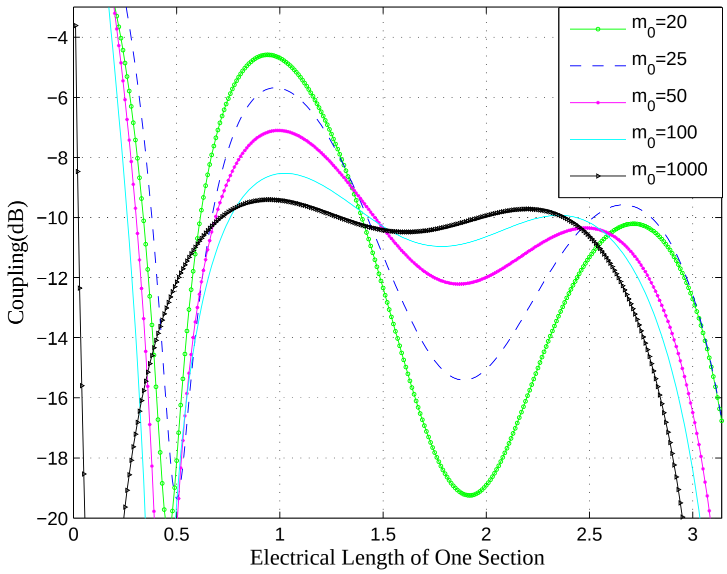

Figure 4.16: Coupling performance with varying junction length.

value. The deterioration depends on even and odd mode impedances of the junction. The deterioration may exist in opposite manner if the choice of even or odd mode impedances for junction are within different boundary conditions. The above mentioned procedure can be followed in both the criteria. The magnitude of deterioration in coupling depends on the junction length therefore junction length should be minimized to minimize the junction discontinuity effect.

4.5 Modified theory of coupled line design with junction discontinuity

In this section, for the compensation of the junction discontinuity effect a novel theoratical procedure has been developed i.e. named as the modidfied theory. The junction discontinuity effect can be estimated in terms of the lumped reactance shown in privious section. Including the junction discontinuity effect even and odd mode impedance of the element-A and element-B can be written as,

$$
\begin{aligned}
Z_{Be_{(eff)}} &= Z_{0eB} + jZ_{j0e}\beta l, \\
Y_{Ae_{(eff)}} &= Y_{0eA} + jY_{j0e}\beta l.
\end{aligned} \tag{4.30}
$$

Where $Z_{Ae_{(eff)}}$ and $Z_{Be_{(eff)}}$ are taken as effective impedance of the element-A and element-B in even mode respectively. The reactive behavior of the junction deteroriate the performance of the coupled lines from desired one. This effect can be compensated by making an oppositive effect in each of the elements.

Using the same, it can be analysed that junction discontinuity effect in element-B and element-A can be compensated by adding capacitive reactance X_C and inductive admittance Y_L respectively. Now $Z_{Be_{(eff)}}$ and $Y_{Be_{(eff)}}$ including compensation can be written as,

$$
\begin{aligned}
Z_{Be_{(eff)}} &= Z_{0eB} + jZ_{j0e}\beta l + X_C, \\
Y_{Ae_{(eff)}} &= Y_{0eA} + jY_{j0e}\beta l + Y_L.
\end{aligned} \tag{4.31}
$$

In modified theory two facts have been explored and utilized for the compensation of junction discontinuity effect. These facts are given as follow,

1. A small increment in length of the quarter-wave coupled element behaves as capacitive in even mode and inductive in odd mode whereas characteristic impedance remains same.

   This fact can be understood with the help of Fig.4.17 where increment in length of an arbitrary coupled element-x is analyzed. From Fig.4.17.(a), even

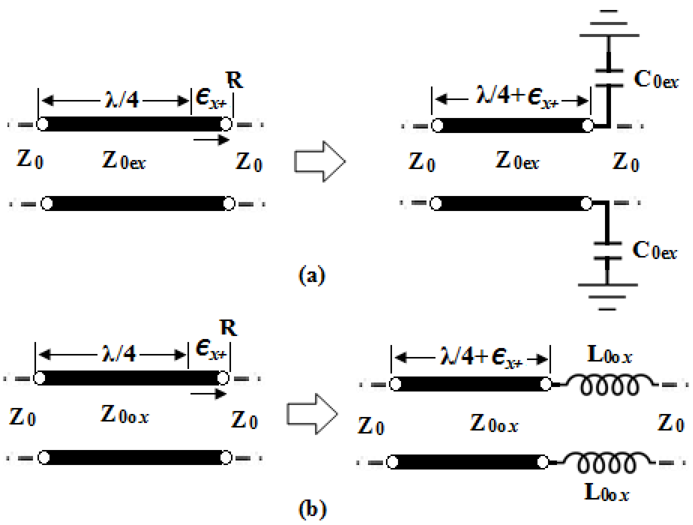

Figure 4.17: Schematic of the of the coupled element-x with small increments in length in (a) Even mode (b) Odd mode.

mode input admittance $Y_{in(eR)}$ at point-R can be written by

$$\begin{aligned} Y_{in(eR)} &= Y_{0ex}\frac{Y_0 + jY_{0ex}\tan(\pi/2 + \beta\epsilon_{x^+})}{Y_{0ex} + jY_0\tan(\pi/2 + \beta\epsilon_{x^+})} \\ &= Y_{0ex}\frac{Y_0 + jY_{0ex}\cot\beta\epsilon_{x^+}}{Y_{0ex} + jY_0\cot\beta\epsilon_{x^+}}. \end{aligned} \tag{4.32}$$

substituting characteristic admittance $Y_0 = 1$, we get

$$\begin{aligned} Y_{in(eR)} &= Y_{0ex}\frac{1 - jY_{0ex}\cot\beta\epsilon_{x^+}}{Y_{0ex} - j\cot\beta\epsilon_{x^+}} \\ &= Y_{0ex}\frac{\beta\epsilon_{x^+} - jY_{0ex}}{Y_{0ex}\beta\epsilon_{x^+} - j} \text{ valid for the } \epsilon_{x^+} < \pi/6. \end{aligned} \tag{4.33}$$

Further, it can be simplified as

$$Y_{in(eR)} = Y_{0ex}^2\frac{\beta^2\epsilon_{x^+}^2 + 1}{\beta^2\epsilon_{x^+}^2 Y_{0ex}^2 + 1} + jY_{0ex}\beta\epsilon_{x^+}\frac{1 - Y_{0ex}^2}{\beta^2\epsilon_{x^+}^2 Y_{0ex}^2 + 1}. \tag{4.34}$$

Here, $Y_{0ex} < 1$, $\epsilon_{x+} < 1$, $\beta < 1$ gives $Y_{0ex}^2\beta^2\epsilon_{x+}^2 <<< 1$ and hence Eqn.4.34 reduces to.

$$Y_{in(eR)} = Y_{0ex}^2 + j\epsilon_{x+}\beta Y_{0ex}(1 - Y_{0ex}^2). \tag{4.35}$$

For $Y_0 = 1$, this also may written as,

$$Y_{in(eR)} = \frac{Y_{0ex}^2}{Y_0} + \frac{j\epsilon_{x+}\beta Y_{0ex}(1 - Y_{0ex}^2)}{Y_0}. \tag{4.36}$$

This equation represents quarter wave admittance transformer with series inductance. It can be noticed that the small increment in length of an arbitrary element-x behaves like shunt capacitance of value $\epsilon_{x+}Y_{0ex}(1 - Y_{0ex}^2)/v$ in the even mode.

In case of odd mode, impedance Z_{ineR} at point-R is given as

$$Z_{ineR} = Z_{0ox}^2 + j\beta\epsilon_{x+}Z_{0ox}(1 - Z_{0ox}^2). \tag{4.37}$$

It reveals, a small increment in length of an element behaves like series inductance of value $\beta\epsilon_{x+}Y_{0ex}(1 - Y_{0ex}^2)/v$ in odd mode.

Series inductance in odd mode and shunt capacitance in even mode for small increment in length of an element-x are found equal therefore,

$$jY_{0ex} = jX_{0ox} = j\beta\epsilon_{x+}Y_{0ex}(1 - Y_{0ex}^2). \tag{4.38}$$

The above equation in terms of shunt capacitance C_{0ex} and series inductance L_{0ox} can be written as

$$L_{0ox} = C_{0ex} = \epsilon_{x+}Y_{0ex}(1 - Y_{0ex}^2)/v \tag{4.39}$$

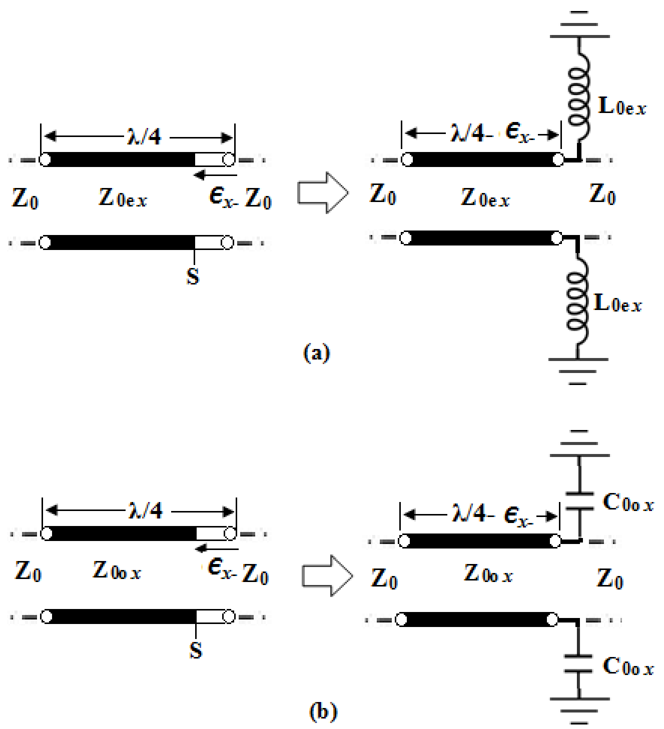

Figure 4.18: Schematic of the of the element-x with small decrement in length (a) Even mode (b) Odd mode.

2. A small decrement in the length of the quarter-wave coupled element behaves as inductive in even mode and capacitive in odd mode whereas characteristic impedance remains same. This fact can be proved with the help of Fig.4.18 where decrement in length of an arbitrary coupled element-x is analyzed. Input admittance $Y_{in(eS)}$ at point-S in Fig4.18.(a) is given by

$$\begin{aligned} Y_{in(eS)} &= Y_{0ex}\frac{Y_0 + jY_{0ex}\tan(\pi/2 - \beta\epsilon_{x-})}{Y_{0ex} + jY_0\tan(\pi/2 - \beta\epsilon_{x-})} \\ &\approx Y_{0ex}\frac{\beta\epsilon_B + jY_{0ex}}{Y_{0ex}\beta\epsilon_{x-} + j}\text{valid for the } \epsilon_{x-} < \pi/6. \end{aligned} \tag{4.40}$$

above can be simplified as

$$Y_{in(eS)} = \frac{Y_{0ex}^2}{Y_0} - \frac{j\beta\epsilon_{x^-}Y_{0ex}(1 - Y_{0ex}^2)}{Y_0}. \tag{4.41}$$

This equation represents quarter wave admittance transformer with series inductance. This implies that small increment in length of an element behaves like shunt inductance of value $1/\beta\epsilon_{x^-}Y_{0ex}(Y_{0ex}^2 - 1)v$ in the even mode.
In case of odd mode, impedance Z_{inoS} at point-S is given by

$$Z_{inoS} = Z_{0ox}^2 - j\beta\epsilon_{x^-}Z_{0ox}(1 - Z_{0ox}^2). \tag{4.42}$$

This states, a small decrement in length of an element behaves like series capacitance of value $1/\beta\epsilon_{x^-}Z_{0ox}(1 - Z_{0ox}^2)v$ in odd mode.
Series capacitance in odd mode and series inductance in even mode for small decrement in length of an element are found equal, this one has

$$jX_{0ox} = jY_{0ex} = j\beta\epsilon_{x^-}Z_{0ox}(1 - Z_{0ox}^2). \tag{4.43}$$

In terms of series inductance L_{0ex} and shunt capacitance C_{0ox} can be expressed as

$$L_{0ex} = C_{0ox} = 1/\beta\epsilon_{x^-}Y_{0ex}(Y_{0ex}^2 - 1)v \tag{4.44}$$

From Eqn.4.44 one can notice that the compensation of the junction discontinuity effect in 3-element coupled line section can be made by making increment in the length of element-B and decrement in the length of element-A.
Let the increment in element-B, ϵ_{B+} and decrement in element-A, ϵ_{A-} are made to provide the needful compensation reactace and admitance as given in Eqn.5.4.

The values of ϵ_{B+} and ϵ_{A-} can be calculated with the help of Fig.4.19.(a) and (b).

Compensation with element-B in matched condition can be expressed as,

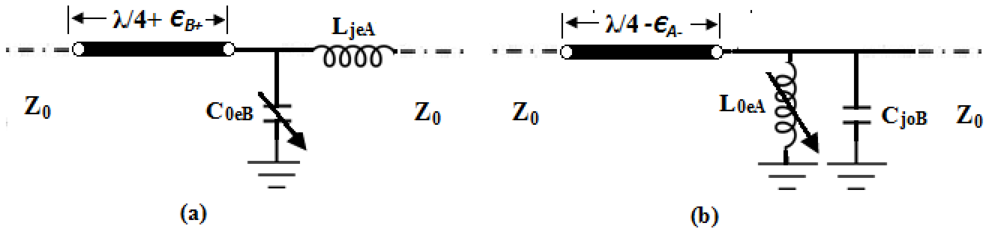

Figure 4.19: Equivalent of altered elements including the effect of junction discontinuity (a)Element-A (b)Element-B.

$$Z_{0eB} = \sqrt{\frac{X_{j0eB}}{Y_{0eB}}}. \tag{4.45}$$

Using Eqn.5.4 and Eqn.4.38, value of ϵ_{B+} can be written as

$$\epsilon_{B+} = \frac{Z_{0eB}Z_{j0e}l}{(Z_{0eB}^2 - 1)}. \tag{4.46}$$

Compensation with element-A in matched condition can be written as,

$$2\pi f\sqrt{L_{0eA}C_{jeA}} = \sqrt{X_{0eA}Y_{jeA}} = 1. \tag{4.47}$$

By using Eqn.5.4 and Eqn.4.44, value of ϵ_{A-} can be written as

$$\epsilon_{A-} = \frac{Y_{j0e}l}{Z_{0oA}(1 - Z_{0oA}^2)}. \tag{4.48}$$

From Eqn.4.30, it can be noticed that the effective even mode impedances of element-B and element-A increases and decreases respectively. Due to this effect maxima at upper end decreases while increases at lower end in coupling parameter.

Thus, compensation i.e. correction can be made by increment ϵ_{B+} in the length of element-B and decrement ϵ_{A-} in the length of element-A. This modification has been incorporated in the 3-element coupled lines section. The schematic of the modified section and it,s signal flow graph are shown in Fig.4.20 and Fig.4.21. respectively.

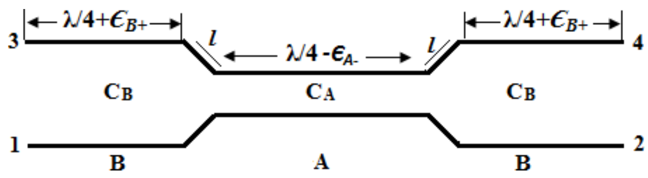

Figure 4.20: Schematic of the modified stepped 3-element coupled section.

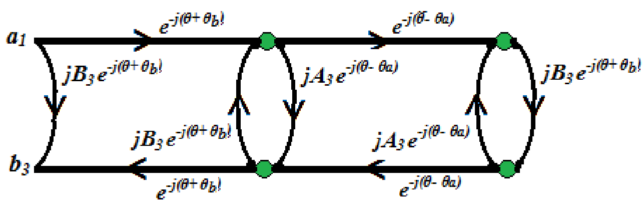

Figure 4.21: Reduced signal flow graph for the modified 3-element 8.34 ± 0.2 coupled lines section.

From Fig.4.21, coupled signal b_{3m} for the modified 3-element coupled line section can written as.

$$b_{3m} = jB_3'.e^{-j(\theta+\theta_a)} + jA_3'.e^{-j(3\theta+2\theta_b-\theta_a)} + jB_3'.e^{-j(5\theta+3\theta_b-2\theta_a)}. \tag{4.49}$$

Where, θ_a and θ_b are electrical length corresponding ϵ_{A-} and ϵ_{B+} that values are given as

$$\theta_a = \beta\epsilon_{A-} \text{ and } \theta_b = \beta\epsilon_{B+}. \tag{4.50}$$

4.6 Generalizing compensation theory to n-element

In 3-element coupled lines section, compensation of the junction discontinuity effect is made by incrementing in the length of element-B and decrementing in the length of element-A. This can be generalized for n-element coupled lines section as shown in Fig.4.22. The resultant alteration required for element A, B C.... are $2\epsilon_{A^-}$, $(\epsilon_{B^+} - \epsilon_{B^-})$ and $(\epsilon_{C^+} - \epsilon_{C^-})$...... respectively.

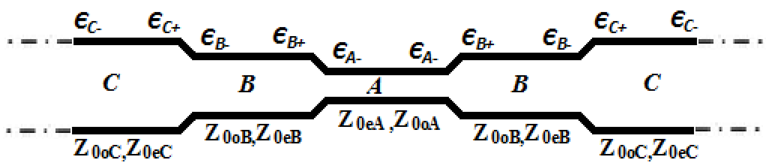

Figure 4.22: Schematic of the n-element coupled lines section.

The increment and decrement required in the length of any arbitrary element-x of impedance Z_{0ox},Z_{0ox}, can be written as

$$\epsilon_{x^-} = \frac{Y_{j0ex^-} l_{x^-}}{Z_{0ox}(1 - Z_{0ox}^2)}, \quad \epsilon_{x^+} = \frac{Z_{0ex} Z_{j0ex^+} l_{x^+}}{(Z_{0ex}^2 - 1)}. \tag{4.51}$$

Where, Y_{j0ex^-} is the even mode admittance, l_{x^-} is length of the junction and ϵ_{x^-} is the decrement to be made in the length of element-x. Similarly, Z_{j0ex^+} is the even mode impedance, l_{x^+} length of the junction and ϵ_{x^+} is the increment to be made in the length of element-x.

4.7 Application of modified theory in design of 3-element, 8.34±0.2dB coupled section

The 8.34±0.2dB coupled section uses element-A and element-B of even mode impedance $Z_{0eA} = 1.7848$ and $Z_{0eB} = 1.07434$ i.e normalized with $Z_0 = 50\Omega$. The strip-line junctions of even mode impedance $Z_{j0e} = 1.312$ and length $\lambda_0/80$ at center frequency 75MHz is employed to connect element-A and element-B. For the compensation of junction discontinuity effect ϵ_{A^-} and ϵ_{B^+} are calculated as

$$\epsilon_{A^-} = \frac{Y_{j0e}l}{Z_{0oA}(1 - Z_{0oA}^2)}$$

Where $l = \lambda_0/80$ at center frequency. That gives

$$\epsilon_{A^-} = \frac{Y_{j0e}l}{Z_{0oA}(1 - Z_{0oA}^2)} = \frac{0.56028 \times (\lambda_0/80)}{0.56028(1 - 0.56028^2)} = 0.0248\lambda_0.$$

Now,

$$\epsilon_{B^+} = \frac{Z_{0eB}Z_{j0e}l}{(Z_{0eB}^2 - 1)} = \frac{1.07434 \times 1.312 \times (\lambda_0/80)}{(1.07434^2 - 1)} = 0.015265\lambda_0 = 0.015265.$$

Now making use of Eqn.4.50, θ_a and θ_b can be calculated as

$$\begin{aligned} \theta_a = \left(\frac{2\pi}{\lambda}\right)(0.0248\lambda_0) &= (2 \times 0.0248\pi)\left(\frac{\lambda_0}{\lambda}\right) \\ &= (0.0496\pi)\left(\frac{\theta}{\theta_0}\right) \\ \text{using same procedure} \;\; \theta_b &= (0.03053\pi)\left(\frac{\theta}{\theta_0}\right). \end{aligned}$$

Where $\theta_0 = \pi/2$. Using Eqn.4.49, b_{3m} is calculated and plotted using MATLAB and is shown in Fig.4.23.

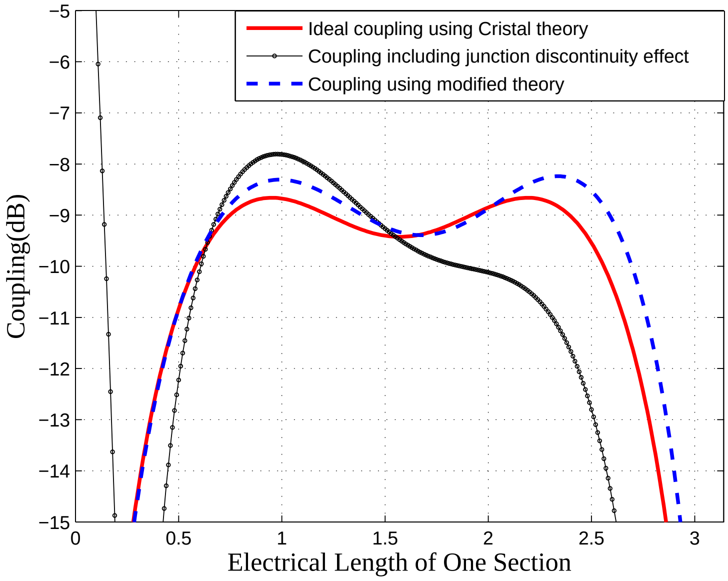

Figure 4.23: Comparison of the calculated coupling of the 3-element, 8.34±0.3dB coupled line section using MATLAB.

The coupling performance using modified theory is found in agreement to the ideal coupling using Cristal theory as shown in Fig.4.23. To verify the effectiveness of the modified theory, calculated modification is incorporated in model used HFSS simulation and simulation is performed. The perspective comparison of coupling and output S-parameters obtained from the HFSS simulation and theoratically calculted parameters using modified theory is shown in Fig.4.24 and Fig.4.25, where effectiveness of the modified theory is proven.

Note:-Junction discontinuity effect is derived in terms of capacitance or inductance values. These derived values are also useful for the previous method, where junction discontinuity effect is compensated using capacitor or open stub. Therefore junction

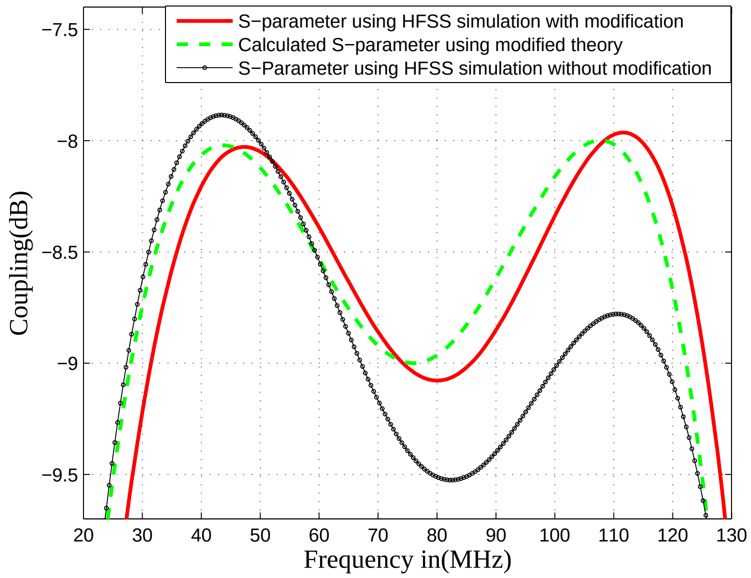

Figure 4.24: Comparison of coupling results obtained from HFSS simulation and modified theory.

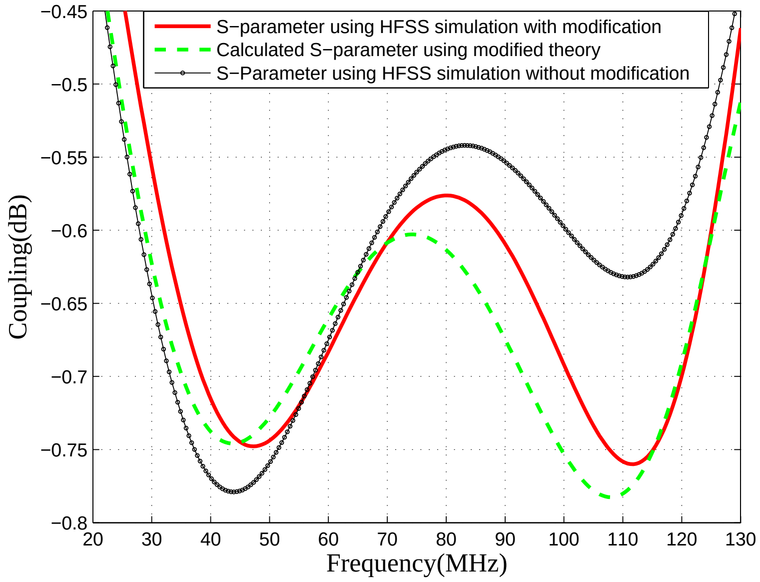

Figure 4.25: Comparison of output results obtained from HFSS simulation and modified theory.

discontinuity analysis is also useful for other available compensation techniques. Modified theory is a simple approach by which junction discontinuity effect can be compensated without increasing the structure complexity.

4.8 Results and Discussion

Junction discontinuity effect is comprehensively investigated while designing of 3-element, 8.34±0.2dB coupled line section. Coupling and output S-parameters obtained from HFSS simulation are seen deviated from the expected results due to junction discontinuity effect. The left and right extremes in coupling performance are found 7.56dB and 8.87dB as shown in Fig.4.9 whereas its magnitude decreases continuously. This effect is also observed in the output S-parameters where magnitude is found increasing in the prescribed band. The left and right extremes of the output parameters are found −0.835dB and −0.63dB as shown in Fig.4.9. Both the maxima of the coupling and output S-parameters should be equal in the prescribed bandwidth whereas these are seen unequal due the effect of junction discontinuity. The simulated coupling performance for element-A and element-B as shown Fig.4.7 and Fig.4.8 are found in close agreement to the calculated values i.e. 6.15dB and 22.54dB. This shows that element-A and element-B are perfectly designed. Therefore, undesirable effect of the junction discontinuities is confirmed. A generalized theoretical procedure has been developed where analytical equivalence of junction discontinuity effect is derived for the known parameters. The equivalent of junction discontinuity parameter is incorporated into Cristal theoretical tabulated parameters for 3-element, 8.34±0.2dB coupled line section and coupling S-parameters are calculated as shown in Fig.4.15. The calculated left and right maxima of coupling parameter of 3-element coupled line section are deviated

from the Cristal theoretical results and deviation is found in same manner as simulated results, shown in Fig.4.9.
To include the junction discontinuity parameter at the designing stage, a modified theory has been developed. The 3-element, 8.34±0.2dB coupled line section is designed by using modified theory and the calculated results are shown in Fig.4.23. Both the maxima i.e. approximately 8.25dB are found equal and result verifies the Cristal equal ripple theory outcomes. To verify the effectiveness of the modified theory, calculated modification is incorporated in HFSS simulation of 8.34±0.2dB coupled line section. In simulation results, left and right maxima of the coupling performance are found 8.15dB and 8.1dB respectively as shown in Fig.4.24 where in output performance same are found −0.74dB and −0.765dB respectively i.e. shown in Fig.4.25. Here it can be seen that HFSS simulation results are found in close agreement to expected results.

4.9 Conclusion

Junction discontinuity effect on multi-element coupled lines performance and its diminution is presented using novel theoretical approach. The reactive effect of junction discontinuity is derived and incorporated with even and odd modes analysis of the coupled element where negative effect of junction discontinuity on S-parameters of 3-element coupled lines section is presented and verified with the HFSS simulation result. Modified theory is explored, applied and proven effective in compensation of the junction discontinuity effect. The modified theory is also generalized for n-element coupled lines section. Using developed theoretical approach, junction parameters can be included in Cristal theory where tabulated even mode impedances of coupled elements can be optimized for specified junction parameter. It is expected that the developed modified theory will help in the design of high power hybrid couplers.

5

Design and development of ultra-wideband 3dB hybrid coupler for ICRF heating in tokamak

5.1 Introduction

In privious chapter an analysis of the broadband multi-element coupled lines in conjuction with junction discontinuity effect is presented. The junction discontinuity effect deteriotes the performance of the multi-element coupled lines and the deterioation in terms of coupling and output performances are studied. For the high power handling capability coupled lines system generially be oversized. As the size of the system increses, the discontinuity effect become prominant which deteriorates the performance in such a way the one can not achive the disired performance without considering of it at the designing stage. Modified theory for the compensation of junction discontinuity effect is proposed which takes into account of it at the designing stage.

In this chapter, design and development process of a 200kW, 3dB tandem hybrid coupler for 38 to 112MHz frequency range is presented. The modified theory for the compensation of the junction discontinuity effect is revisited and compensation is applied in designed model. The fabrication of the designed model is performed where broad side coupled strip-line conductors are arranged in a particular configuration and placed in the grounded metallic enclosure. Air as dielectric is used to minimize the insertion loss. The central conductors are supported with the acrylic studs. The dielectric stud induces the capacitive discontinuity. The discontinuities effect due to the junction and supporting studs are compensated using the modified theory. The fabricated model is characterized and tasted, where obtained results are found in close agreement with the calculated ones, which take into account the effect of the discontinuities. The experience with concept, design and development procedure have imparted sufficient knowledge that one can utilized it in the development of the broadband hybrid couplers for the high power applications in HF, VHF and UHF band.

The concept, design and simulation of 3$\pm$0.2 hybrid coupler is described in Section-5.2. Analysis of the discontinuities in coupled lines and it,s compensation are explained in section-5.3 and 5.4 respectively. Application of compensation theory in design of proposed 3$\pm$0.2 hybrid coupler and its optimization with supporting studs is presented in section-5.5. Fabrication process, results and discussion are explained in section-5.6 and section-5.7 respectively. Finally, conclusions are given in section-5.8.

5.2 Concept, design and simulation

Design and development process of a ultra-wideband 3±0.2dB tandem hybrid coupler of 200kW power handling capability and 38 to 112MHz frequency range is presented. For overall 3±0.2dB of coupling, two 8.34±0.1dB TEM broadside coupled strip-line sections are connected in tandem so that wider coupling gap can be provided i.e. essential for 200kW power handling capability. As we diacussed that the multi-octave bandwidth can be achieved by means of cascading several quarter-wavelength elements. Therefore each of the 8.34±0.1dB coupled section are designed with 3-elements to achive the desired bandwidth. The top and cross section view of the proposed 3dB hybrid coupler is shown in Fig.5.1. It consists of two stepped strip-line central conductors which are arranged one above other and placed in the grounded metallic enclosure. Air as dielectric is used to minimize the insertion loss. The central conductor is supported with the acrylic studs. The structure drawing shown in Fig.5.1 has symmetry along the line L and one of the symmetrical portions represents 8.34±0.1dB coupled line section. Each of the 8.34 ± 0.1dB coupled line section consists of element-B, element-A and element-B in series where junction of length l is physically employed for joining of these elements. Privious theory [20] has been utlized for the designing of the 8.34 ± 0.1dB coupled section, where coupling coefficient for element-A and element-B, calculated as $C_A = 0.5222 = -6.123$dB and $C_B = 0.07074 = -22.896$dB respectively. Two 8.34 ± 0.1dB sections are connected in tandem with 50Ω connecting lines(shown as C.Lines in Fig.5.1) to get the desired coupling of 3 ± 0.2dB.

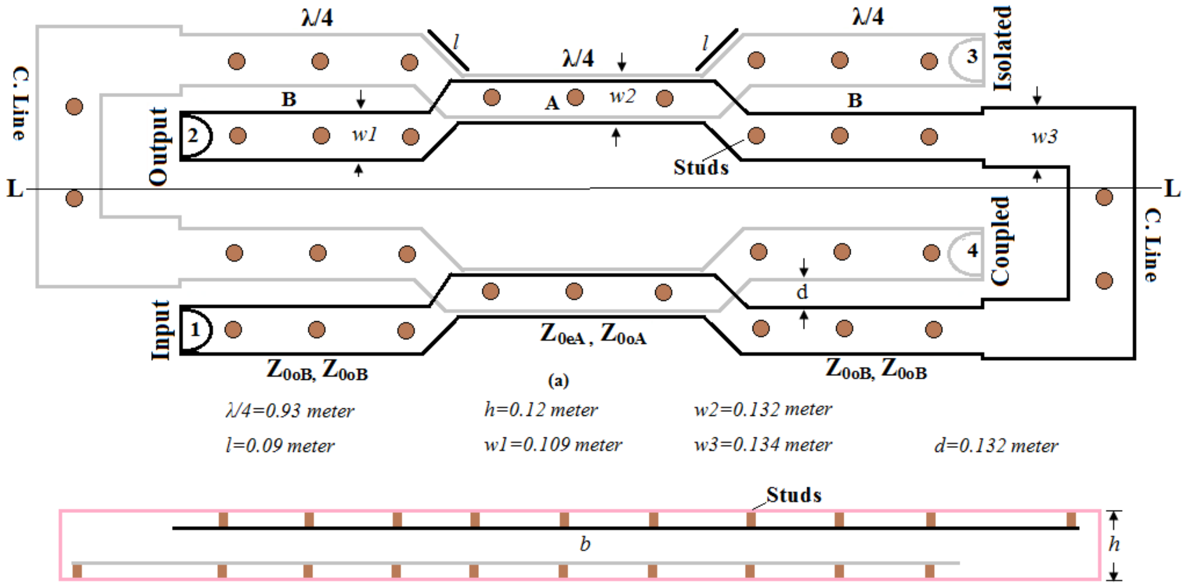

(b)

Figure 5.1: Perspective top and cross section view of the proposed 3 ± 0.2dB hybrid coupler.

HFSS Simulation results of the designed model

Structural design parameters of element-A, element-B and 50Ω connecting lines as shown in Fig.5.1 are calculated using known equations [11,35,44] and the resulting model is simulated with HFSS software. The earlier theory [20] states that the coupling and output parameters of the multi-element coupled lines should represent equal ripple graph in frequency band, where both the maxima/minima should be equal with specified value of tolerance. In the simulation results, these parameters are found significantly deteriorated from the theoretical prediction, as shown in Fig.5.2. The maxima at upper and lower end of the frequency band are seen to be unequal including significantly low minima. The discrepancy is investigated and found associated with the reactive effect of discontinuities in the coupled lines.

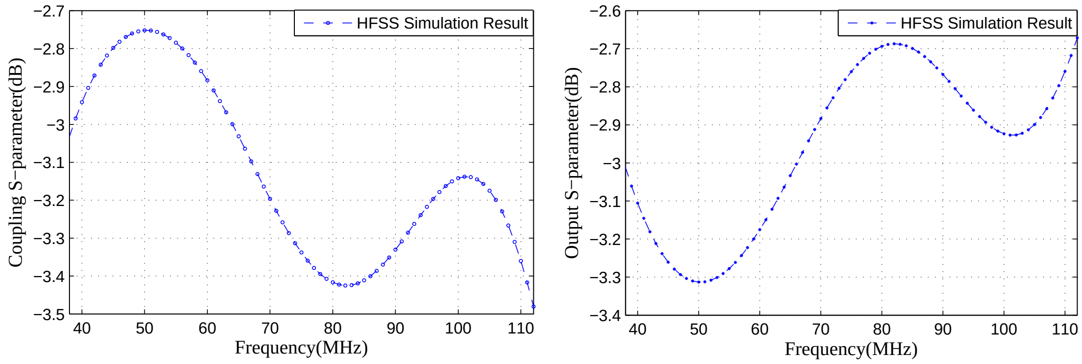

Figure 5.2: Simulation results in terms of S-parameter.

5.3 Analysis of discontinuities in the coupled lines

5.3.1 Discontinuity due to junction

Schematic of the 3-element coupled line section including junction of length l is shown in Fig.5.3. The effect of junction discontinuity in 3-element coupled lines section can be estimated as lumped reactance that may be series inductance and shunt capacitance [52]. Including this estimation, electrical equivalent of the given 3-element coupled lines section for even and odd modes are shown in Fig.5.4

As described in previous section, each of the element are designed for the specified

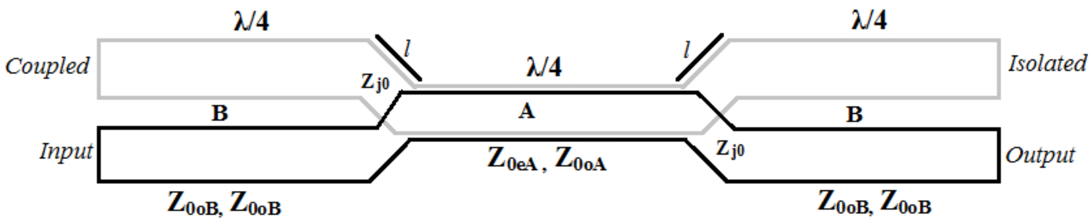

Figure 5.3: Schematic of 3-element coupled lines section.

value of even and odd mode impedance. Therefore, the estimation of the junction

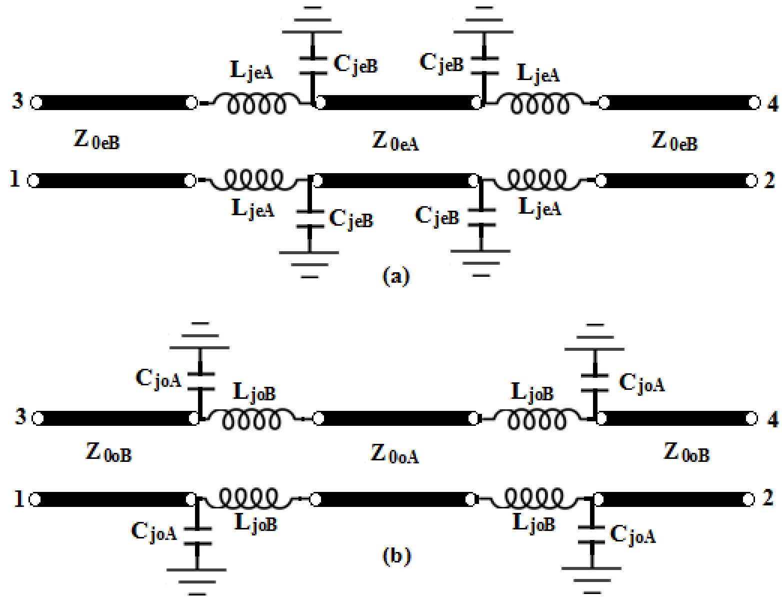

Figure 5.4: Equivalent of 3-element coupled lines section including junction discontinuity effect in (a) Even mode (b) Odd mode.

discontinuity effect on the each of the element-A and element-B is made separately. In case of element-A, the parameters L_{jeA} and C_{joA} represent the junction discontinuity equivalent inductance in even mode and capacitance in odd mode respectively. Similarly, in case of element-B, the parameters C_{jeB} and L_{joB} represent the junction discontinuity equivalent capacitance in even mode and inductance in odd mode respectively [52]. These can be expressed as follows:

$$L_{jeA} = C_{joA} = Z_{j0e} l / v,$$
$$L_{joB} = C_{jeB} = l / (Z_{j0e} v). \tag{5.1}$$

Where, Z_{j0e} and v are the junction even mode impedance and velocity of propagation of wave respectively. The analysis with the help of Fig.5.4 implies following facts:

1. The junction discontinuity effect is estimated in terms of the lumped reactance which deteriorates the even and odd mode impedance. Consequently, coupling and output parameters also altered.

2. Effective impedance $Z_{eB_{(eff)}}$ of the element-B and admittance $Y_{eA_{(eff)}}$ of element-A including junction discontinuity effect [52] can be given by,

$$
\begin{aligned}
Z_{eB_{(eff)}} &= Z_{in(eAQ)} \approx Z_{0eB} + jZ_{j0e}\beta l, \\
Y_{eA_{(eff)}} &= Y_{in(eBP)} \approx Y_{0eA} + jY_{j0e}\beta l.
\end{aligned} \tag{5.2}
$$

   From the above expression it can be analyses that junction discontinuity effect produces an additional reactance of $jZ_{j0e}\beta l$ with element-B and $jY_{j0e}\beta l$ with element-A which increases effective impedance and admittance of element-B and element-A respectively. These variation are directly proportional to the operating frequency and length of the junction.

3. Hence, junction discontinuity effect increases the effective even mode impedance of element-B and decreases the effective impedance of the element-A. The resultant effect causes coupling parameter decreases with increasing the frequency and both the maxima at upper and lower end of the frequency band become unequal including significantly low minima in the 3-element coupled line section.

The effect of the junction discontinuity is demonstrated analytically in privious chapter. To study the effect of junction discontinuity by increasing the junction length, a 3-element 8.34dB coupled lines section has been designed and simulated using software HFSS. Initially, lengths of the element-A and element-B are taken as quarter wavelength at the center frequency 80MHz where junction length $l =$

0.09*meter*. By making the variation in junction length in step of $\epsilon = 0.02meter$ simulation is performed. Result obtained from simulation is shown in Fig.5.5, which indicates that deterioration in coupling parameter become more significant with increasing the length of junction.

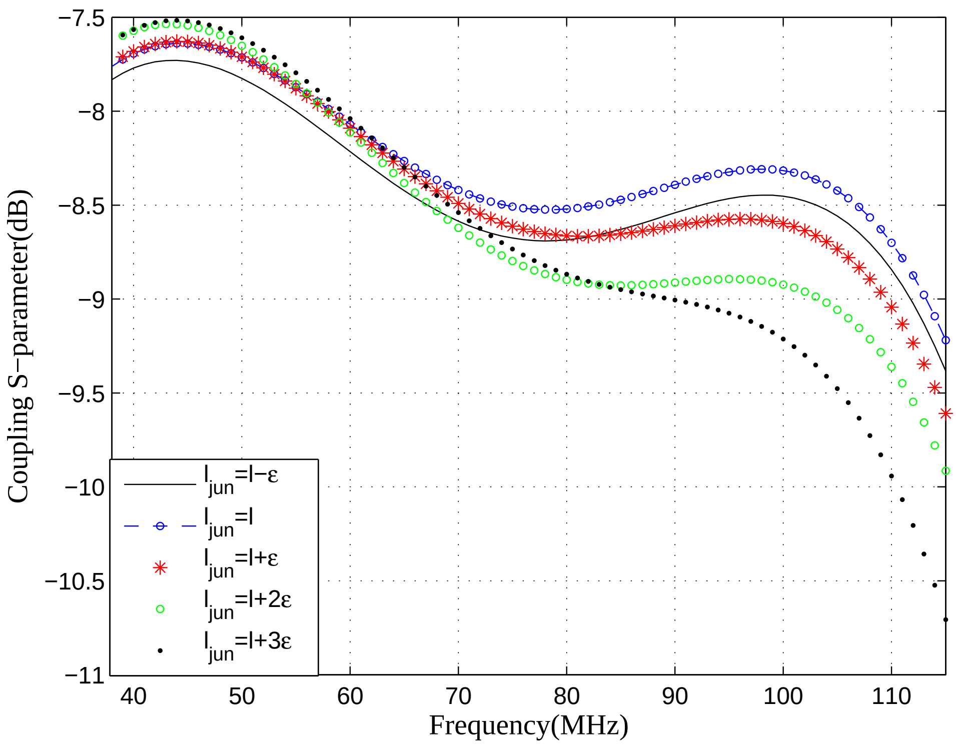

Figure 5.5: Coupling performance of the 3-element 8.34dB coupled lines section by varying length of the junctions.

5.3.2 Discontinuity due to Supporting Studs

Air as dielectric is used to minimize the insertion loss. The central conductor are supported by the dielectric studs that introduce additional capacitive discontinuity in the coupled line section. Capacitive reactance due to the supporting dielectric stud, X_{stud} that is given as

$$X_{stud} = 1/2\pi f C_{stud} \tag{5.3}$$

5.4 Compensation Theory for the junction discontinuity

Compensation of the junction discontinuity effect in element-B and element-A can be done by adding capacitive reactance X_C and inductive admittance Y_L explained in privious chapter and $Z_{B_{(eff)}}$ and $Y_{B_{(eff)}}$ are written as,

$$\begin{aligned} Z_{B_{(eff)}} &= Z_{0eB} + jZ_{j0e}\beta l + jX_C, \\ Z_{A_{(eff)}} &= Y_{0eA} + jY_{j0e}\beta l + jY_L. \end{aligned} \tag{5.4}$$

To provide the X_C and Y_L for the need full copensatation modified theory can be applied. As per modified theory, junction discontinuity effect can be compensated by incorporating the appropriate alteration in element-B and element-A. To demonstrate the fact a 3-element 8.34dB coupled lines section has been designed and simulated using HFSS. Initially, length L_A of element-A and L_B of element-B are taken as quarter wavelength at 80MHz. As per compensation theory, variation in length of element-A and element-B has been done by incrementing in L_B and decrementing in L_B in step of $\epsilon = 0.02meter$. For constant junction length of $l = 0.09meter$, the results obtained from this variation are shown in Fig.5.6. The results shows, the proposed variation in the length of the elements give the oppositive or corrective effect to the junction discontinuity. So the compensatation can be made by appropriate alteration in element-A and element-B.

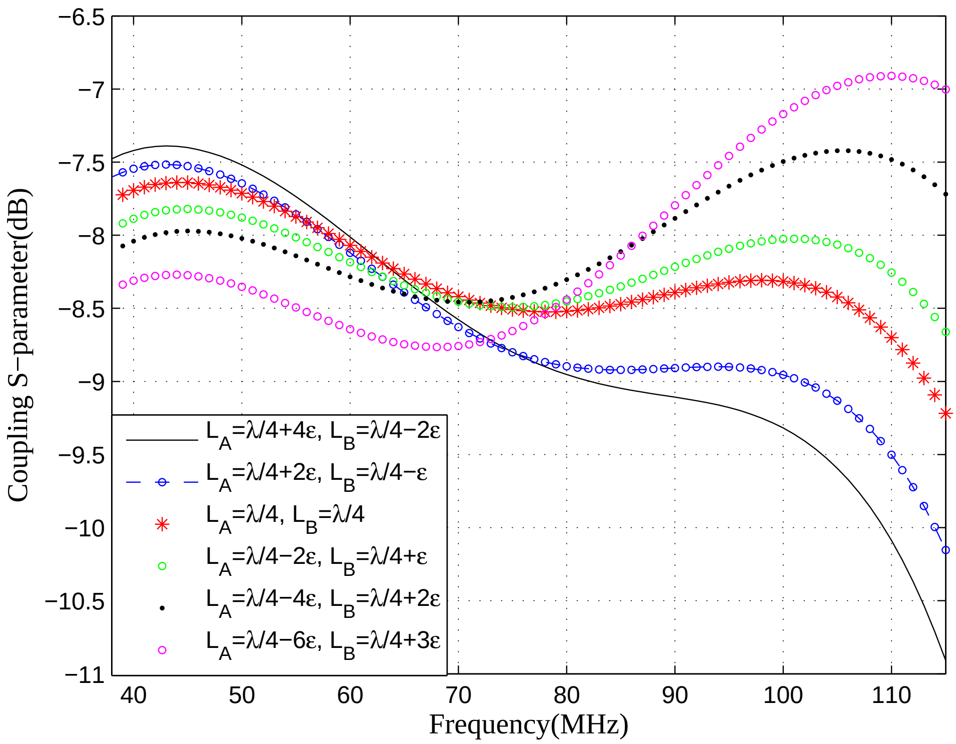

Figure 5.6: Coupling performance of the 3-element 8.34dB coupled lines section with varying length of the elements.

5.5 Junction discontinuity effect compensation and optimization including supporting studs

The discontinuity due to supporting studs must also be included along with junction discontinuity effect for effective compensation so that desired coupling parameters can be obtained practically. The supporting insulating studs induce an additional discontinuity in terms of capacitive reactance. The analysis of the stud

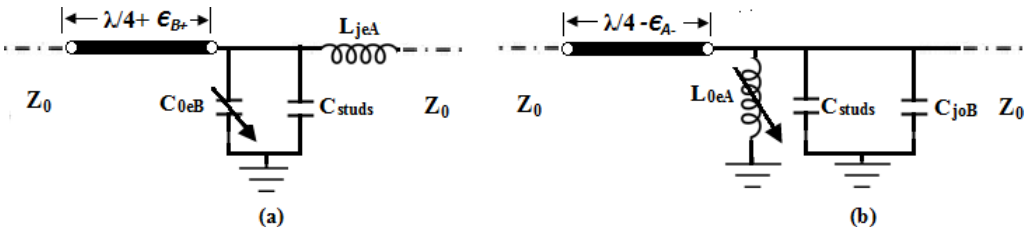

Figure 5.7: Even mode equivalent of altered elements including the effect of discontinuities for (a)Element-A (b)Element-B.

discontinuity effect on element-A and element-B and the possible compensation can be evaluated with the help of Fig.5.7 Even mode impedance of element-B including supporting stud and junction discontinuities can be written as,

$$Z_{0eB} = \sqrt{\frac{X_{j0eB}}{(Y_{0eB} + Y_{studsB})}}. \tag{5.5}$$

The value of ϵ_{B+} i.e. overall compensating increment in the length of element-B by using Eqn.5.3, Eqn.5.4 and Eqn.4.38 can be written as

$$\epsilon_{B+} = \frac{1}{\beta Y_{0eB}\,(1 - Y_{0eB}^2)} \left[\frac{Z_{j0eB}\beta l}{Z_{0eB}^2} - Y_{studB} \right]. \tag{5.6}$$

Even mode impedance of element-A including supporting stud and junction discontinuities can be written as,

$$2\pi f \sqrt{L_{0eA}(C_{jeA} + C_{studsA})} = 2\pi f \sqrt{X_{0eA}(Y_{jeA} + Y_{studsA})} = 1. \tag{5.7}$$

The value of ϵ_{A-} i.e. overall compensating decrement in the length of element-A by using Eqn.5.3, Eqn.5.4 and Eqn.4.44 can be written as

$$\epsilon_{A-} = \frac{(Y_{j0e}\beta l + Y_{studsA})}{Z_{0oA}(1 - Z_{0oA}^2)}. \tag{5.8}$$

This compensation theory including discontinuities due to junction and supporting studs is applied to the proposed 3-element, 8.34±0.2dB coupled section. The design parameters of the proposed 3-element coupled section are given as,
wavelength at central frequency is $\lambda = 3.48meter$, length of the junction is $l = 0.09meter$, capacitance of the studs in element-B is $C_{B(studs)} = 4.806pF$, capacitance of the studs in element-A is $C_{A(studs)} = 3.204pF$, even mode impedance of element-A is $Z_{0eA} = 1.7848$ and of element-B is $Z_{0eB} = 1.07434$. These parameters are used in Eqn.5.7 and 5.8 to calculate ϵ_{B+} and ϵ_{A-}. The calculated values are $0.014429\lambda_0$ and $0.07587\lambda_0$ respectively. These modifications are incorporated in model and simulation is performed using HFSS software. In simulation results as shown in Fig.5.8, it can be seen that after including the modification both the maxima/minima in coupling and output parameter of are become equal and represents the equal ripple graph in the frequency band as earlier theory prescribes [20]. This displays the significance of the compensation theory presented herein.

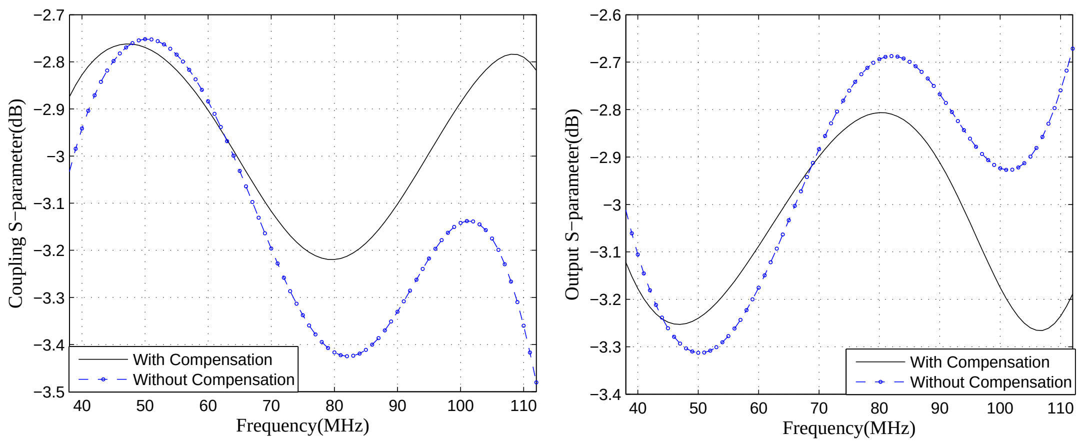

Figure 5.8: Perspective comparison of HFSS simulation results with compensation and without compensation

5.6 Fabrication Process

Designed 3dB tandem hybrid coupler is fabricated with two stepped U-shaped 3mm thick copper strip-line inner conductors that are overlapping in opposite directions.

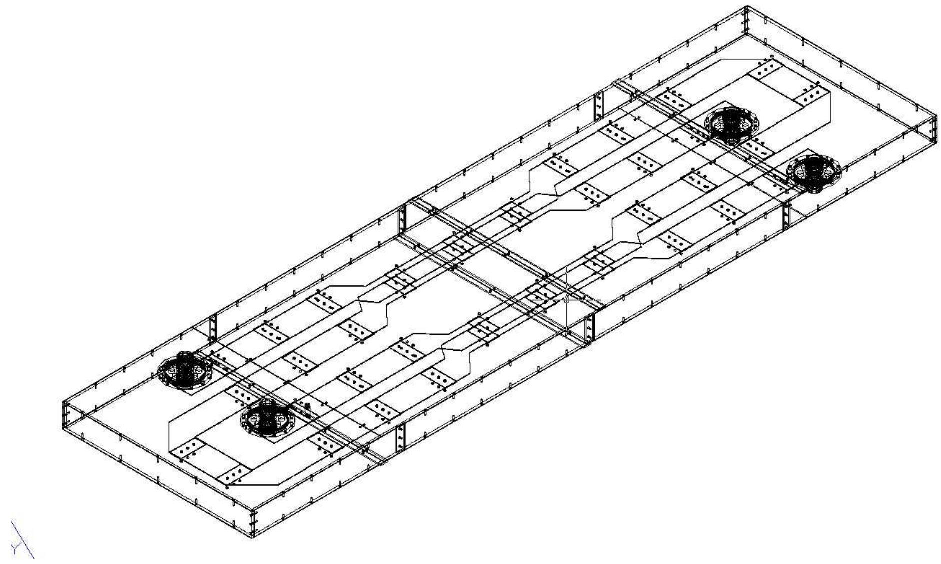

Figure 5.9: Super-view of the assembly drawing of the hybrid coupler

Stepping in U-shaped strip has been made in such a way that its overlapping provides the complete structural configuration of element-A, element-B and connecting lines as per calculation. The strip-widths of the coupled element-A, element-B and connecting lines are taken as 10.9cm, 13.2cm and 13.6cm respectively. The outer conductor rectangular box of inner dimensions $360cm \times 100cm \times$ 12cm is fabricated with the aluminum sheet of $3mm$ mounted on the suitable frame. All of the four ports are made to provide 6inch standard 50Ω coaxial transmission line as the termination. Super-view of the assembly drawing is shown in Fig.5.9, while inner assembly of the fabricated hybrid coupler is shown in Fig.5.10.

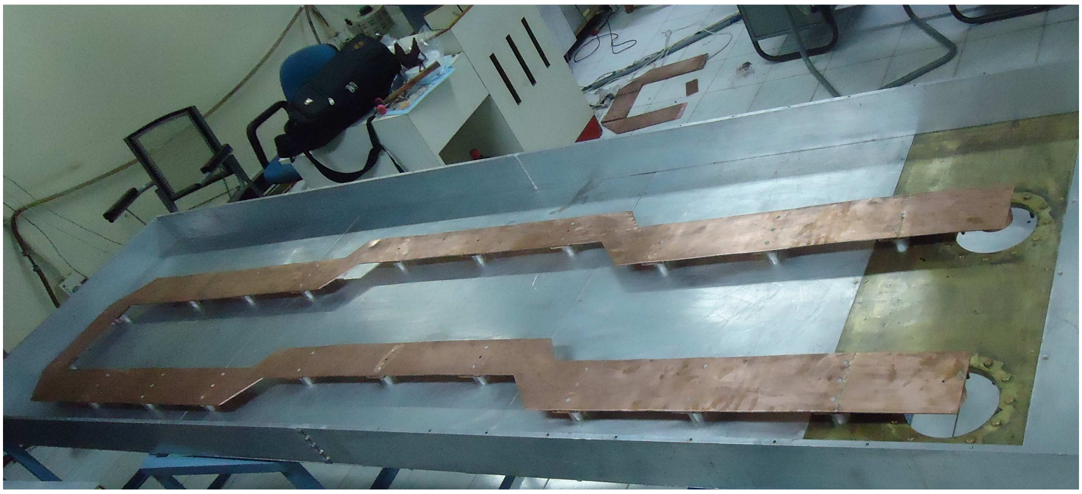

Figure 5.10: Photograph of the fabricated hybrid coupler inner assembly

5.7 Results and discussion

5.7.1 Testing with vector network analyzer(VNA)

A 200kW, 3 ± 0.2dB tandem hybrid coupler has been designed for the frequency range of 38 to 112MHz. The designed model is simulated with the HFSS software. Simulation results are found deviated from the theoretical prediction due to inherent discontinuities. The maxima at upper and lower end of the frequency band are seen to be unequal and displays significantly low minima as shown in Fig.5.2. For compensation of the discontinuities effect, a theoretical procedure has been developed and incorporated in the designed model. Simulation of the compensated model is performed and obtained results are shown in Fig.5.8. The compensated model provides a coupling of -3 ± 0.25dB, output of -3 ± 0.25dB, return loss less than 30dB and isolation value less than -29dB in the frequency range of 38-112MHz. The designed model has been fabricated and tested with vector network analyzer(VNA). The VNA measured parameters in comparison with the HFSS simulation results are shown in Fig.5.11. Test results of the fabricated hybrid coupler provide a coupling of -3 ± 0.2dB, output of -3 ± 0.2dB, return loss less than 27dB and isolation value less than -27dB in the prescribed frequency range.

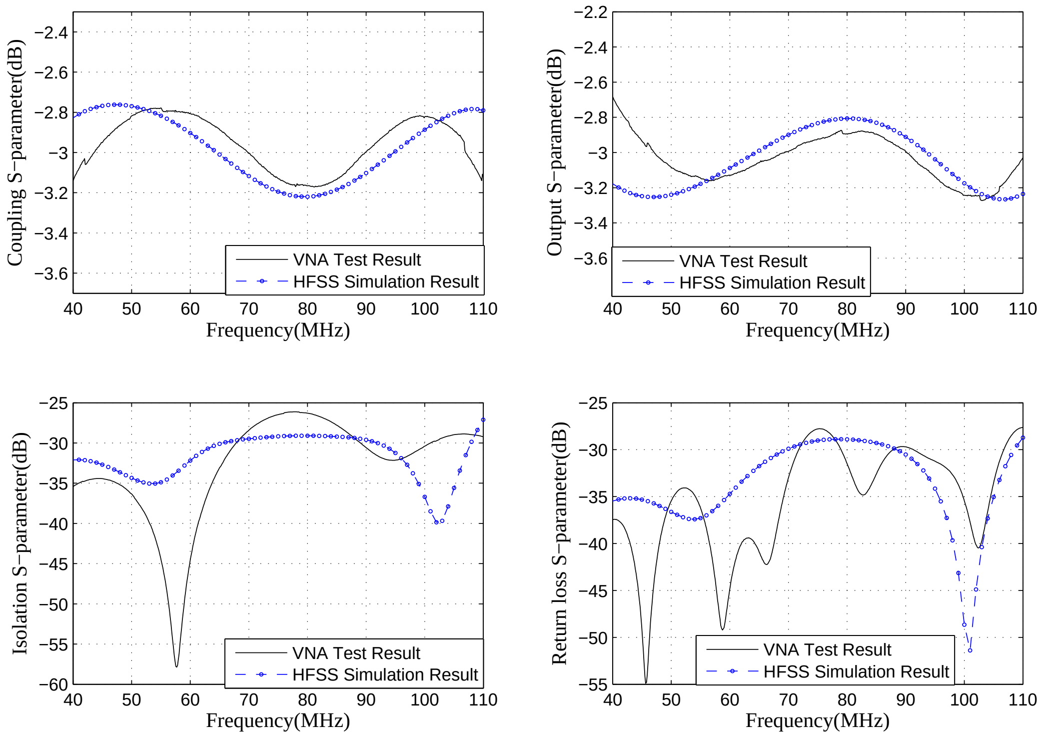

Figure 5.11: Comparison of VNA test Results and HFSS simulation Results

5.7.2 Testing Using 1kW, 91.2MHz cwrf Source

The cwrf power test is conducted with the available 91.2MHz source rated at 1kW. Schematic diagram of cwrf power test setup and resulting waveforms at the input, output, coupled and isolated port are shown in Fig.5.12 and Fig.5.13 respectively. With 800*watt* input, power measured at output coupled and isolated port are

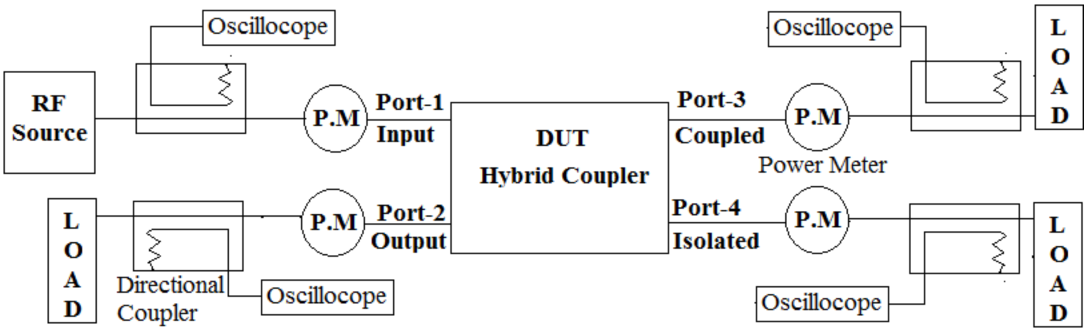

Figure 5.12: Schematic of the cwrf test setup

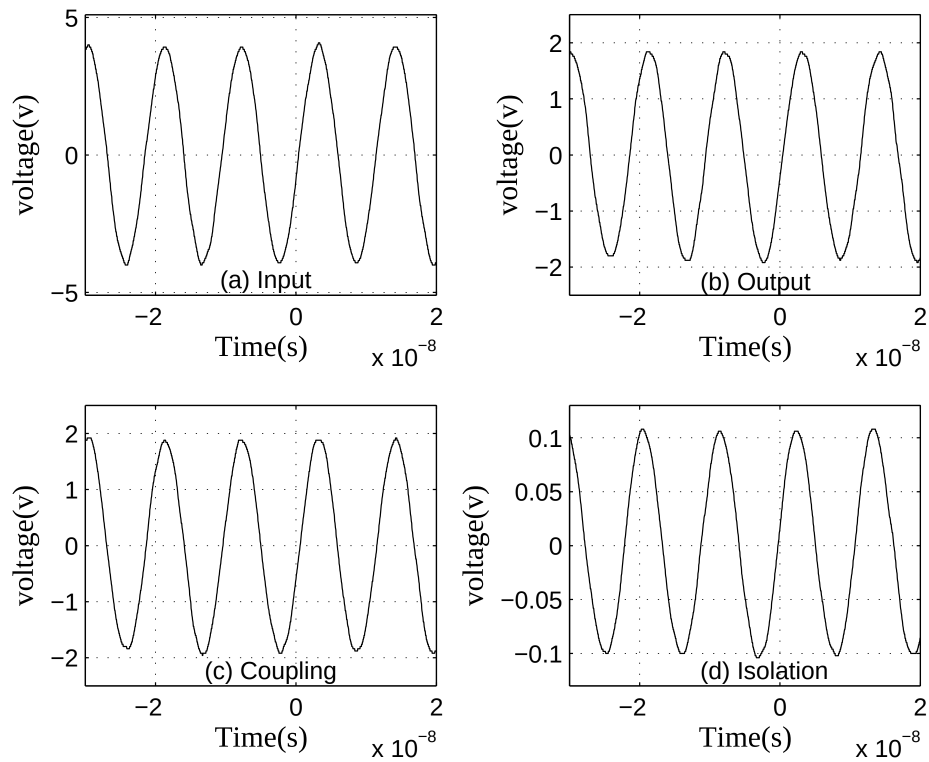

Figure 5.13: Measured cwrf voltage waveforms (a) Input (b) Output (c) Coupling (d) Isolation

392*watt* 405*watt* and 1.5*watt* respectively. Directional coupler along with oscilloscope are connected to obtain sample of forward going power at the input, output, coupled and isolated ports. Voltage waveforms obtained from oscilloscope represent the coupling of 2.95dB, output of 3.105dB and isolation of 27dB at 91.2MHz. The outcomes of this testing confirms to the VNA test results within the tolerance limit at 91.2MHz.

5.7.3 DC Breakdown Testing

The peak power handling capability of the developed hybrid coupler is estimated with insulation resistance breakdown testing between the coupled strip-line conductors and the strip-lines to ground conductor each. The dielectric supporting studs between strip-line conductor and ground outer conductor is the limiting factor due to surface arcing at higher electric field.

Insulation resistance testing between strip-line to ground conductor is performed at $12kV_{dc}$ without any significant leakage current or arcing. This is equivalent to $5.88kV_{rf(peak)}$ [31] i.e. 346kW rf power rating. Average power handling capability of the strip-line must also be confirmed with dielectric and ohmic losses which are responsible for rise in temperature [11]. Device may be used at 350kW average power with $10°C$ rise in temperature from the ambient temperature of $35°C$. Thus, the developed hybrid coupler can handle the 200kW rf power within vswr of 1.73 (if exist) due to mismatch at other ports.

5.8 Conclusion

Design and development process of a 200kW 3-element, 3dB tandem hybrid coupler is presented and its applicability in ICRF heating of the tokamak is discussed. Use of multi-element coupled lines in tandem become essentials at the desired broadband in the high power application. Junction discontinuity effect significantly deteriorates the performance of the multi-element couped lines is comprehensively investigated and explained. For the compensation of the junction discontinuity effect, a theoretical procedure has been developed and generalized for n-element coupled lines section. The same theory is utilized and found effective in optimization of the central conductor supporting studs that induces capacitive reactance. The compensation for observed discontinuity is applied in the development of proposed model, where significance of theory is highlighted. Developed hybrid coupler provides the optimum performance in the prescribed frequency band. The experience with concept, design and development procedure have imparted sufficient knowledge for up-gradating the hybrid coupler to higher power levels in the broadband application. This is planned to develop a 3dB hybrid coupler for 1.5MW power in the frequency range of 30 to 95MHz, particularly for the ion cyclotron resonant heating systems in various tokamaks.

6

Design and development of ultra-wideband 3dB hybrid coupler for ICRF heating in fusion grade reactors

6.1 Introduction

In previous chapter, design and development of a 200kW, 3dB tandem hybrid coupler for 38 to 112MHz frequency range is presented. The modified theory is applied and successfully compensated the junction discontinuity effect [53]. The device is fabricated and tasted for the desired performance. This work has imparted sufficient experience that can be utilized while making of ultra-wideband 3dB hybrid coupler for HF and VHF [53].

In this chapter our objective is to design a hybrid coupler for 1.5MW power handling capability in frequency range of 30 to 96MHz for ICRF heating in fusion grade reactor. The peak power handling capability is limited by the maximum voltage that can be applied without causing dielectric breakdown. Here, air is utilized as a dielectric. At the atmospheric temperature and pressure the breakdown strength of dry air is approximately 30.0kV/cm [16, 31]. Thus, the maximum electric field on inner strip and hence maximum power handling capability is restricted by coupling gap and gap between lines to ground. Therefore, spacing between conductors is needed to be higher for the high power handling capability. Thus, coupled lines cross-section become larger. The maximum permissible spacing is governed by the onset of TE and TM modes [17]. To restrict the lowest order TE modes, average circumferential distance of coupled cross-section must not be exceeded about one wavelength. The mode conversion from TEM to TE or TM modes represents a source of power loss and resulting deterioration in coupling, output, return loss and isolation characteristic. As permissible limit of the gaps are restricted hence the power handling capability. The problem must be alleviated. In this chapter our objective is to achieve the spacing and coupling gap beyond maximum permissible limit so that design of proposed 1.5MW ultra-wideband hybrid coupler may be possible.

Section-6.2 explains the multi-element coupled lines in ultra-high power application. The concept design and simulation of the designed 1.5MW hybrid coupler are described in section-6.3. The fabrication drawings are illustrates in section-6.4 while simulation results have been discussed in section-6.5. Finally, conclusion is presented in section-6.6.

6.2 Multi-element coupled lines in ultra-high power application

In multi-element coupled lines wider bandwidth is achieved by cascading several sections of the coupled lines, each section having an electrical length $\theta = \pi/2$ at center frequency. The bandwidth increases with increase in the number of elements. The odd numbers of the coupled element are cascaded in symmetrical configuration where middle element is more tightly coupled as compared to the side one. Structural configuration of the coupled lines can be selected on the basis of coupling values. The schematic of the 8.34dB, 3-element coupled lines section is shown in Fig.6.1. Power handling capability of the coupled transmission lines can be increased with increase in gap/spacing and hence resulting parameters like junction length strip-width also increase. The significance of the structural changes with power handling capability can be clarified with aid of Fig.6.1 where subsection (a) and (b) define the structural changes of 3-elements coupled line section for low and high power.

In previous chapter, effect of junction discontinuity is studied and found more significant at high power because of larger structural dimensions of the coupled lines. A theoretical procedure has been developed for the compensation of this effect. The theory is applied in development 200kW ultra-wideband hybrid coupler and found effective. The higher modes of TE and TM can propagate at higher frequencies due to increase in dimension of the strip-line beyond the certain limit. This should be avoided because mode conversion from TEM to TE or TM modes represents a source of power loss. Hence system experiences the increase of the return loss and isolation while increasing the spacing and strip-width beyond permissible limit.

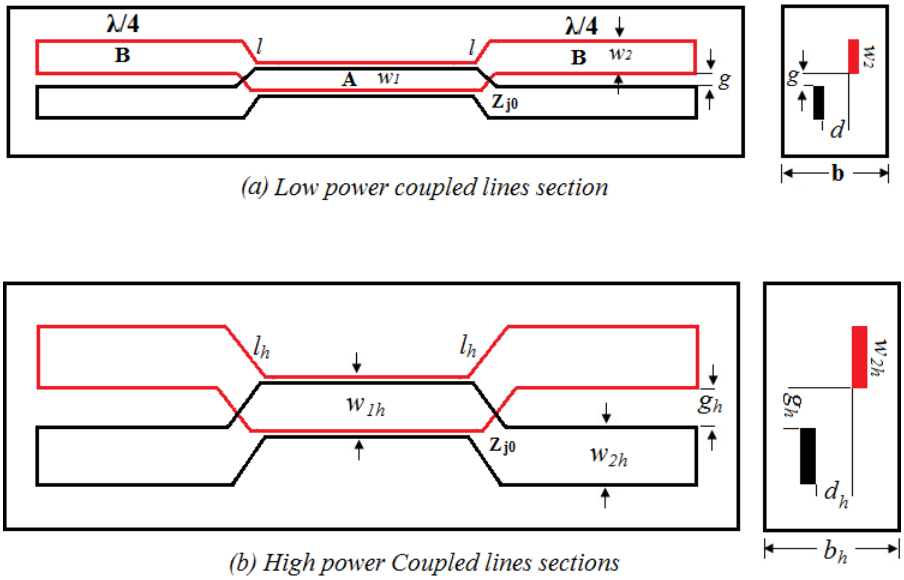

Figure 6.1: Schematic of the (a)top and side view of low power, (b)top and side view for high power multi-element coupled lines.

Thus, the structural size of the coupled lines can not be increased beyond certain value. The TM is not propagated in case the strip-line of impedance $Z_0 \leq 120$ and $(w/b \geq 0.215)$ for HF and VHF range. Therefore only TE mode is considered herewith. The lowest order TE mode can propagate when the spacing b, d and

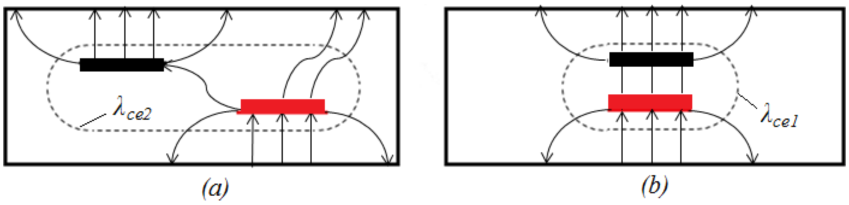

Figure 6.2: Electric field lines for lowest TE modes in (a)Element-B and (b)Element-A

strip-width w are such that the average circumferential distance as indicated by the dotted line in Fig.6.2 exceed about one wavelength. The cut-off wavelength of

TE mode i.e. λ_{ce} can be expressed in terms of strip-line parameters as [44],

$$\begin{aligned}\lambda_{ce(A)} &= \sqrt{\epsilon_r}\left[2w_1 + 2\pi(d+2t)\right], \\ \lambda_{ce(B)} &= \sqrt{\epsilon_r}\left[4w_2 + 2g + 2\pi(d+2t)\right]\end{aligned} \tag{6.1}$$

Thus, TE mode cut-off frequency for element-A, $f_{c(A)}$ and element-B, $f_{c(B)}$ can be expressed as,

$$\begin{aligned}f_{c(A)} = \frac{c}{\lambda_{ce(A)}} &= \frac{c}{\sqrt{\epsilon_r}\left[2w_1 + 2\pi(d+2t)\right]}, \\ f_{c(B)} = \frac{c}{\lambda_{ce(B)}} &= \frac{c}{\sqrt{\epsilon_r}\left[4w_2 + 2g + 2\pi(d+2t)\right]}\end{aligned} \tag{6.2}$$

In case of 200kW hybrid coupler as presented in previous chapter, the respective structure dimensions are given as,

$$\begin{aligned}w_1 &= 0.109m, \quad w_2 = 0.132m, \quad d = 0.04m \\ t &= 0.003m, \quad g = 0.0172m, \quad \epsilon_r = 1.\end{aligned}$$

Substituting these parameters in Eqn.6.2 we get,

$$\begin{aligned}f_{c(A)} &= \frac{3\times10^8}{\left[2\times0.109 + 2\times3.14\times0.046\right]} = 1.25GHz, \\ f_{c(B)} &= \frac{3\times10^8}{\left[4\times0.132 + 2\times0.0172 + 2\times3.14\times0.046\right]} = 348MHz.\end{aligned} \tag{6.3}$$

It can be seen that the cut-off frequency for the TE mode in element-A is 1.25GHz and in element-B is 348MHz. That means, above to 348MHz, TE mode can propagate in the 8.34±0.2dB coupled lines section which consist of element-A and element-B. This device is fabricated to operate in the frequency range of 40-

110MHz. Thus, it can safely be used without any deterioration in the results. In HFSS simulation, it is found that the hight of outer conductor must be taken $0.40m$ for required spacing to limit the electric field within the 1.0MV/m. For the 1.5MW power handling capability in the frequency range 30-96MHz same respective strip-line dimension are calculated as,

$$\begin{aligned} w_{1h} &= 0.39m, \;\; w_{2h} = 0.56m, \;\; d_h = 0.153m \\ t_h &= 0.005, \;\; g_h = 0.205m, \;\; \epsilon_r = 1 \end{aligned}$$

Using Eqn.6.2, cut-off frequency for element-A, $f_{hc(A)}$ and element-B, $f_{hc(B)}$ are calculated as,

$$f_{hc(A)} = 166MHz, \quad f_{hc(B)} = 80MHz. \tag{6.4}$$

It can be seen that above the 80MHz higher mode TE can be excited in the 8.34±0.2dB coupled lines section. Therefore, required spacing for 1.5MW can not be achieved using this configuration. It can also be noticed that the strip-line width $w_2 = 0.56m$ is calculated for the required spacings. Application of such a large dimension strip-line conductor in HF and VHF frequency range is difficult due to the many other reasons like,

- Large dimension of the coupled lines create the structural configuration conflict between element-A and element-B and junction discontinuity effect become more prominent.
- To maintain the spacified gaps between of the bulky copper inner coupled strip-lines over the required length is very difficult and small deviation from specified structural dimension induces, huge deterioration in performance.

6.3 Concept, design and simulation of the 1.5MW 3dB hybrid coupler

For 1.5MW power handling capability, required spacing can not be achieved in privious model due to the excitation of the TE modes as explained in previous section.

Now the strip-line width can be reduced by increasing the impedance. For 1.5MW power handling capability, two 100Ω ultra-wideband 3dB hybrid coupler are connected in parallel to achieve the required spacing at reduced strip-width. By using this concept, strip-width can be reduced with ratio of 4 approx. as compared to 50Ω, 3dB hybrid coupler without affecting the ground spacing. Schematic of the 1.5MW hybrid coupler using two 100Ω, 3dB couplers is shown in Fig.6.3. Here, each of 8.34 ± 0.2 coupled lines section is designed for 100Ω. The structural design parameters of element-A, element-B and connecting lines as shown in Fig.6.3 can be calculated using known equations [11,35,44]. The structural parameters of the strip-line for the proposed 1.5MW are calculated as,

$$\begin{aligned} w_1 &= 0.121m, \;\; w_2 = 0.152m, \;\; d = 0.072m \\ t &= 0.005m, \;\; g = 0.1851m, \;\; \epsilon_r = 1 \end{aligned}$$

Using these dimension $f_{c(A)}$ and $f_{c(B)}$ are calculated as,

$$f_{c(A)} = 396MHz, \quad f_{c(B)} = 200MHz. \tag{6.5}$$

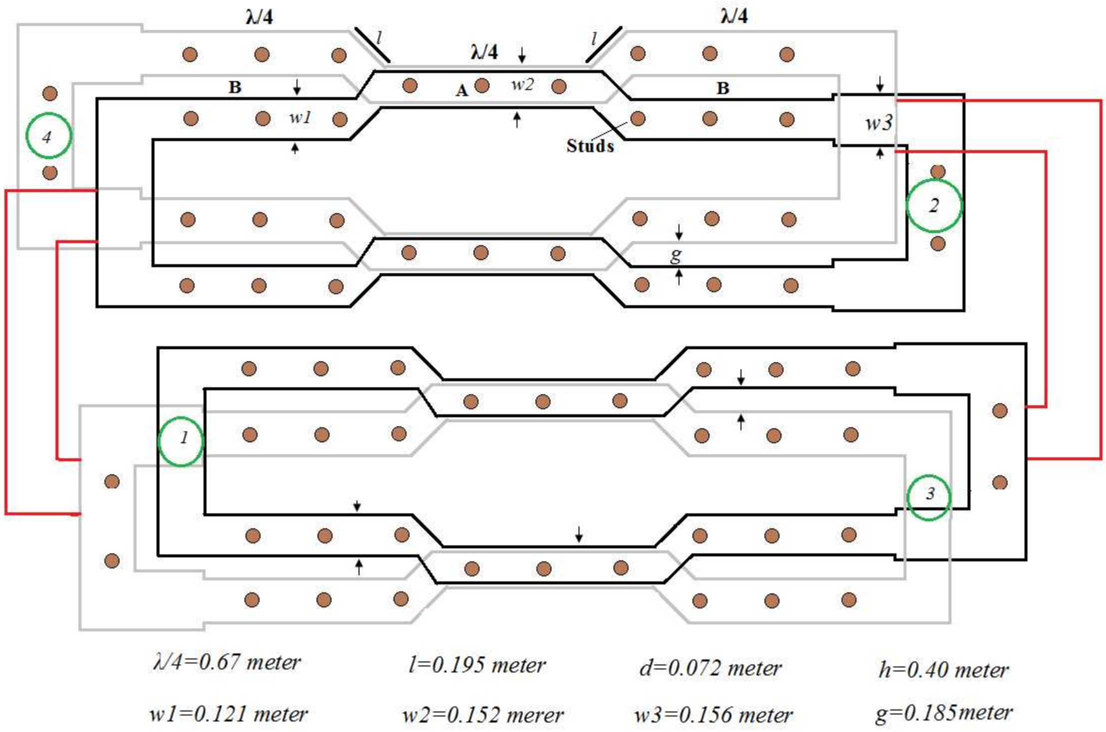

Figure 6.3: Schematic of 1.5MW, 3dB hybrid coupler.

This is observed that designed hybrid coupler can work in the required frequency range of 30-96MHz without excitation of higher TE modes. The inner strip-line dimensions are also reduced in the ratio of 4 and it is found appropriate. Therefore, other problem associated to the bigger size of the inner strip-line is also alleviated. The resulting model using these structural parameters is simulated with HFSS software and the electric field plot is shown in Fig.6.4 Here, maximum electric field is found below the safe limit of 1.0MV/m at 1.5MW input. Thus, the designed hybrid coupler is verified for the 1.5MW power handling capability. The simulation results are shown in Fig.6.5

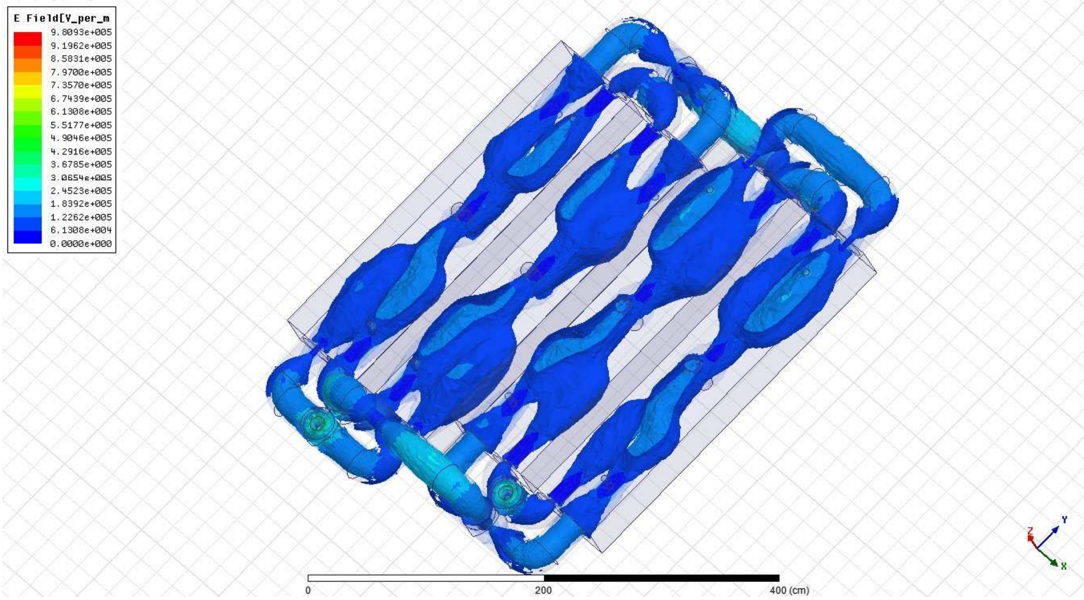

Figure 6.4: Electric field plot.

6.4 Fabrication drawing of the hybrid coupler

Fabrication drawing of the designed hybrid coupler is shown in Fig.6.6, where two identical 100Ω hybrid couplers are arranged on one above other. These are connected with $9\frac{1}{8}$inch, 100Ω transmission lines. Each of the rectangular box have inner space of $3.40m \times 1.0m \times 0.4m$ and designed to fabricate with aluminum sheet of 5mm thickness. Total space used by the device is approx. $5.0m \times 2.5m \times 2.0m$. Each rectangular box contains two 8.34±0.2dB coupled lines sections. Each of the section has two stepped 5mm thick copper strip-line conductors that are overlapped on each other in a particular manner. Perspex holders are provided to hold the strip-line conductor inside the outer conductor box. The 100Ω coaxial transmission lines are used to connect two 8.34±0.2dB coupled lines sections. The detailed dimension of the inner strip-line are shown in Fig.6.3. All of the four ports are made to provide $9\frac{1}{8}$inch, 50Ω coaxial transmission line as the termination required.

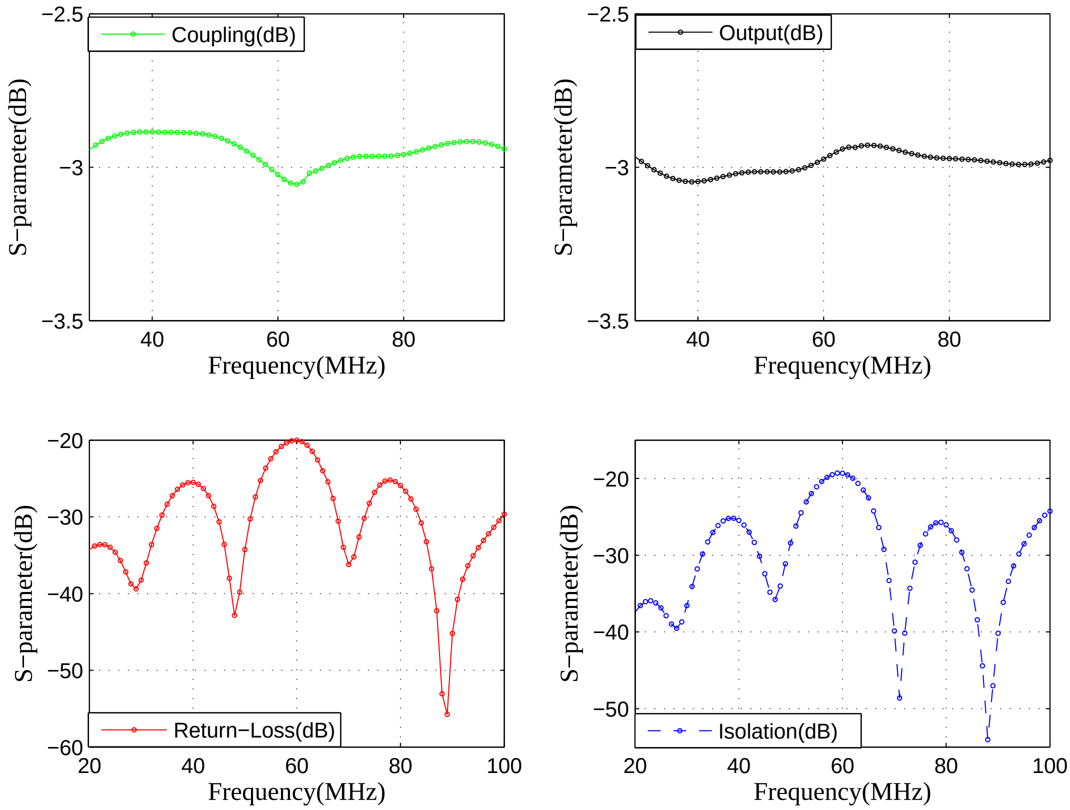

Figure 6.5: Simulation Results.

6.5 Result and discussion

A 1.5MW, 3 ± 0.2dB tandem hybrid coupler has been designed for the ultra-wideband of 30 to 96MHz. To achieve the required spacing for 1.5MW power handling capability two 100Ω hybrid couplers are connected in parallel. The designed model is simulated with HFSS software. Simulation results are found providing coupling of -3 ± 0.25dB, output of -3 ± 0.25dB, return loss less than 20dB and isolation value less than -21dB in the frequency range of 30-90MHz.

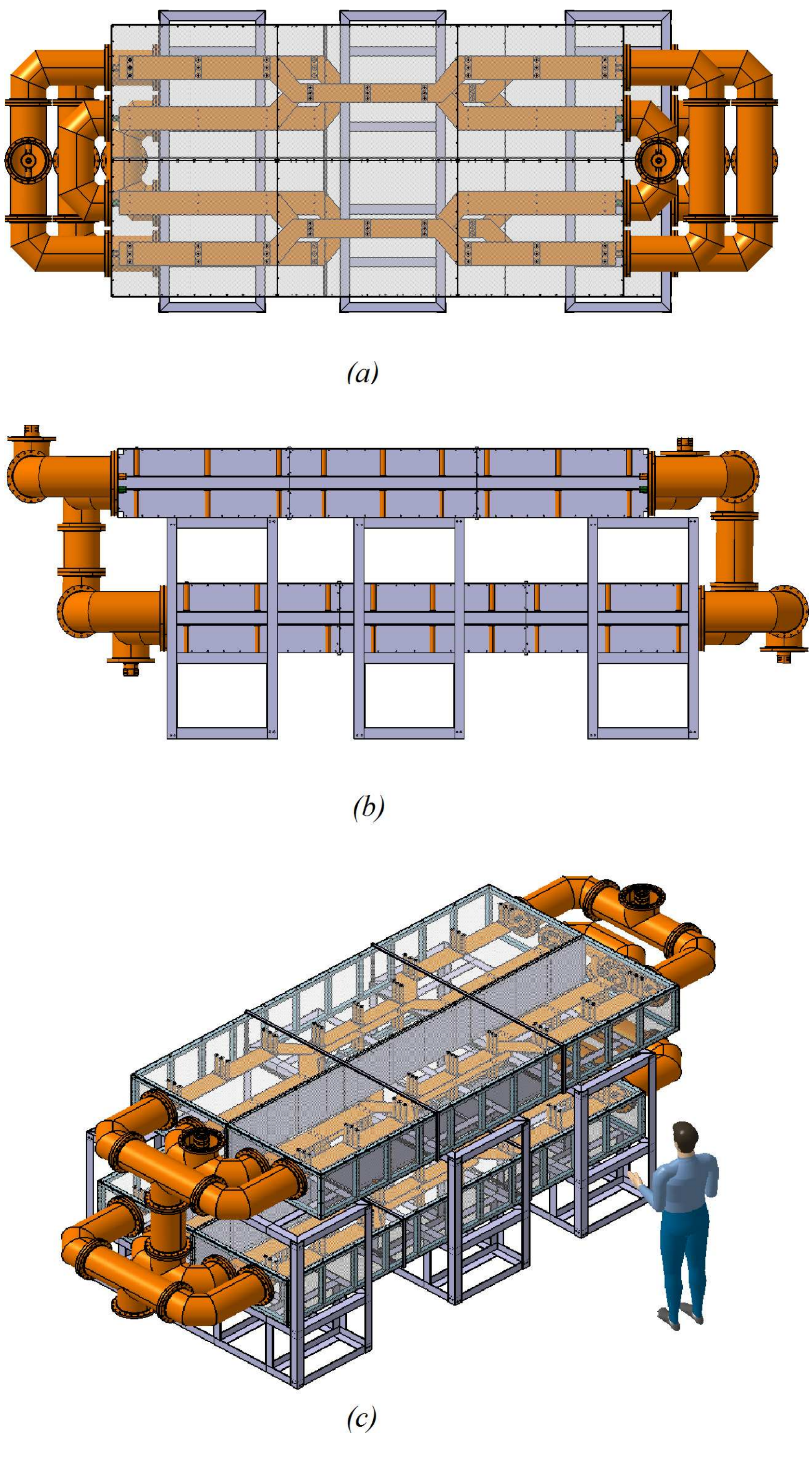

Figure 6.6: Assembly drawing of the designed 1.5MW 3dB hybrid coupler (a)Top view (b) Side view (c)Super view.

The maximum electric field on the structure is found below 1.0MV/m. The results are found as per our objective.

6.6 Conclusion

Design, simulation and fabrication drawing of the 1.5MW 3dB hybrid coupler in the ultra-wideband of 30-96MHz is presented. The propagation of higher modes is main obstacle. The problem has been alleviated in this chapter. The practical experience previous development is utilized in the designing of this device. The device is found performing for the required values in the simulation results. The fabrication of the such big and complicated device needs sufficient time and not a part of the thesis. The final model is very expected to provide with acceptable results. Therefore the future work may be focus on the fabrication of the device.

7

Conclusions

This thesis is devoted to establish a concept, design and development procedure for the fabrication of ultra-wideband 3dB hybrid coupler for the ICRF heating of the tokamak. The systematic design approach and fabrication drawings of 1.5MW, ultra-wide band, 3dB hybrid coupler for the HF and VHF range are presented. This challenging task has been completed in several steps. The design, fabrication and testing of 2.5 kW narrow band and 200kW ultra-wideband hybrid couplers are being carried out as the intermediate stages. In order to investigate the applicability of the fabricated device in the desired regime, numerous theoretical and experimental techniques have been explored. These are added as new contributions to the present literature. The fabricated hybrid couplers have successfully created the process for indigenous development. In high power HF and VHF applications, bigger size of the device creates several unexpected complications due to fabrication constraints and the outcomes can be observed in terms of poor performance. In particular, 200kW hybrid coupler is fabricated with dimension of $3.60m \times 1.0m \times 0.12m$. Fabrication of the such a large device within the perfect tolerance and maintains the spacified gaps between inner coupled strip-lines over the required 3.6m length is very difficult. The small deviation from specified structural dimension induces, huge deterioration in performance. Thus, the deterioration due to structural tolerances need to be compensated in final experimental model. This work has provided with the experience of theoratical modeling, simulation, fabrication and testing of the high power rf componants in HF and VHF. The practices that are learnt and adopted at intermidate stages are utilized and found very helpful in designig process of 1.5MW multi-element ultra-wideband 3dB hybrid coupler. Thesis claims the design and development of broadband multi-element coupled lines of very high power handling capability that is not reported earlier. This is found that junction discontinuity effect descrepency is great obstacle behind it and the development of a high power multi-element coupled line is not possible without considering it.

The developed broadband coupled lines can also be used to achieve the wider bandwidth in RF components such as, balanced mixer, phase correlator, balanced amplifier, balanced modulator, attenuator, power measurements and antenna array networks. These components are utilized in the area of satellite communication, cellular, broadcast, defense and aerospace.

Because of its wide application ranging from fusion devices to industries, this is essential part of active research.

7.1 Summary

The major achievements of the thesis can be summarize as,

- The initial concept, design, fabrication and test procedure of a 91.2MHz, 2.5kW prototype 3dB tandem hybrid coupler has been developed.

- A novel patch compensation technique is explored and applied to optimize the performance of hybrid coupler in general.

- The above said prototype has successfully created the process for indigenous development of 2.5kW, 3dB hybrid coupler at any required frequency in 20 to 120MHz range.

- The comprehensive study of the broadband multi-element coupled lines, in conjunction with the junction discontinuity effect is presented, and its appliability in high power rf regime is discussed.

- In multi-element coupled lines, junctions are employed for the joining of coupled elements. These junctions produces undesirable reactance that deteriorates the performance of multi-element coupled lines. The reactive effect of junction discontinuity is derived in terms of lumped capacitance and inductance and incorporated in the previous theory. Ultimately the negative effect of junction discontinuity is verified with HFSS simulation result.

- Modified theory including compensation of junction discontinuity effect is explored, applied and proven effective. This theory has been applied in design of 3-element 8.34$\pm$0.2dB coupled lines and found substantially effective in compensation of junction discontinuity discrepancy.

- The modified theory is also extended for compensation of junction discontinuity effect in n-element coupled lines section to make it useful for other applications.

- Design and development of the ultra-wideband 200kW, 3dB hybrid coupler for the 40-110MHz is presented where significance of the modified theory is highlighted.

- The final objective of the thesis has been completed with design and fabrication drawings of 1.5MW 3dB hybrid coupler in the frequency range of 30 to 96MHz. This design has been simulated with HFSS and verified for desired performance.

7.2 Future scope

In tokamak, hanging boundary conditions for the fields lead to a hanging plasma load. In many cases the field pattern is dominated by an exponential decay up to the location where the plasma density is high enough for the wave to start propagating. Consequently the loading is sensitive to changes of the plasma density and the density gradient in front of the antenna. The fields and thus the antenna loading can also be affected by changes in absorption of the wave inside the plasma, or by variations of the fields excited by neighboring straps. Changes occur in both the real and imaginary parts of the antenna impedance. The fast variations such as giant ELMs have time scale of few $100\mu s$. Such fast variations are very difficult to match.

The plasma offers continuous variable mismatched impedance and therefore, significant amount of the rf power is reflected back to the ICRF generator. This may cause of under performance or damage to the rf generator. In ICRH systems, 3dB hybrid coupler is used as rf power divider, power combiner and for providing protection to the rf generator by isolating the reflected power. Reflected power can be isolated by using 3dB hybrid coupler if both of the oupled and output ports are terminated with identical mismatched load. The hybrid coupler ports that are terminated with ICRH antennae inside the tokamak may offers the different load impedance at a particular moment. In such condition, hybrid coupler may fails to protect the rf system from reflected power. In that case faster matching system is required to cope with the faster variations of the plasma load impedance. The available matching techniques such as vacuum variable capacitors and shorted stubs are slower as compared to the plasma load variations and are not successful. Up to certain extant ferrite stub is suitable for fast matching of the plasma load variations in milliseconds order. This is found that matching capability of the ferrite stub can be faster if it is mounted on the connecting lines of the hybrid coupler. The connecting lines are of 50Ω non-coupled strip-lines that are used to onnect the two 8.34dB coupled lines in tandem. In a single tandem hybrid coupler two connecting lines present where ferrite stub can be used. This is expected that matching speed can be two times faster as compared to the ferrite stubs used else where.

The future work will focus on the development of an integrated hybrid coupler system including fast ferrite stub for the to enhance the performance of the ICRF system in the tokamak.

Bibliography

[1] X. J. Zhang, Y. P. Zhao, B. N. Wan, X. Z. Gong, Y. Lin, W. Y. Zhang, Y. Z. Mao, C. M. Qin, S. Yuan, X. Deng, et al. Experimental observation of ion heating by mode-converted ion bernstein waves in tokamak plasmas. *Nuclear Fusion*, 52(8):082003, 2012.

[2] A. Becoulet. Heating and current drive regimes in the ion cyclotron range of frequency. *Plasma Physics and Controlled Fusion*, 38(12A):A1, 1996.

[3] Y. C. Saxena et al. Present status of the SST-1 project. *Nuclear Fusion*, 40(6):1069, 2000.

[4] D. Bora, Sunil Kumar, Raj Singh, K. Sathyanarayana, S. V. Kulkarni, A. Mukherjee, B. K. Shukla, J. P. Singh, Y. S. S. Srinivas, P. Khilar, et al. Cyclotron resonance heating systems for SST-1. *Nuclear fusion*, 46(3):S72, 2006.

[5] Yevgen O. Kazakov, V. G. Kiptily, S. E. Sharapov, and D. Van Eester. Search for ion heating scenarios in burning dt plasmas with icrh. In *Proceedings of 12th Technical Meeting on Energetic Particles in Magnetic Confinement Systems, p. P1. 14*, 2011.

[6] J. M. Noterdaeme, Vl. V. Bobkov, S. Brémond, A. Parisot, I. Monakhov, B. Beaumont, Ph. Lamalle, F. Durodié, and M. Nightingale. Matching to elmy plasmas in the icrf domain. *Fusion engineering and design*, 74(1):191–198, 2005.

[7] Djamel Grine, André Messiaen, Michel Vervier, Pierre Dumortier, and Raymond Koch. Summary and results of the study of the hybrid matching op-

tion implementation of the iter icrh system. *Fusion Engineering and Design*, 87(2):167–178, 2012.

[8] P. Dumortier, P. Andrew, G. Bonheure, R. V. Budny, R. Buttery, M. Charlet, I. Coffey, M. de Baar, P. C. de Vries, T. Eich, et al. Confinement properties of high density impurity seeded elmy h-mode discharges at low and high triangularity on jet. *Plasma Physics and controlled fusion*, 44(9):1845, 2002.

[9] Bernard M. Oliver. Directional electromagnetic couplers. *Pro eedings of the IRE*, 42(11):1686–1692, 1954.

[10] E. M. T Jones. Coupled-strip-transmission-line filters and directional couplers. *Microwave Theory and Techniques, IRE Transactions on*, 4(2):75–81, 1956.

[11] Rana Pratap Yadav, Sunil Kumar, and S. V. Kulkarani. Design and development of 3 db patch compensated tandem hybrid coupler. *Review of Scientific Instruments*, 84(1):014702, 2013.

[12] M. Mayoral, I. Monakhov, T. Walden, V. Bobkov, T. Blackman, M. Graham, J. Mailloux, J. Noterdaeme, M. Nightingale, and J. Ongena. Hybrid couplers on the jet icrf system: Commissioning and first results on elms. In *AIP Conference Proceedings*, volume 933, page 143, 2007.

[13] M. Nightingale, F. Durodie, A. Argouarch, G. Berger-By, T. Blackman, J. Caughman, V. Cocilovo, P. Dumortier, D. Edwards, J. Fanthome, et al. Development of the JET ion cyclotron resonance frequency heating system in support of ITER.

[14] Valery A. Dolgashev and Sami G. Tantawi. Effect of rf parameters on breakdown limits in high-vacuum x-band structures. In *AIP Conference Proceedings*, pages 151–165, 2003.

[15] Sami G. Tantawi and Christopher D. Nantista. Active and passive rf components for high-power systems. In *AIP CONFERENCE PROCEEDINGS*, pages 83–100, 2002.

[16] Richard Woo. *Final report on RF voltage breakdown in oaxial transmission lines*. Jet Propulsion Laboratory, California Institute of Technology, 1970.

[17] Paul Shiffres. How much cw power can stripline handle. *Microwaves*, (6):25–34, 1966.

[18] R. Levy. Transmission-line directional couplers for very broad-band operation. *Electrical Engineers, Proceedings of the Institution of*, 112(3):469–476, 1965.

[19] Ralph Levy and Seymour B. Cohn. A history of microwave filter research, design, and development. *Microwave Theory and Techniques, IEEE Transactions on*, 32(9):1055–1067, 1984.

[20] E. G. Cristal and L. Young. Theory and tables of optimum symmetrical tem-mode coupled-transmission-line directional couplers. *Microwave Theory and Techniques, IEEE Transactions on*, 13(5):544–558, 1965.

[21] J. K. Shimizu. Coupled-transmission-line directional couplers. *IEEE Transactions on Microwave Theory and Techniques*, 6(4):403–410, 1958.

[22] Leo Young. The analytical equivalence of tem-mode directional couplers and transmission-line stepped-impedance filters. In *Proceedings of the Institution of Electrical Engineers*, volume 110, pages 275–281. IET, 1963.

[23] Henry J. Riblet. General synthesis of quarter-wave impedance transformers. *Microwave Theory and Techniques, IRE Transactions on*, 5(1):36–43, 1957.

[24] Paul I. Richards. Resistor-transmission-line circuits. *Proceedings of the IRE*, 36(2):217–220, 1948.

[25] H. Seidel and J. Rosen. Multiplicity line in cascade transmission synthesis-part-I. *Microwave Theory and Techniques, IEEE Transactions on*, 13(3):275–283, 1965.

[26] Michael Dydyk. Microstrip directional couplers with ideal performance via single-element compensation. *Microwave Theory and Techniques, IEEE Transactions on*, 47(6):956–964, 1999.

[27] Chul-Soo Kim, Jong-Sik Lim, Dong-Joo Kim, and Dal Ahn. A design of single and multi-section microstrip directional coupler with the high directivity. In *Microwave Symposium Digest, 2004 IEEE MTT-S International*, volume 3, pages 1895–1898. IEEE, 2004.

[28] Sheng-Fuh Chang, Jia-Liang Chen, Yng-Huey Jeng, and Chain-Tin Wu. New high-directivity coupler design with coupled spurlines. *Microwave and Wireless Components Letters, IEEE*, 14(2):65–67, 2004.

[29] Sarmad Al-Taei, Phil Lane, and George Passiopoulos. Design of high directivity directional couplers in multilayer ceramic technologies. In *Microwave Symposium Digest, 2001 IEEE MTT-S International*, volume 1, pages 51–54. IEEE, 2001.

[30] Slawomir Gruszczynski and Krzysztof Wincza. Generalized methods for the design of quasi-ideal symmetric and asymmetric coupled-line sections and di-

rectional couplers. *Microwave Theory and Techniques, IEEE Transactions on*, 59(7):1709–1718, 2011.

[31] Peter A. Rizzi. *Microwave engineering: passive circuits*. Prentice Hall Englewood Cliffs, NJ, 1988.

[32] David M. Pozar. *Microwave engineering*. John Wiley & Sons, 2009.

[33] Robert M. Barrett. Microwave printed circuits–the early years. *Microwave Theory and Techniques, IEEE Transactions on*, 32(9):983–990, 1984.

[34] M. V. Schneider. Microstrip lines for microwave integrated circuits. *Bell System Technical Journal*, 48(5):1421–1444, 1969.

[35] Seymour B. Cohn. Parallel-coupled transmission-line-resonator filters. *Microwave Theory and Techniques, IRE Transactions on*, 6(2):223–231, 1958.

[36] Harlan H. Howe. *Stripline circuit design*. Artech House Dedham, M. A., 1974.

[37] Robert E. Collin. *Foundations for microwave engineering*. John Wiley & Sons, 2007.

[38] K. C. Gupta, Tatsuo Itoh, and Arthur A. Oliner. Microwave and rf education-past, present, and future. *Microwave Theory and Techniques, IEEE Transactions on*, 50(3):1006–1014, 2002.

[39] Rick Sturdivant. Fundamentals of packaging at microwave and millimeter-wave frequencies. In *RF and Microwave Microelectronics Packaging*, pages 1–23. Springer, 2010.

[40] I. J. Bahl and K. C. Gupta. Average power-handling capability of microstrip lines. *IEE Journal on Microwaves, Optics and Acoustics*, 3(1):1–4, 1979.

[41] Amendra Koul, Marina Y. Koledintseva, Scott Hinaga, and James L. Drewniak. Differential extrapolation method for separating dielectric and rough conductor losses in printed circuit boards. *Electromagnetic Compatibility, IEEE Transactions on*, 54(2):421–433, 2012.

[42] Gary Brist, Stephen Hall, Sidney Clouser, and Tao Liang. Non-classical conductor losses due to copper foil roughness and treatment. *Proc. Electron. Circuits World Conv*, 10:22–24, 2005.

[43] W. L. Firestone. Analysis of transmission line directional couplers. *Proceedings of the IRE*, 42(10):1529–1538, 1954.

[44] Bharathi Bhat and Shiban K. Koul. *Stripline-like transmission lines for microwave integrated circuits.* New Age International, 1989.

[45] Boris Markovich Kats, Valery Petrovich Meschanov, and Alexander Lvovich Khvalin. Synthesis of superwide-band matching adapters in round coaxial lines. *Microwave Theory and Techniques, IEEE Transactions on*, 49(3):575–579, 2001.

[46] Ch. Person, L. Carre, E. Rius, J. Ph. Coupez, and S. Toutain. Original techniques for designing wideband 3d integrated couplers. In *Microwave Symposium Digest, 1998 IEEE MTT-S International*, volume 1, pages 119–122. IEEE, 1998.

[47] C. Person, J. P. Coupez, S. Toutain, and M. Morvan. Wideband 3 db/90 coupler in multilayer thick-film technology. *Electronics Letters*, 31(10):812–813, 1995.

[48] M. Nakajima, E. Yamashita, and M. Asa. New broad-band 5-section microstrip-line directional coupler. In *Microwave Symposium Digest, 1990., IEEE MTT-S International*, pages 383–386. IEEE, 1990.

[49] Roland B. Ekinge. A new method of synthesizing matched broad-band tem-mode three-ports. *Microwave Theory and Techniques, IEEE Transactions on*, 19(1):81–88, 1971.

[50] Sang-Gyu Kim and Kai Chang. Ultrawide-band transitions and new microwave components using double-sided parallel-strip lines. *Microwave Theory and Techniques, IEEE Transactions on*, 52(9):2148–2152, 2004.

[51] Seymour B. Cohn and Ralph Levy. History of microwave passive components with particular attention to directional couplers. *Microwave Theory and Techniques, IEEE Transactions on*, 32(9):1046–1054, 1984.

[52] Rana Pratap Yadav, Sunil Kumar, and Sanjay Kulkarni. An analysis of junction discontinuity effects in multi-element coupled lines and its diminution at designing stage. *Progress In Electromagnetics Research B*, 56:25–49, 2013.

[53] Rana Pratap Yadav, Sunil Kumar, and S. V. Kulkarni. Design and development of ultra-wideband 3 db hybrid coupler for ion cyclotron resonance frequency heating in tokamak. *Review of Scientific Instruments*, 85(4):044706, 2014.